REPORT DOCUMENTATION PAGE

Form Approved OMB NO. 0704-0188

1. REPORT DATE (DD-MM-YYYY)	2. REPORT TYPE	3. DATES COVERED (From - To)
06-08-2014	MS Thesis	-

4. TITLE AND SUBTITLE
Binding Energy of Quantum Bound States in X-shaped Nanowire Intersection

5a. CONTRACT NUMBER
W911NF-11-1-0189

5b. GRANT NUMBER

5c. PROGRAM ELEMENT NUMBER
206022

6. AUTHORS
Subash Nepal (student),, Igor Bondarev (advisor)

5d. PROJECT NUMBER

5e. TASK NUMBER

5f. WORK UNIT NUMBER

7. PERFORMING ORGANIZATION NAMES AND ADDRESSES
North Carolina Central University Graduate
Office of Sponsored Programs
1801 Fayetteville St.
Durham, NC 27707 -3129

8. PERFORMING ORGANIZATION REPORT NUMBER

9. SPONSORING/MONITORING AGENCY NAME(S) AND ADDRESS (ES)
U.S. Army Research Office
P.O. Box 12211
Research Triangle Park, NC 27709-2211

10. SPONSOR/MONITOR'S ACRONYM(S)
ARO

11. SPONSOR/MONITOR'S REPORT NUMBER(S)
58986-PH-REP.30

12. DISTRIBUTION AVAILIBILITY STATEMENT
Approved for public release; distribution is unlimited.

13. SUPPLEMENTARY NOTES
The views, opinions and/or findings contained in this report are those of the author(s) and should not contrued as an official Department of the Army position, policy or decision, unless so designated by other documentation.

14. ABSTRACT
The question of the possible existence of the quantum bound states (localized states) due to special geometries has been a long standing problem in quantum theory. Knowledge of quantum bound states in crossed nanowire system is very important in understanding the properties of spatially confined nanostructures which are promising candidates for device applications such as transistors, amplifiers, switches, biosensors, photo-detectors, solar cells, lasers and light-emitting diodes. This study focuses mainly on investigating the angular dependence of the lowest bound

15. SUBJECT TERMS
Quantum Wires, Crossed Nanowires, Trapped Electron States, Quantum Dots

16. SECURITY CLASSIFICATION OF:			17. LIMITATION OF ABSTRACT	15. NUMBER OF PAGES	19a. NAME OF RESPONSIBLE PERSON
a. REPORT	b. ABSTRACT	c. THIS PAGE			Igor Bondarev
UU	UU	UU	UU		19b. TELEPHONE NUMBER: 919-530-6623

Report Title

Binding Energy of Quantum Bound States in X-shaped Nanowire Intersection

ABSTRACT

The question of the possible existence of the quantum bound states (localized states) due to special geometries has been a long standing problem in quantum theory. Knowledge of quantum bound states in crossed nanowire system is very important in understanding the properties of spatially confined nanostructures which are promising candidates for device applications such as transistors, amplifiers, switches, biosensors, photo-detectors, solar cells, lasers and light-emitting diodes. This study focuses mainly on investigating the angular dependence of the lowest bound energy state for the model system of an electron trapped at the intersection of two identical narrow channels (nanowires) crossed at an arbitrary angle. When the channels are perpendicular, such a classically unbound system is known to possess a quantum bound state. We used the variational principle to obtain the general criterion to study the role of tilted geometry for the existence of bound state of an electron in such a quantum system. Using suitable trial wave functions, calculations were carried out to estimate the upper bound for the ground state energy of an electron located inside the crossed nanowire system. The results of our calculations show that the bound state energy varies as the squared sine of the intersection angle of the crossed nanowires. We have found that the system is strongly bound when the intersection angle is 90 degree and the system is unbound when the intersection angle is 00. These particular features of the crossed nanowire system can be exploited to design single electron ultra-sensitive switching devices using newly developed lithographic and etching techniques in nanotechnology. Furthermore, our model may be useful to interpret electron transport peculiarities in realistic systems such as semiconductor nanowire films, nanorods and carbon nanotube bundles.

Binding Energy of Quantum Bound States in X-shaped Nanowire Intersection

by

Subash Chandra Nepal

A Thesis (Project) Submitted to

The Faculty of the Graduate School at

North Carolina Central University

In Partial Fulfillment of the Requirements

For the Degree

(Master of Science)

Durham, North Carolina

2014

Binding Energy of Quantum Bound States in X-shaped Nanowire Intersection

by

Subash Chandra Nepal

A Thesis (Project) Submitted to

The Faculty of the Graduate School at

North Carolina Central University

In Partial Fulfillment of the Requirements

For the Degree

(Master of Science)

Durham, North Carolina

2014

Approved by

_____

Committee Chair

_____

Committee Members

ABSTRACT

The question of the possible existence of the quantum bound states (localized states) due to special geometries has been a long standing problem in quantum theory. Knowledge of quantum bound states in crossed nanowire system is very important in understanding the properties of spatially confined nanostructures which are promising candidates for device applications such as transistors, amplifiers, switches, biosensors, photo-detectors, solar cells, lasers and light-emitting diodes. This study focuses mainly on investigating the angular dependence of the lowest bound energy state for the model system of an electron trapped at the intersection of two identical narrow channels (nanowires) crossed at an arbitrary angle. When the channels are perpendicular, such a classically unbound system is known to possess a quantum bound state. We used the variational principle to obtain the general criterion to study the role of tilted geometry for the existence of bound state of an electron in such a quantum system. Using suitable trial wave functions, calculations were carried out to estimate the upper bound for the ground state energy of an electron located inside the crossed nanowire system. The results of our calculations show that the bound state energy varies as the squared sine of the intersection angle of the crossed nanowires. We have found that the system is strongly bound when the intersection angle is 90^0 and the system is unbound when the intersection angle is 0^0. These particular features of the crossed nanowire system can be exploited to design single electron ultra-sensitive switching devices using newly developed lithographic and etching techniques in nanotechnology. Furthermore, our model may be useful to interpret electron transport peculiarities in realistic systems such as semiconductor nanowire films, nanorods and carbon nanotube bundles.

ACKNOWLEDGMENTS

First and foremost, I am grateful to my supervisor Dr. I. V. Bondarev for his mentorship in the completion of my thesis work and for his sponsorship throughout the course of my studies. I am thankful to Dr. Benjamin Crowe and Dr. B. Vlahovic for their moral support and inspiration during the time of thesis work. I extend my thanks to Dr. Areg Meliksetyan for his valuable time in going through the mathematical details for preparing the initial draft of this work. I am also thankful to the faculty members of the Physics Department at NCCU for providing motivation and good academic environment to accomplish this thesis project. Lastly, I wish to thank my wife, lovely daughter, mother, uncle and nephew for giving homely support throughout my work.

CONTENTS

I. INTRODUCTION

A. Literature Review: History and Background

The current progress in lithographic and etching techniques in semiconductor technology make it much easier to design low dimensional quantum systems such as quantum wells (two dimensions), quantum wires (one dimension) and quantum dots (zero dimension). The smallness yet finiteness of these structures invoke quantum mechanical effects into play. The motion of an electron in a narrow crossed channels has been studied previously by Schult, Ravenhall and Wyld [1]. This paper report the detailed calculations designed to determine whether quantum effects can cause the trapping of single electron at the intersection of wires. The potential shape have been ignored but considered the channels such that the potential is zero within the cross region and infinite outside. Schult et al. solved the free particle Schrödinger equation using two methods for the square geometry [Fig.1].

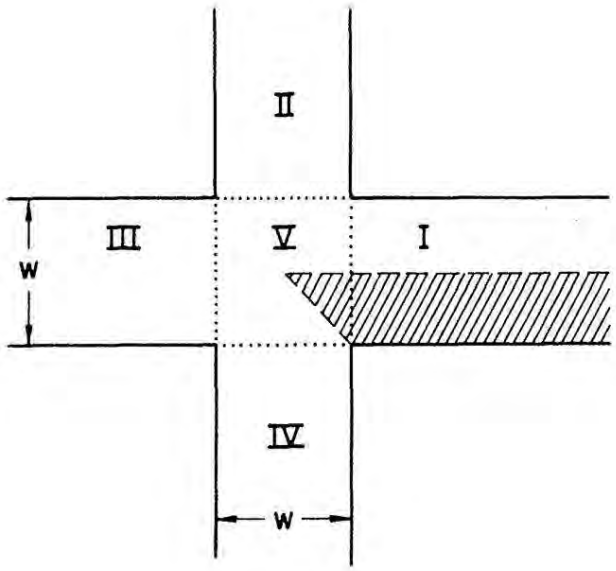

FIG. 1. The geometry of 2D crossed wires of same width (w) intersecting at right angle.

They have computed the energy and the wave function for an electron caught at the intersection of the two narrow channels intersecting at right angle. Their first model was a

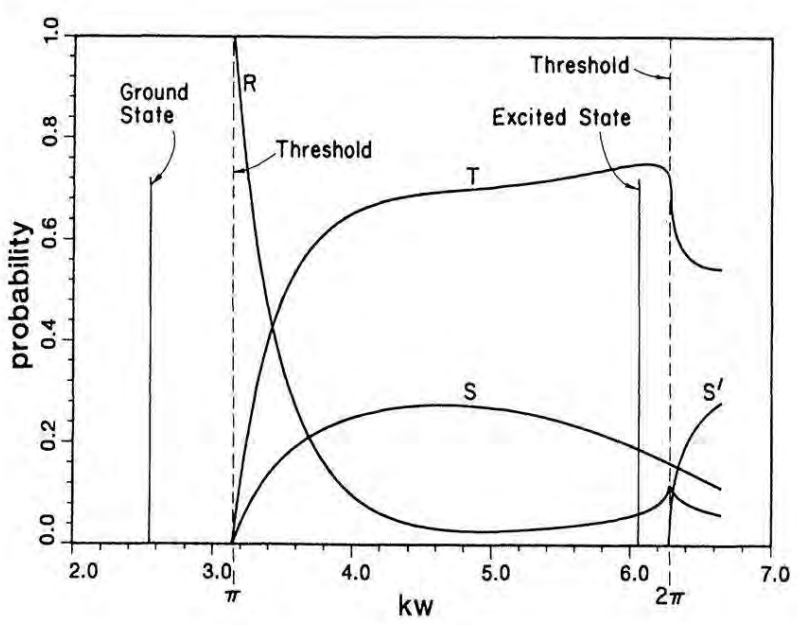

FIG. 2. Properties of a crossed-wire system, as a function of kw, with w being the width of the wire and the energy given by $E = \frac{\hbar^2 k^2}{2m}$. The bound states are shown as vertical lines. The first vertical line show the bound state energies E_1 and the second one represent excited states. The dotted vertical lines are for the propagation threshold energies for the ground and the excited states respectively. The functions are R, the reflection probability in the incident wire; T, the straight-through transmission probability; S, the probability of sideways transmission into the side wires; and S', the probability of sideways scattering into the second transverse band, $n = 2$. Figure is courtesy of Schult et al. [1].

mesh point method in which they replaced the $2D$ Schrödinger equation

$$\hat{H}\Psi(x, y) = E\Psi(x, y) \tag{1}$$

by a difference equation for the wave function evaluated on a rectangular mesh of points in the $x - y$ plane with discrete evolution in pseudo-time variable, t. They treated the Schrödinger equation as the discretization of the differential equation

$$\frac{\delta\Psi}{\delta t} = \nabla^2\Psi. \tag{2}$$

Taking the initial wave function to be symmetric about the center lines in the x and y directions they computed the energy value to be $E_1 = 0.66E_t$. E_t is the threshold energy

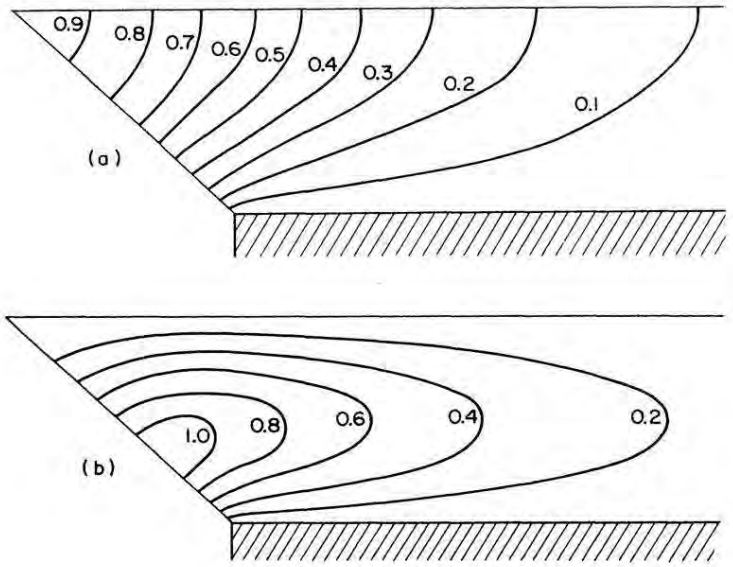

FIG. 3. The bound state wave functions for the ground state. The wave function has steep slope near the corner, concave upward along the channel and convex upwards across the channel. Figure is courtesy of Schult et al. [1].

for free propagation in the open channel, which is given by

$$E_t = \frac{\pi^2 \hbar^2}{2mw^2} \tag{3}$$

where w is the width of the channel and m is the effective mass of an electron. Also for the initial wave function which is odd about the x and y center lines and even about the $x = y$ line, the next bound energy level is at $E_2 = 3.72E_t$, the propagation threshold being at $kw = \pi$ [Fig.2]. This mesh point method gave only the existence of two bound states. Schult et al. used eigenfunctions expansion to solve the differential equation to get higher order bound states. The bound states in case of bent wires in the form of "L" and "T" shaped geometry have been observed. They found that the wave functions near the corners of the intersection varies as $\rho^{2/3}$, where ρ is the distance from the corner [Fig.3]. The presence of corners formed by the intersection of two nanowires is responsible for trapping of the electron. The electron is localized in the square region and cannot propagate along the channel. Furthermore, they estimated the Coulomb energy for the crossed wires. Using the unperturbed wave function, they showed that two electron cannot be bound in the cross

wires because Coulomb repulsion is much greater than (about 10 times) the single-particle binding energy. One of the electron can be bound while the second one, even with opposite spin is pushed into the subband continuum.

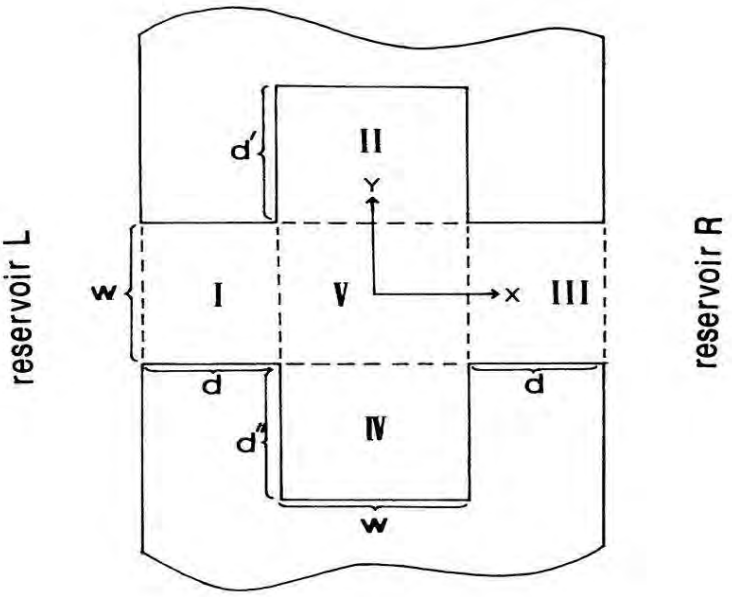

FIG. 4. The geometry of the crossbar structure connecting left and right reservoirs with 2D electrons with equal Fermi energy. The crossbar appear to an electron at the bound state energies nearly infinite.

Berggren and Ji tried to explore the possibility of observing, at least in principle, the bound states in the two intersecting crossed wires by resonant tunneling [2]. The bound states revealed themselves in the electric transport as resonances or antiresonances and the tunneling in the two intersecting wires occur through discrete states. The geometry that they considered consisted of a channel connected to two reservoirs serving as a source and drain. The vertical channel was replaced by a bar of finite length [Fig.4]. They suggested that measurements of the tunneling current could be one of the ways of observing bound states in the cross wires . For such a crossed region, the conductance have been found to be quantized as

$$G = N(2e^2/h) \tag{4}$$

where $N = 1$ or 2. The variation of the conductance as a function of Fermi energy show sharp resonances at E' and E'' which corresponds to the localized states [Fig.5]. The two

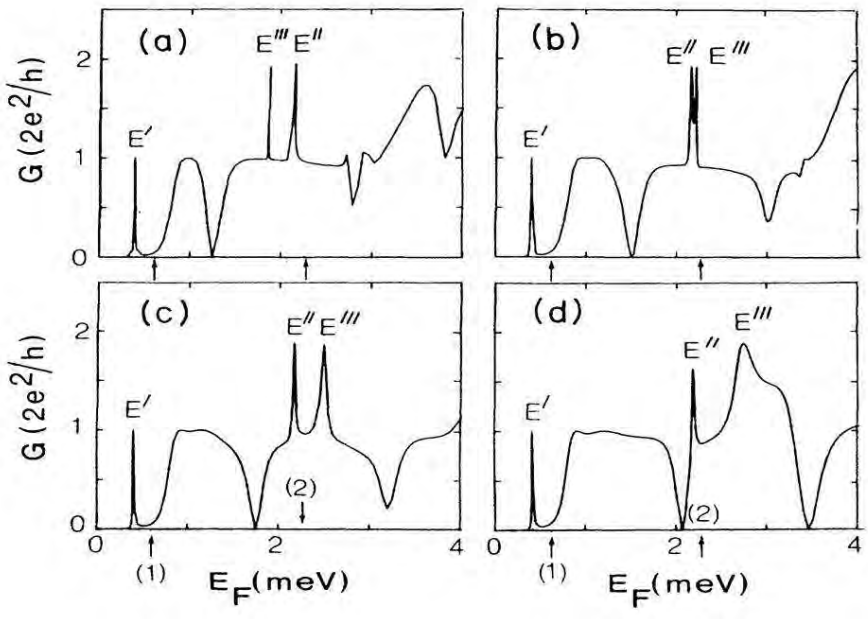

FIG. 5. The conductance as a function of the Fermi energy. The length of the channel connecting 2D electrons and its width are kept constant. The sharp peaks E' and E'' show bound state energies. Figure is courtesy of Berggren et al. [2].

peaks corresponds to the single electron resonant tunneling via bound state energies E_1 and E_2 as estimated by Schult et al. [1].

Soon after the results by Schult et al. for the one electron bound states in an intersecting crossed wires, Berggren and Wang studied the possibility of two electrons being trapped in a finite cross wires intersection [3]. The structure that they considered consisted of an infinite horizontal channel intersected by a finite perpendicular channel [Fig.6]. Their method involved was solving 2D Schrödinger equation self-consistently for each electron taking into account of the Coulomb potential of the other assuming helium atom model. They found that the first electron in the cross region experiences an effectively attractive Coulomb potential while the second is expelled from the central region. This means that no self consistent solution exist for the second electron providing the evidence of Coulomb blockade responsible for the scattering state of two electrons [Fig.7]. Their work supplement the earlier result obtained by Schult et al. [1].

Looking back to the previous work on the transport properties of crossed wires, Ji and Berggren observed that the quantum bound states in the 2D semiconductor structure in

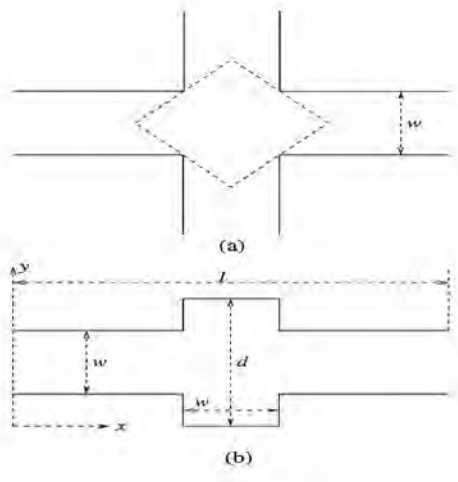

FIG. 6. (a) Schematic view of two intersecting quantum wires with hard walls. The width of the wires is w. (b) View of the modified quantum cross consisting of two horizontal leads and a perpendicular bar with hard walls.

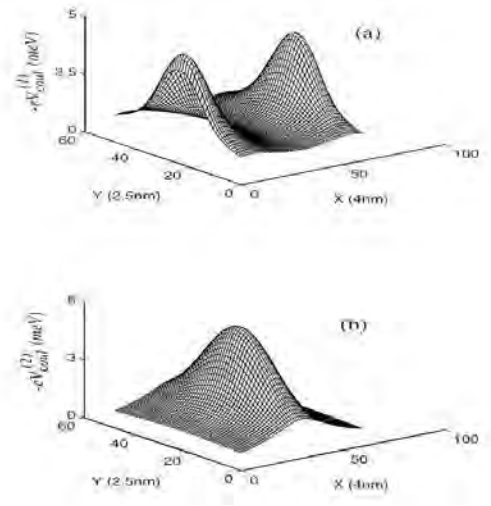

FIG. 7. The Coulomb potential seen by the two electrons: (a) The Coulomb potential for the first electron is taken as attractive potential. In (b), the Coulomb potential for the second electron acts as a potential barrier.

the form of two crossed channels intersecting at right angle give rise to resonant tunneling [4]. The channels that they considered were finite and one of them connect the reservoirs of 2D electron gas on the left and right [Fig.8]. The potential difference was applied across the two reservoirs and conductance values were measured in a structure with the number of

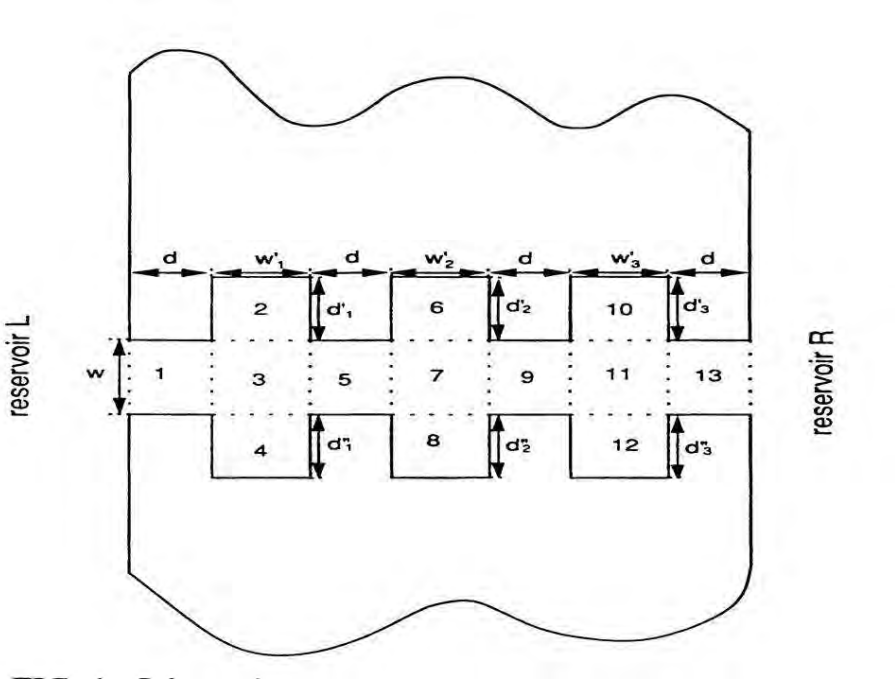

FIG. 8. The geometry of the number of crossbar structures connecting left and right reservoirs with 2D electrons with equal Fermi energy. When the potential difference is applied, electrons flow from left to right. The dashed lines represent the boundaries where the wave functions are matched.

intersections. For the single intersection, the conductance showed a sharp peak below the lowest subband threshold E_t. This peak corresponds to the tunneling through the localized bound states at the center of the cross in case of two infinite intersecting channels [1]. They extended the calculation to a double cross so that the tunneling below the threshold can be assumed to be that through two quantum dots, one held at each intersection. These quantum dots are coupled by a weak potential and the resonance split into two peaks given by E_1 and E_2 [Fig.9]. In the case of number of crosses, the resonant tunneling can be approximated by Kronig-Penny model. There are as many resonance peaks below the lowest subband threshold as there are crosses in the structure connecting two $2D$ electron reservoirs. The calculated value of the conductance reach the maximum value when the quantum dots are well localized to an intersection.

So far, the geometries considered were $2D$ crossed wires intersection enclosing square region with both arms either infinite [1], semi-infinite [3, 4], or finite in length [2]. We have seen the role of bound states in the electronic transport properties of two dimensional

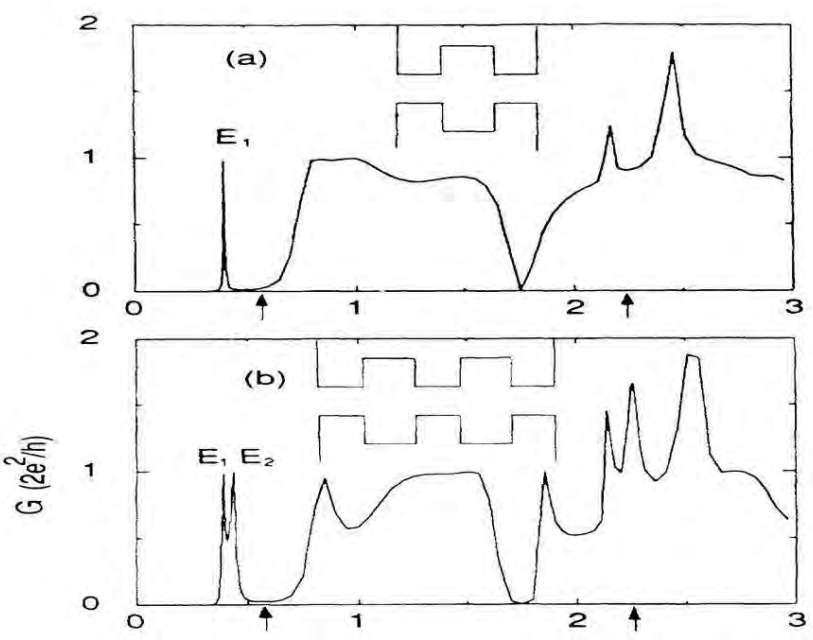

FIG. 9. The calculated conductance at zero temperature as a function of Fermi energy E. E_1, E_2 and E_3 denote the energies at which resonant tunneling via states resembling quantum dots takes place. Figure is courtesy of Ji et al. [4].

crossed structures and some of the methods of observing the localized states. No external field, such as electric or magnetic, was applied to the crossed wires system.

Ravenhall, Wyld and Schult took another approach to probe further into the same problem but in the presence of external magnetic field. Hence, they studied rigorously the effect of magnetic field on the bound states at the crossed junction of nanowires under ballistic approximation in which they neglected the electron-electron interaction [5]. The crossed wires intersect at right angle and the magnetic field was applied perpendicular to the plane of the intersecting wires [Fig.10]. The method they used was an extension for the zero field case to the case of a magnetic field of arbitrary strength. In their model, the voltage that appear across top and bottom of the wire along y-direction gave the Hall voltage (V_{YY}).They calculated the current (I_{XX}) along x-direction which depends strongly on the bound states at the junction. The Hall resistance was obtained using

$$R_H = \frac{V_{YY}}{I_{XX}} \tag{5}$$

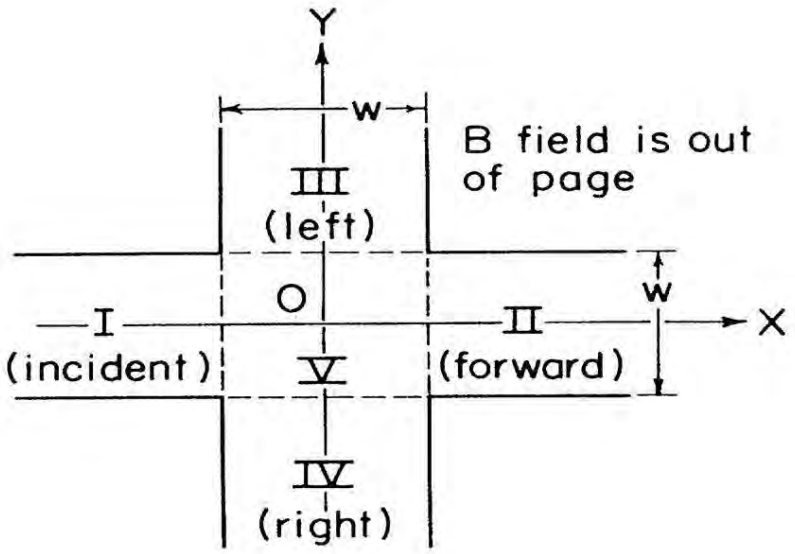

FIG. 10. The four-terminal junction used to study the effect of magnetic fields on the bound state at the intersect.

and compared with

$$R_H = \frac{h}{n_0 e^2} \tag{6}$$

where n_0 is an integer. The ballistic approximation predicts, even for zero field, bound states at the junction and also the variation of the scattering probabilities with energy at the threshold for the opening of new channels. They observed that with non-zero magnetic field new structures are associated with virtual and resonant states located at the junction that becomes $2D$ Landau levels for large value of the magnetic field [Fig.11].

Immediately after the results for $2D$ system of crossed wires were published, the quantum transmission properties of an electron in a crossed junction of two out-of-plane wires have been numerically investigated by Takagaki and Ploog [6]. They considered $3D$ junction with two identical rectangular cross wires connected at right angles on top of each other [Fig.12]. They assumed zero potential within the channels and infinite outside, so that for a given mode (i, j), the threshold for the propagation is given by $(i^2 + j^2)E_t$. In such a structure of crossed junctions, an electron can be transmitted in the direction perpendicular to its incidence. Their calculations show that when these wires are not coupled, the electron gets simply transmitted in the forward direction without any reflection. However, if the coupling

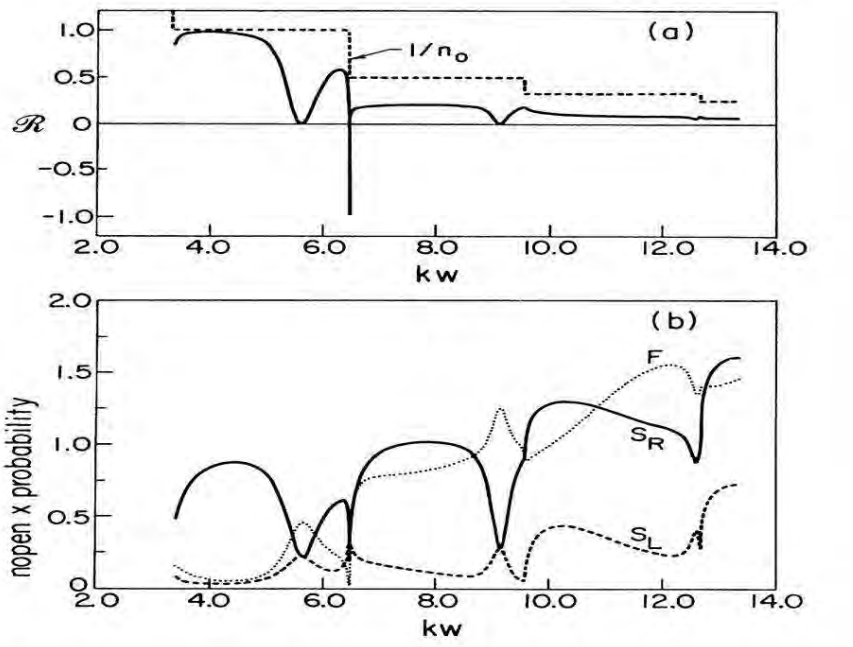

FIG. 11. The dimensionless Hall resistance as a function of kw for dimensionless magnetic field $B = 6.0$. Figure is courtesy of Ravenhall et al. [5].

is non-zero, the electron gets reflected with probability (T_R) or transmitted in the forward direction with probability (T_F) and into each end of the upper wire with probability (T_S) such that

$$T_F + 2T_S + T_R = N, \tag{7}$$

where $N \approx \pi E_F/4E_t$ is the number of propagating modes in the channels for an electron moving with Fermi energy E_F. The transmission exhibits resonance due to quasibound states in the intersection region even if the device consist of straight wires. In the $2D$ in-plane crossed wires junction the incident mode does not couple with the bound states due to parity miss-match hence, no resonances occur in the transmission. The appearance of transmission resonances due to quasibound states gave the strong evidence of the quantum-mechanical behavior of the scattering phenomena (see Fig.13). Furthermore, they calculated the bend resistance R_B, which is always negative for $2D$ crossed junction, can have positive value around the resonances in the $3D$ junction (see Fig.14).

An idealized geometry of $3D$ junction with a single crossing studied by Takagaki and Ploog have limitations with regard to the realistic system associated with number of crossings. Recent experiments on carbon nanotube crossed with a semiconducting one have

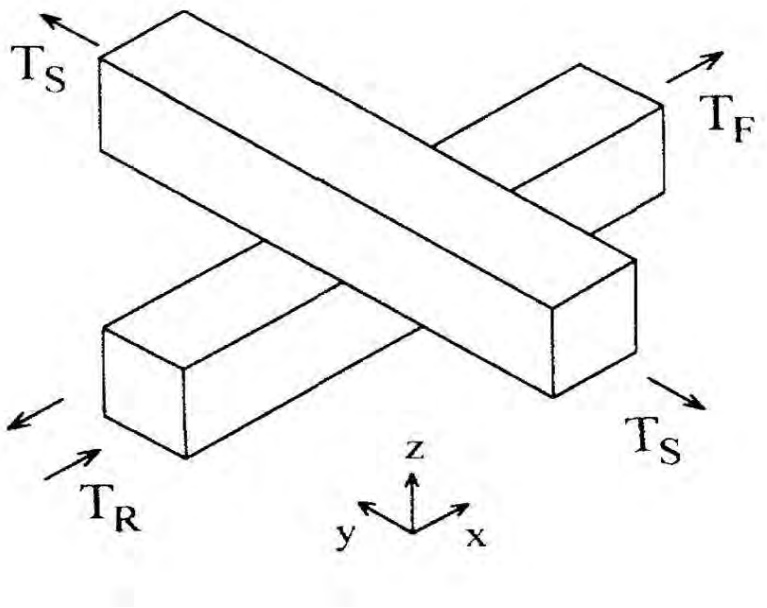

FIG. 12. Schematic view of the out-of-plane crossed wires junction. Two rectangular waveguides are connected at right angles on top of each other. The width of the waveguides are assumed to be equivalent. An electron is injected from the lower waveguides.

shown the existence of bound states at the crossing which are not due to disorder. With an objective at clarifying this problem, Makogon, Jeu and Smith made a detailed study of tunneling effects in crossed $1D$ systems in the presence of potential barriers for the massive quasiparticle excitations [7]. Makagon et al. considered a system composed of two layers of crossed quantum wires with interlayer coupling separated by a distance (see Fig.15).

Apart from ballistic approximation, they took into account of the electron-electron interactions in their calculations to study the tunneling properties in different cases such as - free electron case, single crossing of two crossed wires and more general case that include inhomogeneous potential. In the case of single crossing of two crossed wires, they observed that in addition to the scattering states, bound state solutions were possible. The appearance of bound states was due to the presence of tunneling. However, they obtained the bound states energy much smaller than computed numerically by Schult et al.

As reported earlier in a classic paper by Schult et al., corners in the crossed wire system acted as traps which were responsible for the existence of localized states [1]. This feature was further studied by Avishai, Bessis, Giraud and Mantica in the case of open geometries

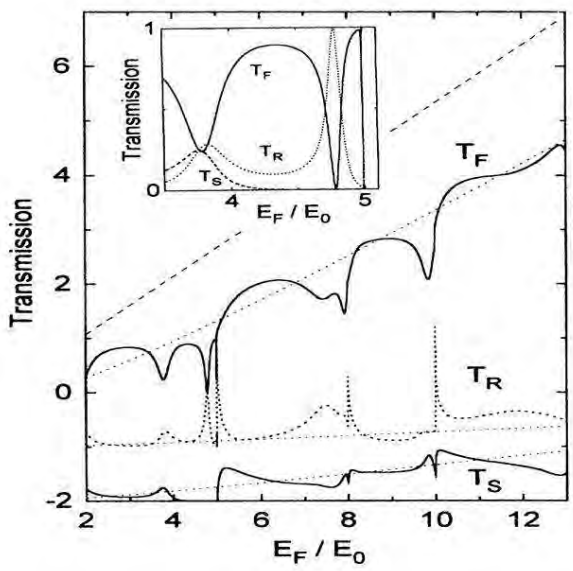

FIG. 13. Transmission probabilities as a function of energy. The thin lines represent the classical transmission probabilities. Figure is courtesy of Takagaki and Ploog [6].

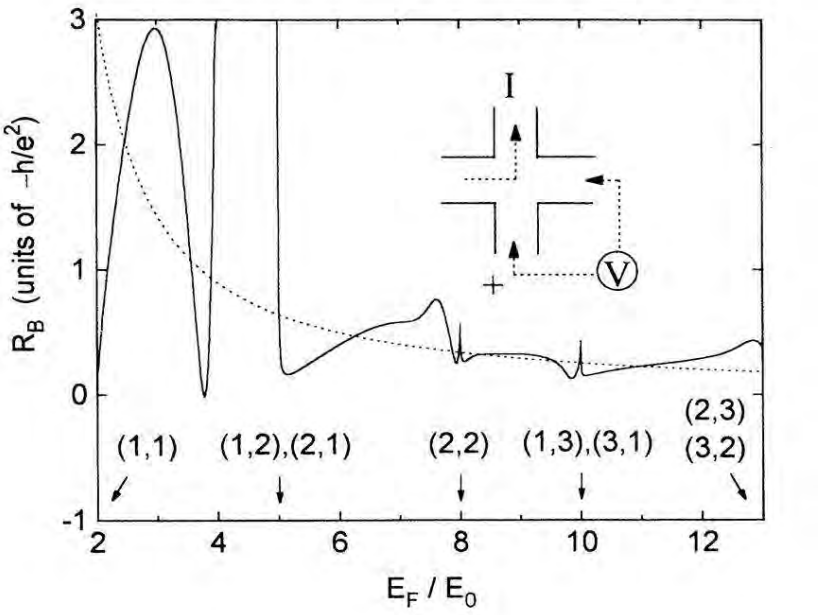

FIG. 14. Bend resistance as a function of energy. The classical of R_B with the zero-point motion correction is represented by dotted line. The arrow indicate the propagation threshold for modes (i, j). The inset illustrate the current and voltage probe configuration. Figure is courtesy of Takagaki and Ploog [6].

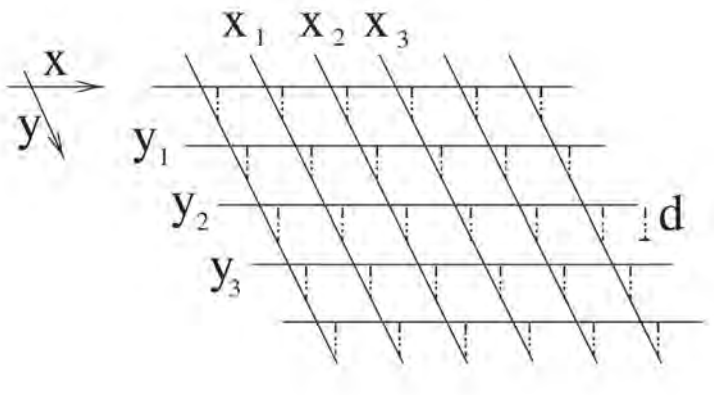

FIG. 15. Two dimensional array of crossed wires separated by a distance d.

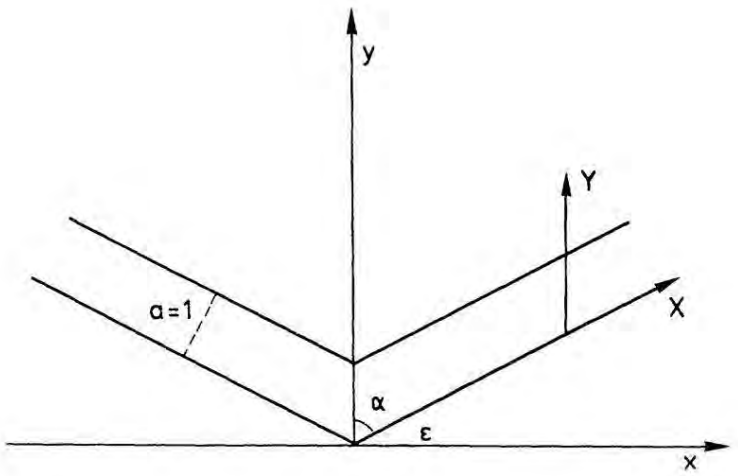

FIG. 16. Geometry used for the existence of a bound state.

[8]. In this paper Avishai et al. reported the problem of quantum bound states in open system with geometrical constraints on free propagation without any explicit potentials. In such case, the Schrödinger equation was reduced to a pure Helmholtz equation with just the kinetic energy operator. The constraints imposed by the boundary conditions on the wave functions were strong enough to generate bound states in a completely open geometries which, classically, do not show any trapped states. They considered two $2D$ semi-infinite wires joined by a sharp angle known as "broken strips" (see Fig.16). They

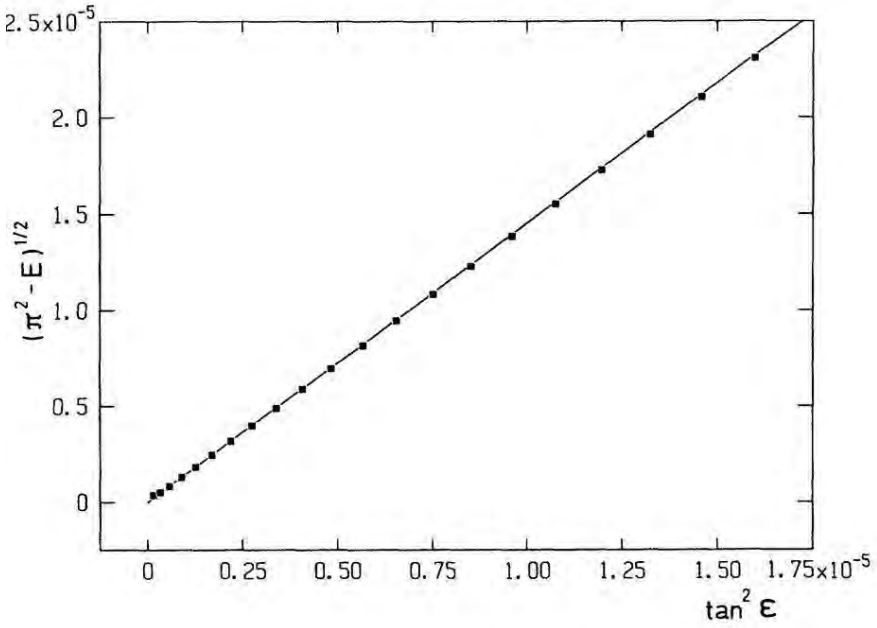

FIG. 17. The linearity of $(\pi^2 - E)^{1/2}$ as a function of $\tan^2 \epsilon$. Figure is courtesy of Avishai et al. [8].

used the variational principle to calculate the energy of an electron in the bent strip. Their result proved the existence of at least one bound state for an arbitrarily small angle and the binding energy was found to be proportional to the fourth power of the sine of the bent angle. They extended their geometry for the case of a crossed wires at right angle and calculated the energy (see Fig.17). They estimated numerically, the upper bound to the ground state energy as $E = 0.94\pi^2$ as compared to the energy $E = 0.92\pi^2$ obtained by Schult et al. and $0.93\pi^2$ by Exner and Seba [9].

In order to apply the phenomenon of quantum bound states, Takagaki and Ploog considered the more realistic situation through atomistic approach to the crossed junction problem [10]. They investigated the quantum transport properties in cross junctions delineated in an anisotropic two dimensional electron gas. They modeled their anisotropic system using square tight-binding lattice with nonidentical nearest-neighbor hopping amplitudes in the direction that are orthogonal to each other. The model they used consisted of a symmetrically shaped crossed junction defined by a square lattice inclined with respect to the anisotropy direction (see figure Fig.18). They assumed that the probabilities of an electron turning into the left-hand-side and right-hand-side leads are different. Hence, they calculated the

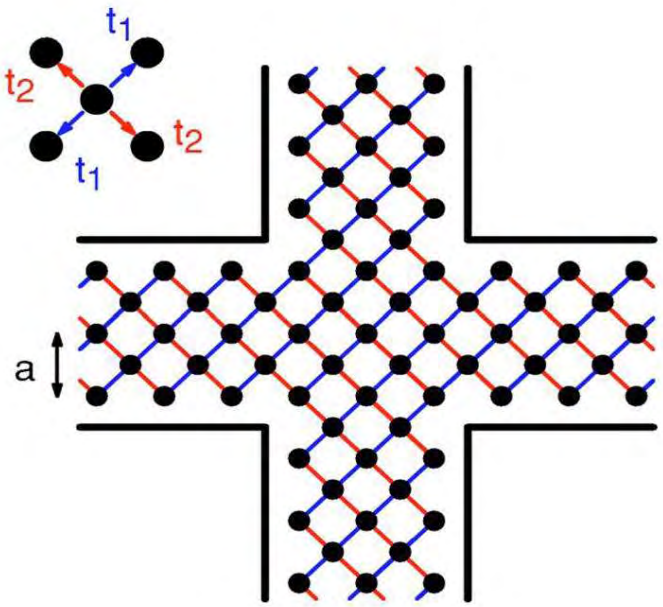

FIG. 18. Geometry for tight-binding model for anisotropic cross junctions when the number of the transverse lattice sites $N = 2$. The solid thick lines indicate boundary of the cross junction. Takagaki and Ploog [10].

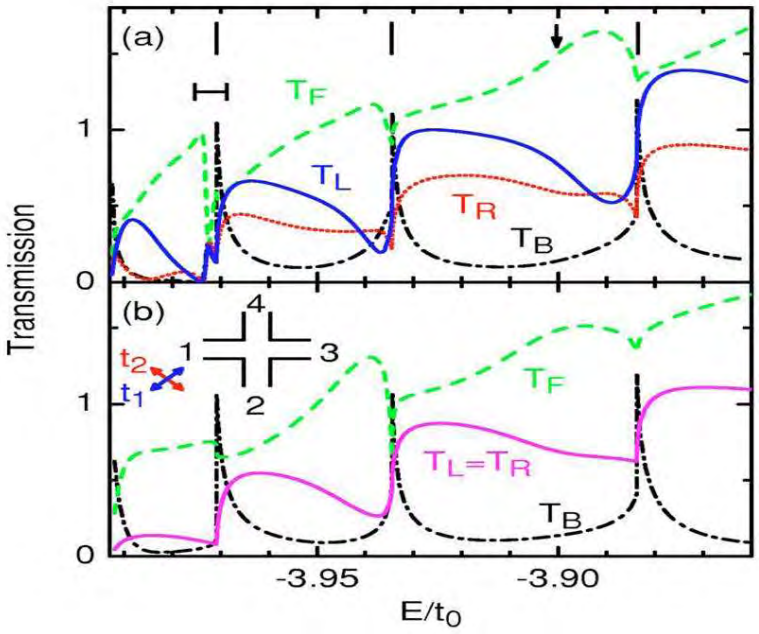

FIG. 19. Energy dependence of transmission probabilities in a symmetrically shaped cross junctions in the absence of magnetic field. Figure is courtesy of Takagaki and Ploog [10].

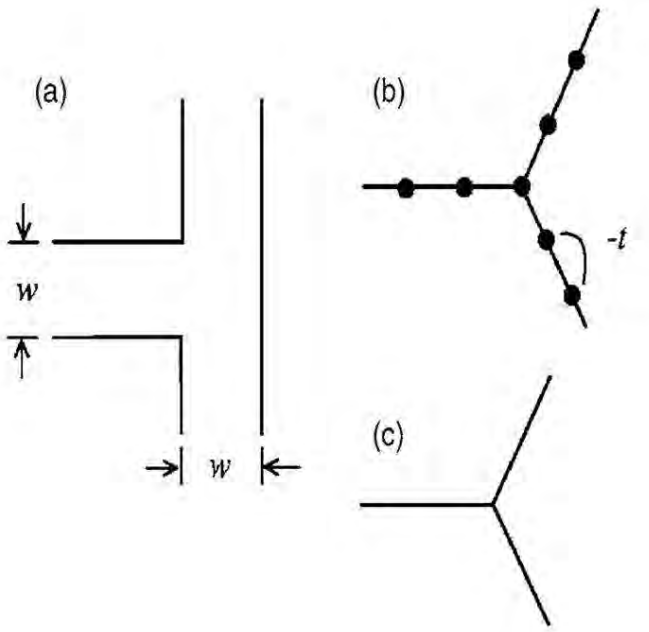

FIG. 20. (a) The original Y junction of Q1D channels considered here, (b)the reformulated Y junction of tight-binding channels, and (c) the effective Y junction of 1D channels affiliated with connection scheme.

transmission probabilities quantum-mechanically using tight-binding model and found that transmission into the right-hand-side lead was larger than that into the left-hand-side lead for lower-lying modes. Takagaki et al. observed that anisotropy played the role of breaking the symmetry of the electronic state and the transport symmetry, giving rise to a transmission resonance through a quasibound state in the cross junction and a finite Hall resistance despite the absence of magnetic field respectively (see Fig.19). The magnitude of Hall resistance was found to depend weakly on the number of occupied subbands in the leads. The most essential features of Hall resistance they observed was switching of the polarity of the Hall resistance associated with the subband thresholds that occurred in the quantum mechanical regime.

The three-leg junction of one dimensional channels (Y junction) have been studied by Voo et al. (see Fig.20). In such geometry, they proposed a scheme to connect the wave function on different one-dimensional ($1D$) branches of the junction [11]. Their model took into account of the difference in the widths of the quasi-one-dimensional ($Q1D$) channels in different systems. They tested their scheme by comparing results from a doubly con-

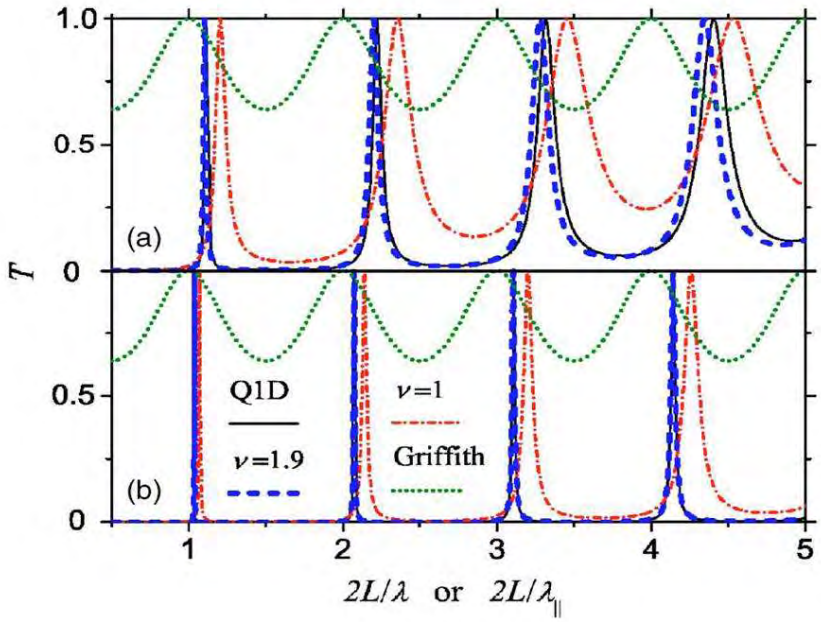

FIG. 21. The transmission probability T is plotted versus the dimensionless longitudinal wave number in the case of quasi-one-dimensional channels and in case one dimensional channels for identical channel widths. Figure is courtesy of Voo et al. [11].

nected one-dimensional system and a related quasi-one-dimensional system. The scheme they suggested may be useful in constructing one-dimensional effective models out of quasi-one-dimensional channels. Voo et al. used tight-binding model to reformulate the two-dimensional Schrödinger equation and imposed the condition of continuity of wave function at the N-leg junction of one dimensional channels. They calculated the transmission probabilities for the $Q1D$ channels and $1D$ channels as a function of the wave number for the case identical legs of the Y junction (see Fig.21). The two results obtained from their model agreed with each other, although the strength of the attractive nature of the Y junction was underestimated.

In summary, the question of the possible existence of quantum bound (trapped, localized) states by special geometry has been a long standing problem in quantum theory. In particular, different geometries of the crossed nanowire intersections explored earlier both in two and three dimensions, have shown the existence of bound states. The ways of observing these states by means of measurement of conductance were proposed theoretically using two dimensional electron gas models. The effects of the external magnetic field on the

cross-wire system were also studied which helps to develop scheme of observing the localized states through the measurement of the quantum Hall resistance. The presence of the bound states at the crossed nanowire intersections greatly affect the electron tunneling properties. Also, quantum bound states are responsible for observed anomaly in the transmission and reflection properties in crossed nanowires systems such as carbon nanotube bundles and films. Many literature sources, till now, looked into the effect of localized states on the electron tunneling behavior for nanowires crossed at right angle, but failed to take into account the dependence of the localized state binding energy on the (*arbitrary*) intersection angle. Hence, the objective of this thesis work is to analyze the angular dependence of the bound state energy for the model system of an electron trapped at the intersection of two identical narrow channels (quantum wires) crossed at an arbitrary angle [12]. When the channels are perpendicular, such a classically unbound system is known to possess a quantum bound state. In what follows, we set up the model for the problem and investigate the angular dependence of the electron bound state energy in the oblique cross-wire system.

II. STATEMENT OF THE PROBLEM

A. Objective

The main objective of the present work is to analyze the angular dependence of the bound state energy for the model system of an electron trapped at the intersection of two identical narrow channels (quantum wires) crossed at an arbitrary angle (see Fig.22). The potential is zero inside the cross-wire system and infinite outside, which is shown by the shaded regions. The shaded (blue) regions represent that these two dimensional region of space is not accessible for an electron. Thus, the motion of an electron is confined within the cross region, the channels of which extend to infinity. The intersection region of the cross-wire system is in general a rhombus of side $2b$ and the width of each nanowires is $2a$. It is well known that when the intersection geometry of the cross-wire system is a square, such a classically unbound system possess a quantum bound state [1]. The motion of a quantum particle,

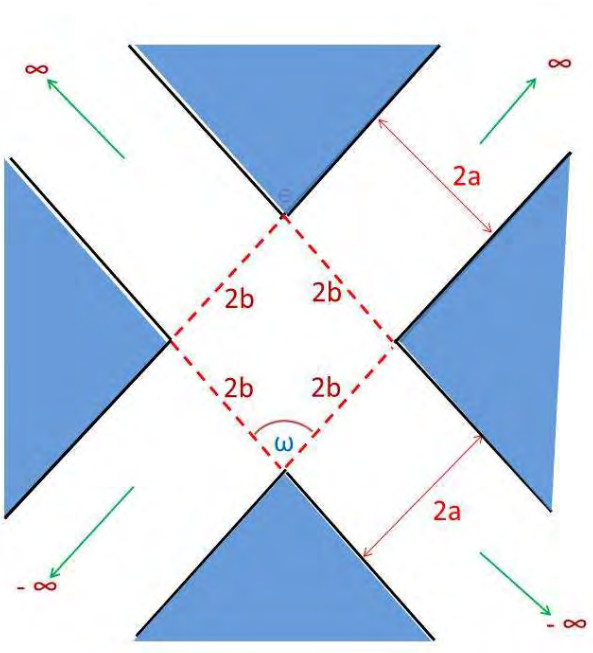

FIG. 22. Nanowires in a skewed geometry. The potential is zero inside the cross-wire system and infinite outside. The shaded (blue) regions represent the regions not accessible for an electron. The motion of an electron is confined within the cross. The intersection region of the cross-wire system is a rhombus of side $2b$, the acute angle between its sides is ω and the width of each nanowires is $2a$.

such as an electron, obeys the Schrodinger equation, as determined by its Hamiltonian. Earlier literature sources (see Chapter I), show that such an electron may either remain localized in a small region of space (a bound state) or diffuse through the entire system (a scattering state). We are particularly interested in two-dimensional crossed nanowires with the condition that they intersect at an arbitrary angle. Previous studies on the cross-wires systems have revealed that an electron in such a system may either be confined within the intersection region in a localized state or decay along the channels of the crossed wires. These quantum bound states are responsible for the observed anomaly in the transmission and reflection properties of crossed nanowires systems. Various methods of observing these states by means of measurement of conductance were also proposed theoretically using two dimensional electron gas models. Furthermore, much work has been done both in two and three dimensional realistic system, finding new approach to observe the effects of the localized states on the optical properties of the material. We extend this knowledge by analyzing the ground states binding energy of an electron in the skewed geometry, which until now have not been studied. Applying variational principle, we investigate conditions for a general criterion for the existence of a bound state and the role of tilted geometry in the bound state energy of an electron. Also, the theory developed in this work might be useful to interpret electron transport peculiarities in realistic systems such as semiconductor nanowire films and carbon nanotube bundles. We assume that our results may have practical applications in the fields of materials science and in the design of quantum information devices. Therefore, the understanding of electron tunneling properties in these cross-wires system is of extreme relevance for device applications. The main objectives of this thesis work can be enumerated as follows:

1. To formulate the problem of cross-wire system in the skewed geometry and to study angular dependence of the bound state energy for an electron trapped at the intersection.

2. Use the results of this model to interpret the electron transport properties in a realistic systems.

In the following section, we describe the procedure to study the cross-wire system in the skewed geometry.

B. Geometry of Nanowires

We consider the coordinate system (x, y) rigidly fixed at the origin $(0, 0)$ which is the center of the crossed nanowires intersection (see figure 23(a)). We define two coordinate systems attached with each nanowires. The coordinate system (x_1, y_1) describes the horizontal channel such that x_1-axis is along the channel and y_1-axis is perpendicular to the channel as shown in the figure 23(b). Similarly, the coordinate system (x_2, y_2) is such that x_2-axis is along the vertical channel . The origin of all the coordinate systems coincides but are different in their orientations and preserve right-handedness. These coordinate systems are related to the original coordinate system by the following transformation relation

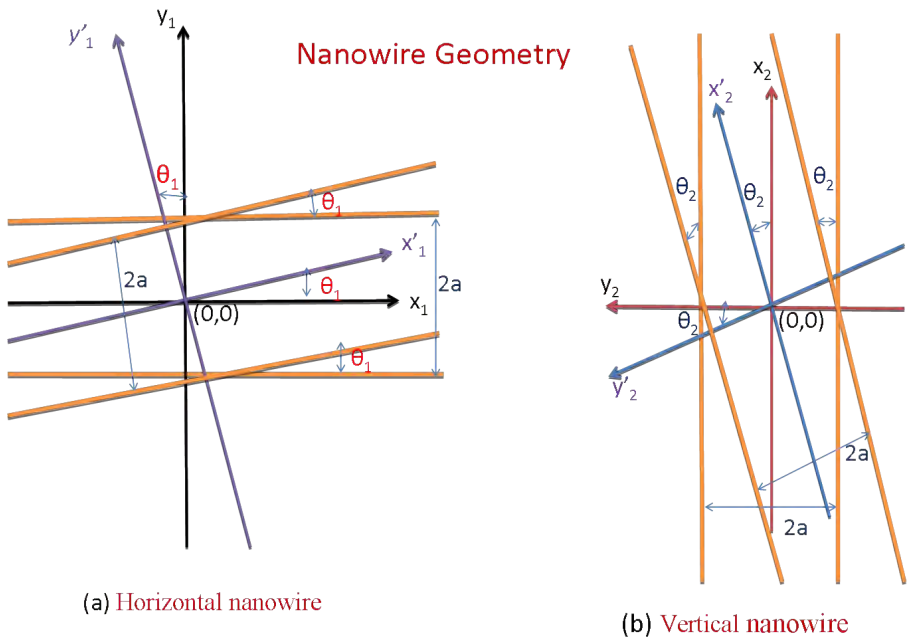

FIG. 23. The diagram (figure is highly exaggerated for clarity) show the coordinate systems used for the X-shaped quantum nanowires. The two nanowires (of equal width $2a$)are shown separately: (a) The coordinate system rigidly fixed to the horizontal nanowire (channel along x-axis) is rotated counterclockwise by an angle θ_1. (b) The coordinate system rigidly fixed to the vertical nanowire (channel along y-axis) is rotated counterclockwise by an angle θ_2.

$$\begin{pmatrix} x_1 \\ y_1 \end{pmatrix} = \begin{bmatrix} 1 & 0 \\ 0 & 1 \end{bmatrix} \begin{pmatrix} x \\ y \end{pmatrix} = \begin{pmatrix} x \\ y \end{pmatrix} \tag{8}$$

and

$$\begin{pmatrix} x_2 \\ y_2 \end{pmatrix} = \begin{bmatrix} 0 & 1 \\ -1 & 0 \end{bmatrix} \begin{pmatrix} x \\ y \end{pmatrix} = \begin{pmatrix} y \\ -x \end{pmatrix} \tag{9}$$

The above transformation relation describes the orientation of the new axes attached to each nanowires relative to the axis fixed at the center of the cross. All of these three coordinate systems are orthogonal. The unit vectors corresponding to direction of the axes of these coordinate systems satisfy

$$\mathbf{x}.\mathbf{y} = \mathbf{x}_1.\mathbf{y}_1 = \mathbf{x}_2.\mathbf{y}_2 = 1 \tag{10}$$

Up to now nothing has been done to the geometry of the crossed nanowires. The configuration is still the same. We describe below a scheme to get the geometry appropriate to our problem. To begin with, the horizontal channel is rotated in counter-clockwise direction by an angle θ_1 with respect to the original coordinate system (x_1, y_1). The coordinate transformation is given by

$$\begin{aligned} \begin{pmatrix} x_1' \\ y_1' \end{pmatrix} &= \begin{bmatrix} \cos\theta_1 & -\sin\theta_1 \\ \sin\theta_1 & \cos\theta_1 \end{bmatrix} \begin{pmatrix} x_1 \\ y_1 \end{pmatrix} \\ &= \begin{bmatrix} \cos\theta_1 & -\sin\theta_1 \\ \sin\theta_1 & \cos\theta_1 \end{bmatrix} \begin{pmatrix} x \\ y \end{pmatrix} \end{aligned} \tag{11}$$

In the next step, we rotate the vertical channel without affecting the horizontal one. Then the coordinate transformation for the rotation of the vertical channel in counter-clockwise direction by an angle θ_2 relative to the original coordinate system (x_2, y_2) is given by

$$\begin{aligned} \begin{pmatrix} x_2' \\ y_2' \end{pmatrix} &= \begin{bmatrix} \cos\theta_2 & -\sin\theta_2 \\ \sin\theta_2 & \cos\theta_2 \end{bmatrix} \begin{pmatrix} x_2 \\ y_2 \end{pmatrix} \\ &= \begin{bmatrix} \cos\theta_2 & -\sin\theta_2 \\ \sin\theta_2 & \cos\theta_2 \end{bmatrix} \begin{pmatrix} y \\ -x \end{pmatrix} \\ &= \begin{bmatrix} \sin\theta_2 & \cos\theta_2 \\ -\cos\theta_2 & \sin\theta_2 \end{bmatrix} \begin{pmatrix} x \\ y \end{pmatrix} \end{aligned} \tag{12}$$

It is clear from the above transformation that

$$x_1' = x\cos\theta_1 - y\sin\theta_1, \quad y_1' = x\sin\theta_1 + y\cos\theta_1 \tag{13}$$

$$x_2' = x\sin\theta_2 + y\cos\theta_2, \quad y_2' = -x\cos\theta_2 + y\sin\theta_2 \tag{14}$$

Now, we have two choices to select the new coordinate system. For the present configuration, we take (x_1', x_2') as the new basis with the axes along x_1' and x_2' direction which we relabel them by x' and y' respectively. Hence, the nanowires intersection geometry referred to the

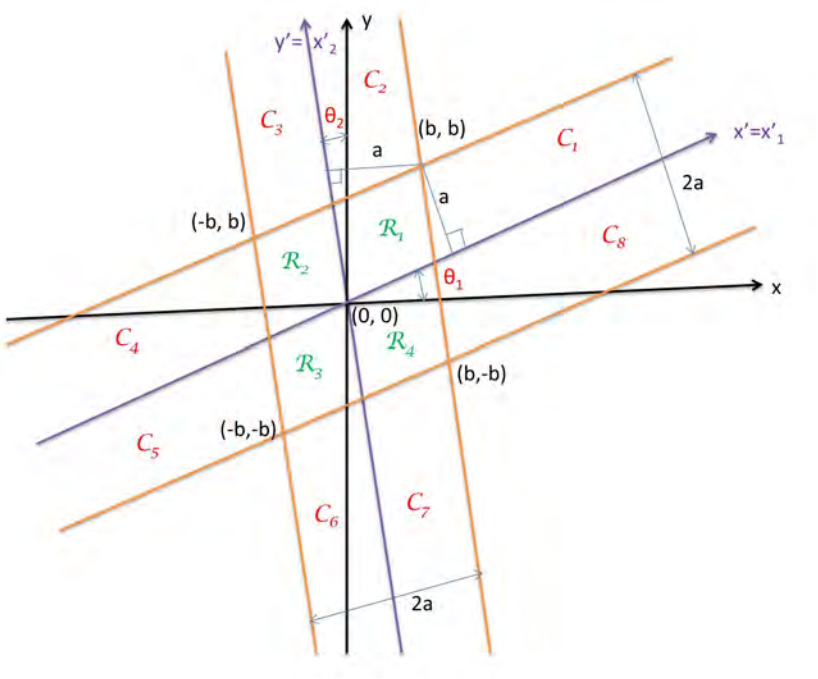

FIG. 24. The figure shows the intersection geometry of two nanowires after two successive orthogonal transformations. The intersection region is a rhombus of side $2b$. The width $(2a)$ of the nanowires remains constant in the new geometry.

new coordinate system (x_1', x_2') is a rhombus (see figure 24). The corners of this rhombus are related to the width of the channel and the angle between the axes. The new and the final coordinate system (x', y') is related to the original system through the following transformation formula

$$\begin{pmatrix} x' \\ y' \end{pmatrix} = \begin{pmatrix} x_1' \\ x_2' \end{pmatrix} = \begin{bmatrix} \cos\theta_1 & -\sin\theta_1 \\ \sin\theta_2 & \cos\theta_2 \end{bmatrix} \begin{pmatrix} x \\ y \end{pmatrix} \tag{15}$$

The determinant of the transformation matrix from the unprimed to the primed set is given by

$$\Delta = \begin{vmatrix} \cos\theta_1 & -\sin\theta_1 \\ \sin\theta_2 & \cos\theta_2 \end{vmatrix}$$

$$= \cos\theta_1 \cos\theta_2 + \sin\theta_1 \sin\theta_2$$
$$= \cos(\theta_1 - \theta_2) = \cos\theta \tag{16}$$

The angular difference $\theta = (\theta_1 - \theta_2)$ gives the angle by which one nanowire is rotated with respect to the other. In other words, this is the measure of asymmetry of the crossed nanowires as shown in the figure 24. If two wires are rotated such that $\theta_1 = \theta_2$ then they intersect symmetrically at right angle. If however the condition $\theta_1 - \theta_2 = \pi/2$ is satisfied, then the two wires completely overlap and form a single wire. The inverse transformation from the primed system to the unprimed system is given by the following transformation relation:

$$\begin{pmatrix} x \\ y \end{pmatrix} = \frac{1}{\Delta} \begin{bmatrix} \cos\theta_2 & \sin\theta_1 \\ -\sin\theta_2 & \cos\theta_1 \end{bmatrix} \begin{pmatrix} x' \\ y' \end{pmatrix} \tag{17}$$

The Jacobian of the transformation from the unprimed to the primed set is given by

$$\begin{aligned} J\left(\frac{x,y}{x',y'}\right) = \frac{\partial(x,y)}{\partial(x',y')} &= \begin{vmatrix} \frac{\partial x}{\partial x'} & \frac{\partial x}{\partial y'} \\ \frac{\partial y}{\partial x'} & \frac{\partial y}{\partial y'} \end{vmatrix} \\ &= \begin{vmatrix} \cos\theta_2/\Delta & sin\theta_1/\Delta \\ -\sin\theta_2/\Delta & \cos\theta_1/\Delta \end{vmatrix} \\ &= \frac{1}{\Delta^2} \begin{vmatrix} \cos\theta_2 & \sin\theta_1 \\ -\sin\theta_2 & \cos\theta_1 \end{vmatrix} \\ &= \frac{1}{\Delta^2} (\cos\theta_1 \cos\theta_2 + \sin\theta_1 \sin\theta_2) \\ &= \frac{1}{\Delta^2} \cos(\theta_1 - \theta_2) = \frac{1}{\Delta^2} (\Delta) = \frac{1}{\Delta} = \sec\theta \end{aligned} \tag{18}$$

The first and second partial derivatives transform from the unprimed coordinates system to the primed set as

$$\begin{aligned} \frac{\partial}{\partial x} &\equiv \frac{\partial x'}{\partial x}\frac{\partial}{\partial x'} + \frac{\partial y'}{\partial x}\frac{\partial}{\partial y'} \equiv \cos\theta_1 \frac{\partial}{\partial x'} + \sin\theta_2 \frac{\partial}{\partial x'} \\ \frac{\partial^2}{\partial x^2} &\equiv \cos^2\theta_1 \frac{\partial^2}{\partial x'^2} + \sin^2\theta_2 \frac{\partial^2}{\partial y'^2} + 2\cos\theta_1 \sin\theta_2 \frac{\partial^2}{\partial x' \partial y'} \\ \frac{\partial}{\partial y} &\equiv \frac{\partial x'}{\partial y}\frac{\partial}{\partial x'} + \frac{\partial y'}{\partial y}\frac{\partial}{\partial y'} \equiv -\sin\theta_1 \frac{\partial}{\partial x'} + \cos\theta_2 \frac{\partial}{\partial y'} \\ \frac{\partial^2}{\partial y^2} &\equiv \sin^2\theta_1 \frac{\partial^2}{\partial x'^2} + \cos^2\theta_2 \frac{\partial^2}{\partial y'^2} - 2\sin\theta_1 \cos\theta_2 \frac{\partial^2}{\partial x' \partial y'} \end{aligned}$$

The 2D Laplacian operator in the new coordinates system becomes

$$\nabla^2 \equiv \frac{\partial^2}{\partial x'^2} + \frac{\partial^2}{\partial y'^2} - 2\,\sin(\theta_1 - \theta_2)\frac{\partial^2}{\partial x'\partial y'} \equiv \nabla'^2 - 2\,\sin\theta\frac{\partial^2}{\partial x'\partial y'} \tag{19}$$

The Hamiltonian operator in the new coordinate system becomes

$$\hat{H} \equiv \frac{-\hbar^2}{2m}\left(\nabla'^2 - 2\,\sin\theta\frac{\partial^2}{\partial x'\partial y'}\right) \tag{20}$$

We consider that the electron is constrained by the potential which is zero inside the channels and infinite outside which is given by

$$\begin{aligned} V(x', y') = 0 \quad &\text{for} \quad |x'| \leq b \quad or \quad |y'| \leq b \\ = \infty \quad &\text{elsewhere} \end{aligned}$$

Our task is to solve the free particle Schrödinger equation for an electron subject to the above potential.

$$\left(\nabla'^2 - 2\,\sin\theta\frac{\partial^2}{\partial x'\partial y'} + \frac{2\,m\,E}{\hbar^2}\right)\Phi(x', y') = 0 \tag{21}$$

This equation clearly describe the behavior of an electron in a two dimensional asymmetric crossed nanowires in new geometry. We take $\theta_1 > \theta_2$ so that $\sin\theta$ is positive. Here, the width of the nanowire channels remain constant. This is the unique problem where there is change in the angle of the intersection of the cross-wire system without any variation in the width. Paranjape calculated the ground-state energy of an electron trapped at the intersection of a cross formed by two quantum wires where the widths of the wires forming the cross were assumed to vary independently [13]. He studied the variation in the energy with the ratio of the widths and observed that the energy decreases as one of the widths is allowed to increase. But our model is based on the angular variation rather than the size of the channels. In what follows, we discuss the approach used to formulate the problem.

C. Method and Assumption

1. Method

The approach used here to study the oblique crossed wires system is based on the variational principle. This is also known as Rayleigh-Ritz variational method which gives a more accurate estimate of the ground state energy than the perturbation theory. It is the non-perturbative method to the approximate calculations of eigenvalues [14]. In what follows, we give a sketch of this method itself [15]. The Schrödinger equation can be derived from the variational principle, which requires that

$$J = \langle\phi|\hat{H}|\phi\rangle \tag{22}$$

is stationary with respect to the independent variation of ϕ and ϕ^* subject to the normalization condition .

$$\langle\phi|\phi\rangle = 1 \tag{23}$$

Using the method of Lagrange multiplier, we construct a function given by

$$J(\varepsilon) = \langle\phi|\hat{H}|\phi\rangle - \varepsilon\langle\phi|\phi\rangle \tag{24}$$

where ε is the undetermined multiplier. The requirement for the function $J(\varepsilon)$ to be stationary leads to

$$\begin{aligned} \delta J(\varepsilon) &= 0 \\ \langle\delta\phi|\hat{H} - \varepsilon|\phi\rangle + \langle\phi|\hat{H} - \varepsilon|\delta\phi\rangle &= 0 \end{aligned} \tag{25}$$

One should be cautious in putting each term in the above equation equal to zero because the variations $\langle\delta\phi|$ and $|\delta\phi\rangle$ are not independent. In general, we consider

$$\delta\phi = \delta u + i\delta v \tag{26}$$

where δu and δv are arbitrary real and independent variations. Then we get,

$$\begin{aligned} \delta J(\varepsilon) &= \langle\delta u|\hat{H} - \varepsilon|\phi\rangle + \langle\phi|\hat{H} - \varepsilon|\delta u\rangle + \langle i\delta v|\hat{H} - \varepsilon|\phi\rangle + \langle\phi|\hat{H} - \varepsilon|i\delta v\rangle \\ &= \langle\delta u|\hat{H} - \varepsilon|\phi + \phi^*\rangle - i\langle\delta v|\hat{H} - \varepsilon|\phi - \phi^*\rangle \end{aligned} \tag{27}$$

For arbitrary δu and δv, one can write

$$\begin{aligned}\left(\hat{H}-\varepsilon\right)|\phi+\phi^*\rangle &= 0\\ \left(\hat{H}-\varepsilon\right)|\phi-\phi^*\rangle &= 0\end{aligned} \tag{28}$$

On adding and subtracting these equation, one get

$$\begin{aligned}\left(\hat{H}-\varepsilon\right)|\phi\rangle &= 0\\ \left(\hat{H}-\varepsilon\right)|\phi^*\rangle = \langle\phi|\left(\hat{H}-\varepsilon\right) &= 0\end{aligned} \tag{29}$$

This is equivalent to equating each term in earlier equation to zero. Thus, ε has the significance of real eigenvalue of $\hat{H}$, which is given by

$$\begin{aligned}\hat{H}|\phi\rangle = \varepsilon|\phi\rangle, \quad \hat{H}|\phi^*\rangle &= \varepsilon|\phi^*\rangle\\ \varepsilon = \frac{\langle\phi|\hat{H}|\phi\rangle}{\langle\phi|\phi\rangle} &= \langle\phi|\hat{H}|\phi\rangle = E\end{aligned} \tag{30}$$

Thus, the variational principle leads to a Schrödinger equation. This means that the solution of variational problem is any solution to the time independent Schrödinger equation. In other words, if any variation is allowed

$$\delta\langle\phi|\hat{H}|\phi\rangle = 0 \tag{31}$$

is equivalent to

$$\hat{H}|\phi\rangle = E|\phi\rangle \tag{32}$$

Suppose E is defined as above. Let E_m and ϕ_m be an eigenvalue and the corresponding eigenstate of $\hat{H}$, respectively. Then

$$\begin{aligned}\delta E &= E - E_m\\ &= \langle\phi|\hat{H}|\phi\rangle - E_m\\ &= \langle\phi|\hat{H}|\phi\rangle - \langle\phi|\phi\rangle E_m\\ &= \langle\phi|\hat{H}-E_m|\phi\rangle\end{aligned} \tag{33}$$

If ϕ and ϕ_m differ by $\delta\phi$, that is

$$\phi = \phi_m + \delta\phi \tag{34}$$

Then the variation in energy δE becomes

$$\delta E = \langle \delta\phi | \hat{H} - E_m | \delta\phi \rangle + O\left((\delta\phi)^2\right) \tag{35}$$

It means that to the first order of approximation,

$$\delta E = 0 \tag{36}$$

This is variational principle. Thus, the best approximation to E_m is obtained by varying ϕ, or the parameters on which it depends so that above relation is obeyed. The Hamiltonian operator $\hat{H}$ which is hermitian, generates a complete orthonormal set of eigenfunctions:

$$\hat{H}|\phi_m\rangle = E|\phi_m\rangle, \qquad \langle \phi_m | \phi_n \rangle = \delta_{mn} \tag{37}$$

We now expand the the trial function ϕ in terms of complete orthonormal set of eigenfunctions

$$\phi = \sum_m a_m \phi_m \tag{38}$$

The energy or the expectation value of the Hamiltonian is given by

$$\begin{aligned} E = \langle \phi | \hat{H} | \phi \rangle &= \sum_{m,n} \langle a_m \phi_m | \hat{H} | a_n \phi_n \rangle \\ &= \sum_{m,n} a_m^* a_n E_n \delta_{mn} = \sum_m |a_m|^2 E_m \end{aligned} \tag{39}$$

and

$$1 = \langle \phi | \phi \rangle = \sum_{m,n} a_m^* a_n \langle \phi_m | \phi_n \rangle = \sum_{m,n} a_m^* a_n \delta_{mn} = \sum_m |a_m|^2 \tag{40}$$

If E_0 is the lowest energy among the spectrum E_m, then we have

$$\begin{aligned} E &\geq E_0 \sum_m |a_m|^2 \\ \text{Therefore,} \quad E &\geq E_0 \end{aligned} \tag{41}$$

In order to obtain a upper bound for some k^{th} level E_k of the spectrum, we select a ϕ which is orthogonal to the eigenfunctions $\phi_0, \phi_1, ..., \phi_{k-1}$ for all the lower levels. Then the coefficients $a_1, a_2....., a_{k-1}$ are all zero. The lowest energy which now occurs for E is E_k. It follows that $E \geq E_k$.

In atomic and molecular physics, most methods for finding the energy levels are variational schemes [16]. The Hartree method of self-consistent fields which is one of the ways

to find the central field is the generalization of the variational principle. In many-electron atoms, the trial function ϕ is expressed as a linear combination of known functions u_i as

$$\phi = \sum_{i=1}^{r} c_i u_i \tag{42}$$

where $c_i's$ are the variational parameters. The functions u_i are not necessarily orthogonal so that we have the non-zero overlap integral given by

$$S_{ij} = \langle u_i | u_j \rangle \tag{43}$$

The expectation value of energy E for the above choice of the trial function is given by

$$\begin{aligned} E &= \frac{\langle \phi | \hat{H} | \phi \rangle}{\langle \phi | \phi \rangle} \\ E &= \frac{\sum_{ij} c_i^* c_j H_{ij}}{\sum_{ij} c_i^* c_j S_{ij}} \\ E \sum_{ij} c_i^* c_j S_{ij} &= \sum_{ij} c_i^* c_j H_{ij} \end{aligned} \tag{44}$$

where $H_{ij} = \langle u_i | \hat{H} | u_j \rangle$.

Differentiating both sides with respect to one of the coefficients, say c_k^*, we get

$$\frac{\partial E}{\partial c_k^*} \sum_{ij} c_i^* c_j S_{ij} + E \sum_{j} c_j S_{kj} = \sum_{j} c_j H_{kj} \tag{45}$$

The minimum energy E is obtained by putting

$$\frac{\partial E}{\partial c_k^*} = 0$$

or

$$\sum_{i=1}^{r} c_j \left(H_{kj} - E S_{kj} \right) = 0, \qquad k = 1, 2....., r \tag{46}$$

The corresponding secular equation is

$$\begin{vmatrix} H_{11} - E S_{11} & ... & H_{1r} - E S_{1r} \\ ... & ... & ... \\ H_{r1} - E S_{r1} & ... & H_{rr} - E S_{rr} \end{vmatrix} = 0 \tag{47}$$

Hence, with the given choice of the trial functions the matrix elements H_{ij} of the Hamiltonian and the overlap integrals S_{ij} are evaluated. If an orthonormal basis is used, the above secular

equation is greatly simplified because $S_{ij} = \delta_{ij}$. In this case, the secular determinant becomes

$$\begin{vmatrix} H_{11} - E & ... & H_{1r} - E \\ ... & ... & ... \\ H_{r1} - E & ... & H_{rr} - E \end{vmatrix} = 0 \tag{48}$$

In either case, the secular determinant for r basis functions give rth order polynomial in E which is solved for r different roots, each of which approximates a different eigenvalue. The r roots are the possible values of E, the lowest one being an upper bound to the ground state energy of the molecular system. The variational method is a basis for Hartree-Fock theory and the configuration interaction method used in the electronic structure of atoms and molecules.

In the variational method, a fixed $\hat{H}$ is taken and it can be shown how the matrix element of $\hat{H}$ varies as the trial function is modified. There is a theorem after Hellmann and Feynmann which shows how the energy of a system varies when the Hamiltonian $\hat{H}$, which depends on a parameter β, changes, i.e.,

$$\frac{\partial E}{\partial \beta} = \langle \frac{\partial \hat{H}}{\partial \beta} \rangle \tag{49}$$

The significance of this theorem is that the operator $\frac{\partial \hat{H}}{\partial \beta}$ may be simple in its form. As an example, if $\hat{H} = \hat{H}_0 + \beta x$, then $\frac{\partial \hat{H}}{\partial \beta} = x$, which does not involve $\hat{H}_0$, the unperturbed Hamiltonian. Hence, using trusted trial functions $\frac{\partial \hat{H}}{\partial \beta}$ can be evaluated from which we obtain the energy eigenvalues of the system.

In practice, if we have a trial function ϕ as a function of some variational parameter α, then the expectation value of the Hamiltonian is given by

$$\langle \hat{H}(\alpha) \rangle = \frac{\langle \phi(\mathbf{r}, \alpha) | \hat{H} | \phi(\mathbf{r}, \alpha) \rangle}{\langle \phi(\mathbf{r}, \alpha) | \phi(\mathbf{r}, \alpha) \rangle} \tag{50}$$

The ground state energy is equal to the value of this ratio evaluated using variational parameter (α) that minimizes this ratio. It just involves the evaluation of two integrals without having to solve any differential equation. The variation theorem states that $E \geq E_0$ for any trial function ϕ. The equality holds if the trial function ϕ is the true ground state wave function. A trial function is set up in a flexible form in terms of parameters making a guess. Its parameters are varied to reduce the trial energy E to its lowest value possible. The result

is an upper bound to the ground state energy. The energy approaches the true ground state energy from the top. This means that the energy obtained from the variational method is always above the true ground state energy.

2. Assumption

We assume that the shape of the potential which confines the electron to the channel is not significant in determining the existence of bound state at the intersection of the two wires [1]. This is because only the corners are responsible for the existence of bound state [9]. It has been proved that in a single straight channel bound state does not exist due to absence of corners and bents. Thus, the potential has nothing to do with the electron confinement. In general, potential can be taken to be constant, harmonic oscillator type (parabolic) or any complex function. Hence, it is sufficient to take the potential to be zero within the rhombus region and the semi-infinite channels. The region outside the cross-wire system is inaccessible to an electron as the walls does not allow tunneling. The walls are rigid and impenetrable. We choose proper trial functions and use riational principle to find the upper bound to the ground state energy of the system. The electron is constrained in a X-shaped channels in the primed coordinate, so the trial wave functions are taken as

$$\Phi(x',y') = A\begin{cases} \left(1-\frac{|x'y'|}{b^2}\right)e^{-\alpha} & \text{for} \quad |x'|\leq b,\ |y'|\leq b \\ \left(1-\frac{|y'|}{b}\right)e^{-\frac{\alpha\,|x'|}{b}} & \text{for} \quad |x'|> b,\ |y'|\leq b \\ \left(1-\frac{|x'|}{b}\right)e^{-\frac{\alpha\,|y'|}{b}} & \text{for} \quad |y'|> b,\ |x'|\leq b \\ 0 & \text{otherwise} \end{cases} \tag{51}$$

where A is the normalization constant which may depend on the variational parameter (α) and also on the asymmetry of the wires. These trial functions are such that they vanish outside the rhombus of side $2b$. The origin of the coordinate system (x', y') is taken at the center of the rhombus. The region of localization is a rhombus with the corners at ($\pm b$,$\pm b$), where $b\,\Delta = a$ and $w = 2a$ is the constant width of the nanowires as shown in figure 24. For simplicity, we write the relative rotation and the Jacobian respectively as

$$\theta_1 - \theta_2 = \theta \quad \textit{and} \quad \Delta^{-1} = \sec\theta$$

In the present work that follows, the above relations have been used extensively to avoid computational complexity.

III. TRIAL FUNCTIONS

A. Trial functions for the skewed cross-wire geometry

The shape of the potential is insignificant in determining the bound states in the cross-wire system. The potential is zero within the two dimensional channel and infinite outside it. The electron is located inside the crossed intersection with both channels extending to infinity. An electron is in the region of zero potential so that no external force act on it. It has total energy only due to its two components of momentum (horizontal and the transverse component). It will be clear later in the chapter that when an electron is inside the channel far away from the cross region, the corresponding transverse component of the momentum is quantized. This is a typical property of a quantum wire. This feature drastically changes within the region of intersection of two identical wires. The crossed intersection behaves as two dimensional potential well. The electron can be trapped and bound to the crossed region without any further decay into the continuum of the channel. The electron is locally bound in the crossed wires which is inherently quantum in origin. The trapped state manifest itself as quantum dot in two dimension. The size of quantum dot is determined by the area of intersection and the nature of the corners (sharp edge or rounded). The trial functions is selected making a guess and satisfying some conditions. The trial functions within the intersection region form a roof with rooflines and falls exponentially just outside the rhombus.

$$\Phi(x',y') = A \begin{cases} \left(1-\frac{|x'y'|}{b^2}\right) e^{-\alpha} & \text{for} \quad |x'| \leq b,\ |y'| \leq b \\ \left(1-\frac{|y'|}{b}\right) e^{-\frac{\alpha\,|x'|}{b}} & \text{for} \quad |x'| > b,\ |y'| \leq b \\ \left(1-\frac{|x'|}{b}\right) e^{-\frac{\alpha\,|y'|}{b}} & \text{for} \quad |y'| > b,\ |x'| \leq b \\ 0 & \text{otherwise} \end{cases} \tag{52}$$

where A is the normalization constant which may depend on the variational parameter (α) and also on the asymmetry of the wires. These trial functions are such that they vanish outside the rhombus of side $2b$. The coordinate system (x', y') is taken at the center of the rhombus. The region of localization is a rhombus with the corners at ($\pm b$,$\pm b$), where $b\Delta = a$ and $w = 2a$ is the constant width of the nanowires as shown in the figure 24. Using the coordinate transformation from Chapter 2, the three dimensional plots for typical values of rotation angles (θ) such as $0°, 30°, 45°, 60°$ and $90°$ are neatly displayed. These plots show the behavior of trial functions used in the calculations.

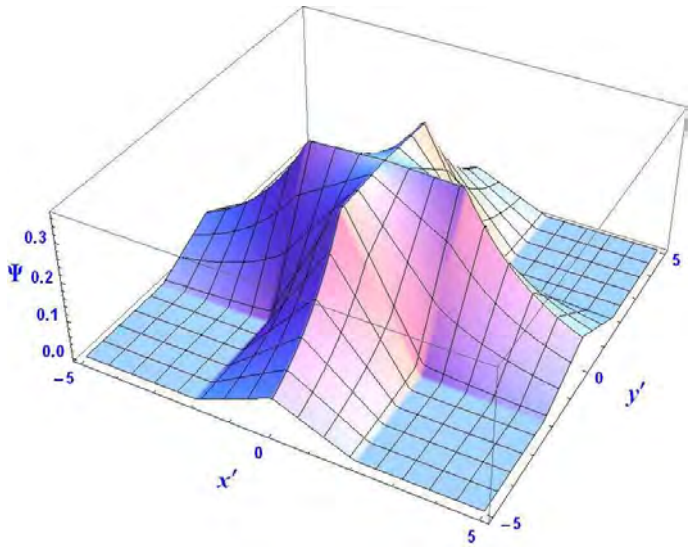

FIG. 25. Trial function for crossed wire system without any rotation ($\theta = 0$), the wires intersect at right angle.

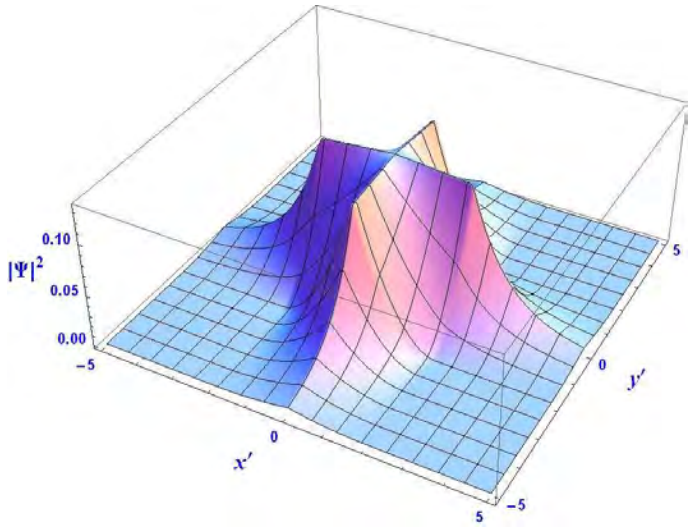

FIG. 26. Probability density for crossed wire system without any rotation ($\theta = 0$), the wires intersect at right angle.

Figure 25 shows the trial function without any rotation of the crossed wire system. These wires intersect at right angle and the region of intersection is a square geometry. The rooflines cross each other at right angle. This configuration has the trial functions decaying exponentially along the channels of the cross and vanishing abruptly at the corners. This feature is more clear from the probability density plot [Fig.26]. The spatial extend of the trial wave function is localized well inside the intersection region and also the probability

density is sharply peaked. This feature make the system more likely to be stable and in fact it is the most stable state.

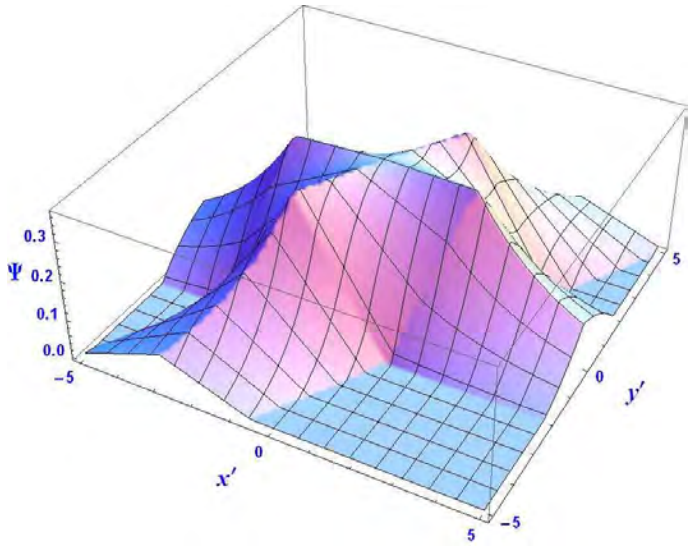

FIG. 27. Trial function for rotation of the axes by angle $\theta = \pi/6$.

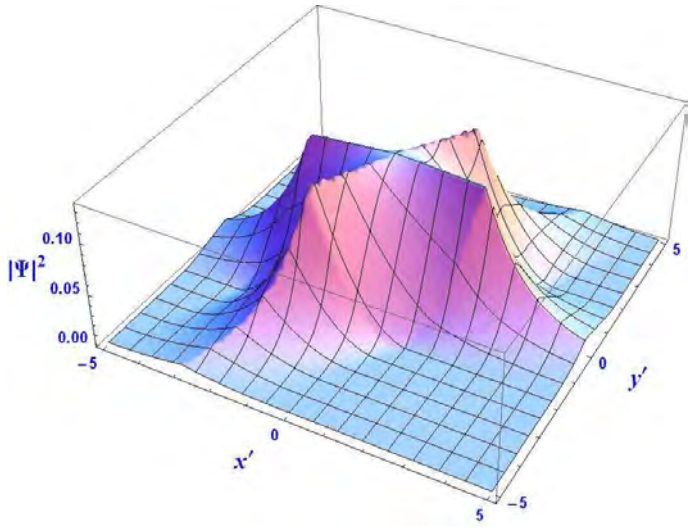

FIG. 28. Probability density for rotation of the axes by angle $\theta = \pi/6$.

Figure [Fig.27] shows the plot of trial function for the crossed wires in which one of the wires is rotated by 30°. These wires intersect at an angle of 60° and the region of intersection is a rhombus. The rooflines cross each other at an angle 60°. This configuration has the trial functions decaying exponentially along the channels of the cross and vanishing at the corners. This feature is more clear from the probability density plot [Fig.28]. The spatial extend of the trial wave function is little bit broaden outside of the intersection region and

also the probability density is less sharply peaked. The system is still stable and not like that of the unperturbed geometry.

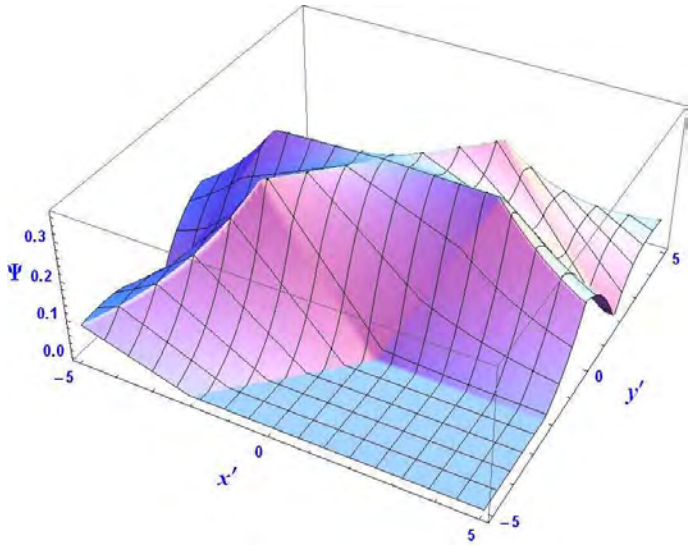

FIG. 29. Trial function for rotation of the axes by angle $\theta = \pi/4$.

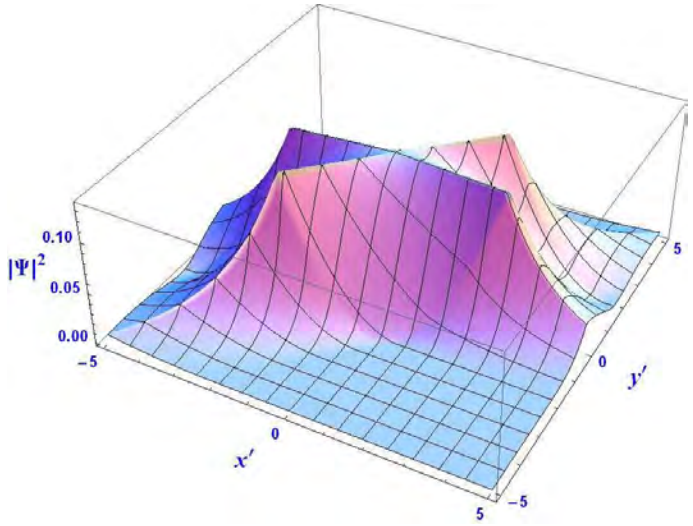

FIG. 30. Probability density for rotation of the axes by angle $\theta = \pi/4$.

Figure [Fig.29] shows the plot of trial function for the crossed wires in which one of the wires is rotated by 45°. These wires intersect at an angle of 45° and the region of intersection is a rhombus. The rooflines cross each other at an angle 45°. This configuration has the trial functions decaying exponentially along the channels of the cross and vanishing at the corners. This feature is more clear from the probability density plot [Fig.30]. The spread of the wave function outside the intersection region is more due to electron tunneling and is

less stable but still it is a bound state.

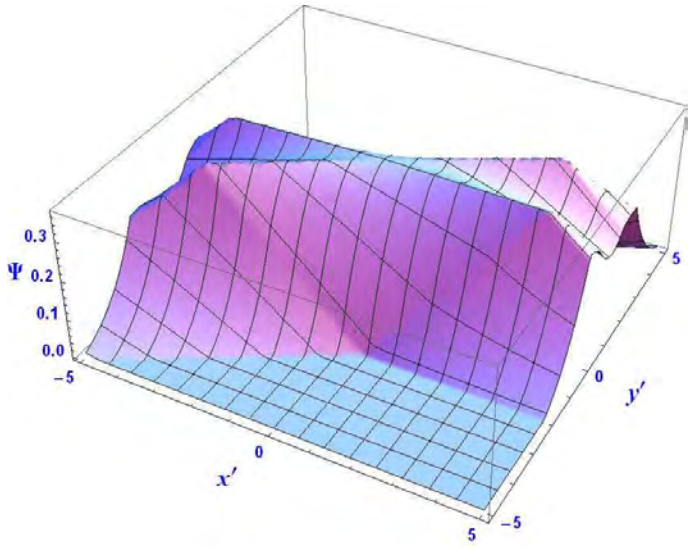

FIG. 31. Trial function for rotation of the axes by angle $\theta = \pi/3$.

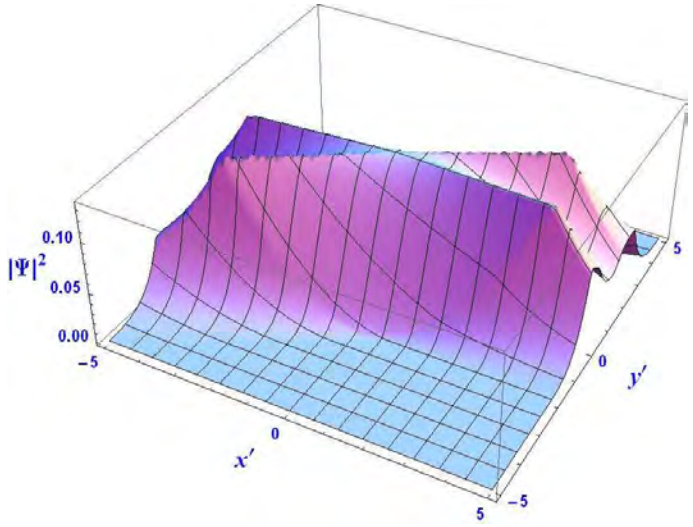

FIG. 32. Probability density for rotation of the axes by angle $\theta = \pi/3$.

Figure [Fig.31] shows the plot of trial function for the crossed wires in which one of the wires is rotated by 60°. These wires intersect at an angle of 30° and the region of intersection is a rhombus. The rooflines cross each other at an angle 30°. This configuration has the trial functions decaying exponentially along the channels of the cross and vanishing at the corners. This feature is more clear from the probability density plot [Fig.32]. The trial wave function is spatially broaden due to electron tunneling and the stability of the system is lowered.

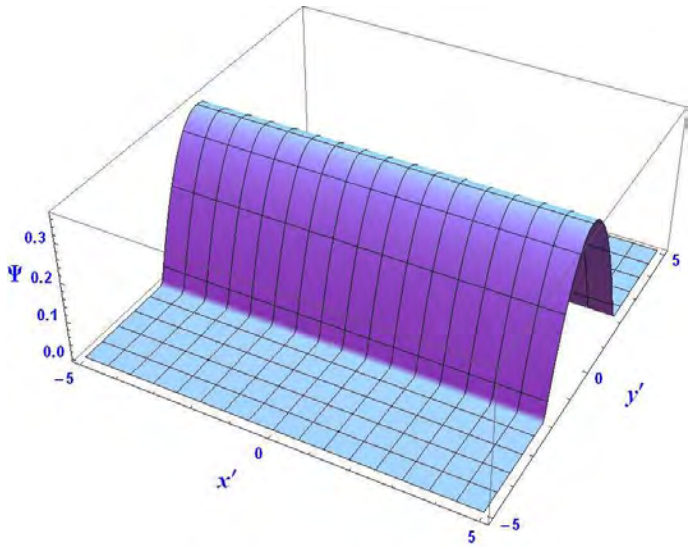

FIG. 33. Trial function for rotation of the axes by angle $\theta = \pi/2$.

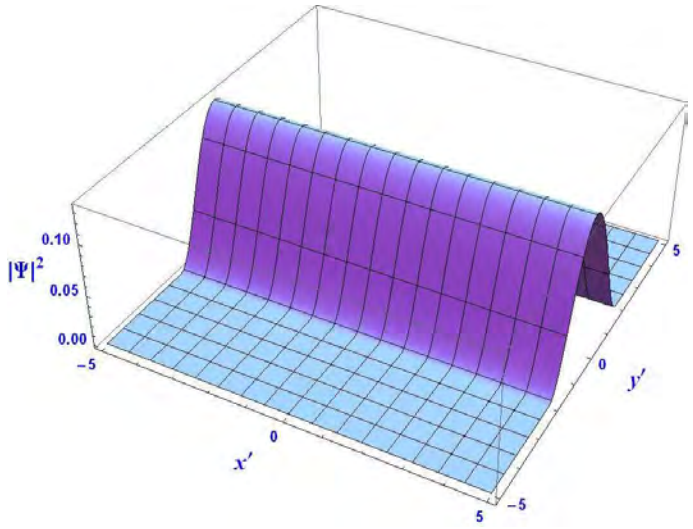

FIG. 34. Probability density for rotation of the axes by angle $\theta = \pi/2$.

Figure [Fig.33] shows the trial function for the crossed wires in which one of the wires is rotated by 90°. These wires merge into a single channel. The two channels completely overlap each other. There are no rooflines. This feature is more clear from the probability density plot [Fig.34]. It will be shown later that this geometry is not favorable to form a quantum bound state. The electron wave function completely spread out along the channels. The probability density show that an electron can exist anywhere along the channel. This is the case of free propagation of an electron along the channels (scattering states).

B. Localization regions of an electron

The electron can be located inside the channel extending to infinity in both direction along x' and y' axes. The geometry of the nanowires intersection is shown in the figure 35. This figure is highly exaggerated so that the different regions can be visualized. Also, evaluation of the normalization constant and the matrix elements of the Hamiltonian requires the regions to be properly specified. It is for this reason, the regions are partitioned accordingly. The intersection region is in general a rhombus with the corners at $(\pm b, \pm b)$. The side of this rhombus is $2b$. The width ($w = 2a$) of the nanowire is same for both the channels. This is because orthogonal transformation to the right-handed coordinate system was used to obtain this oblique geometry which is our model system as discussed in the objective of this work. And under such transformation, width remains invariant. The spatial extend

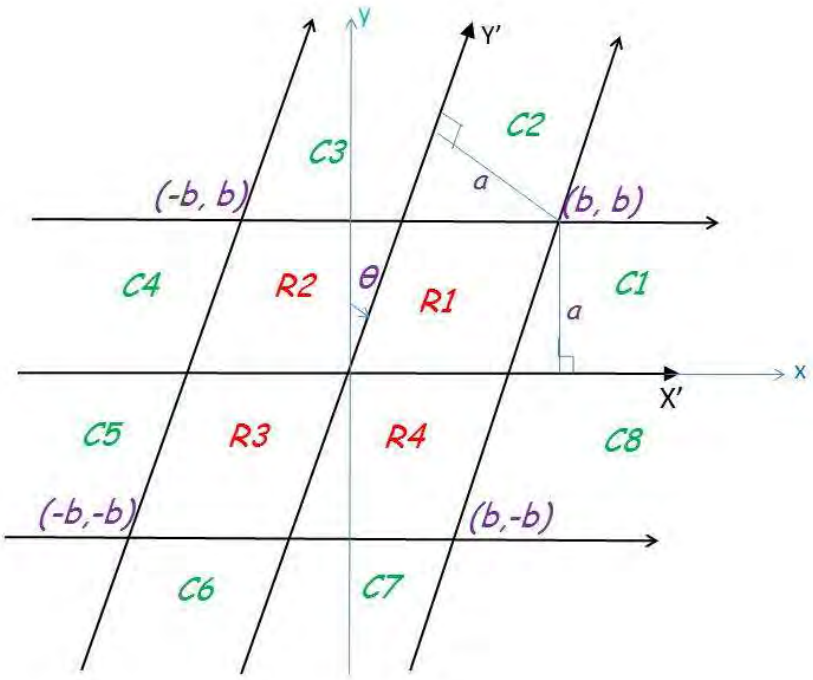

FIG. 35. Localization regions of an electron in the oblique cross-wire system. θ is the angle of rotation of the nanowire and a is the semi-width of the nanowires. The corners of the rhombus are $(\pm b, \pm b)$ referred to the primed coordinate system.

of the wave functions show that the intersection has the greatest probability of electron localization and the probability decreases as we go along the arms of the cross-wire system. In general, there are two regions of localization within the cross-system. The electron may be localized within the intersection region (rhombus) and in the channels. The rhombus can be divided into four parts labeled as R_1, R_2, R_3 and R_4 located in the first, second, third and fourth oblique quadrants respectively. There are four semi-infinite channels in the X-shaped geometry. Each of the four channels (arms) extending to infinity are divided into two portions making eight channels. Hence, there are eight semi-infinite strips labeled as $C_1, ...C_8$. These regions have different geometrical orientation with respect to the origin of the oblique coordinate system. This means that the boundaries in the two dimensional space are different for these regions. The angle θ represent the relative rotation of the channels of the cross-wire system. This fact is clear from the geometry of the nanowires discussed in Chapter II(B). This rotation angle is different from the angle of intersection (ω) of the cross-wire system (see figure 22). In the present work, all the calculations are carried out in terms of the rotation angle θ rather than the angle of the intersection of the cross-wire system (ω).

C. Normalization of the trial functions

To obtain the normalization constant A appearing in the sets of trial functions, the normalization condition in the unprimed coordinate system can be written as

$$\langle \Phi(x,y) | \Phi(x,y) \rangle = \underbrace{\int\int}_{\Omega \in (x,y)} \Phi^*(x,y)\Phi(x,y)dxdy = 1 \tag{53}$$

In the new coordinate system, this condition becomes

$$\underbrace{\int\int}_{\Omega \in (x',y')} \Phi^*(x',y')\Phi(x',y')J\left(\frac{x,y}{x',y'}\right)dx'dy' = 1 \tag{54}$$

where, Ω is the domain of integration.

In practice, it is not required to evaluate the Jacobian for the orthogonal transformation of coordinate system. The Jacobian of the coordinate transformation is a constant (see Eqn.18). Since, variational principle is used, it will appear in both the numerator and denominator of the Rayleigh-Ritz ratio (see Eqn.50), so that it can be ignored. Hence, it is

independent of the coordinate system selected for the calculations as long as the Jacobian is constant. But in the present context, Jacobian is included for convenience even though it does not alter the final result. The integral is evaluated over X-shaped planar regions which represent the two dimensional spatial extend for an electron described by the sets of trials wave functions discussed earlier.

In order to find the normalization constant, we divide the region into four oblique quadrants represented by R_1, R_2, R_3 and R_4 and eight channels labeled as $C_1, C_2, C_3, C_4, C_5, C_6, C_7$ and C_8 as shown in the figure 24. The symmetry of the trial functions in different regions of the nanowire intersection can be used to evaluate these integrals explicitly. In what follows, the steps taken to arrive at the normalization constant will be described for the given sets of trial wave functions. For detailed calculations of the integrals refer to the Appendix I. In order to increase the efficiency of computation, some integrals were evaluated using mathematical handbook [17, 18]. The values of the integrals for the oblique quadrants defined by R_1, R_2, R_3 and R_4 are as follows:

$$R_1 = R_2 = R_3 = R_4 = \frac{11}{18}\, A^2\, b^2\, \sec\theta\, e^{-2\alpha} \tag{55}$$

The total contribution to the normalization integral from the regions R_n is given by

$$\begin{aligned} I_1 &= \sum_{i=1}^{4} R_i = 4\, R_1 \\ &= 4\, \left(\frac{11}{18}\right)\, A^2\, b^2\, \sec\theta\, e^{-2\alpha} \\ &= \frac{22}{9}\, A^2\, b^2\, \sec\theta\, e^{-2\alpha} \end{aligned} \tag{56}$$

and the values of the integrals for eight channels labeled as $C_1, C_2, C_3, C_4, C_5, C_6, C_7$ and C_8 are as follows:

$$C_1 = C_2 = C_3 = C_4 = C_5 = C_6 = C_7 = C_8 = \frac{A^2}{6\alpha}\, b^2\, \sec\theta\, e^{-2\alpha} \tag{57}$$

The total contribution to the normalization integral from the channels C_n is given by

$$\begin{aligned} J_1 &= \sum_{i=1}^{8} C_i = 8\, C_1 \\ &= 8\, \left(\frac{A^2}{6\alpha}\, b^2\, \sec\theta\, e^{-2\alpha}\right) \\ &= \frac{4\, A^2}{3\, \alpha}\, b^2\, \sec\theta\, e^{-2\alpha} \end{aligned} \tag{58}$$

Hence, from the normalization condition, we have

$$\begin{aligned} I_1 + J_1 &= 1 \\ \frac{22}{9}\, A^2\, b^2\, \sec\theta\, e^{-2\alpha} + \frac{4\, A^2}{3\,\alpha}\, b^2\, \sec\theta\, e^{-2\alpha} &= 1 \\ \frac{2\, A^2\, b^2\, \sec\theta\, e^{-2\alpha}}{9\,\alpha}\, (11\alpha + 6) &= 1 \\ A^2 &= \frac{9\,\alpha\, e^{2\alpha}}{2\, b^2\, (11\alpha + 6)\, \sec\theta} \\ A &= \sqrt{\frac{9\,\alpha\, e^{2\alpha}}{2\, b^2\, (11\alpha + 6)\, \sec\theta}} \end{aligned} \tag{59}$$

This is the required normalization constant for the given set of trial functions. The normalized trial functions becomes

$$\Phi(x', y') = \sqrt{\frac{9\,\alpha\, e^{2\alpha}}{2\, b^2\, (11\alpha + 6)\, \sec\theta}} \begin{cases} \left(1 - \frac{|x'y'|}{b^2}\right) e^{-\alpha} & \text{for} \quad |x'| \leq b,\ |y'| \leq b \\ \left(1 - \frac{|y'|}{b}\right) e^{-\frac{\alpha\,|x'|}{b}} & \text{for} \quad |x'| > b,\ |y'| \leq b \\ \left(1 - \frac{|x'|}{b}\right) e^{-\frac{\alpha\,|y'|}{b}} & \text{for} \quad |y'| > b,\ |x'| \leq b \\ 0 & \text{otherwise} \end{cases} \tag{60}$$

In the following Chapters, we retain the original normalization constant as A in the trial functions to carry out the calculations in order avoid the mathematically complicated expression. The value of the normalization constant evaluated above is used explicitly after the final results of the calculations.

IV. EXPECTATION VALUE OF THE HAMILTONIAN

A. Channel matrix elements

The skewed geometry is a cross with the intersection at an arbitrary angle enclosing a region which is a rhombus of side $2b$. The arms of this rhombus extend to infinity in both horizontal and vertical directions. These arms are called channels of the cross-wire system (see figure 35). These channels are labeled as $C_1, C_2, C_3, C_4, C_5, C_6, C_7$ and C_8. Although, there are only four channels but for the computational convenience, each channel is taken as two portions making eight channels. Each of these channels are identical in width but are different with respect to the orientation relative to the origin. Also, calculation of matrix elements of the Hamiltonian for the channels require boundaries of the area enclosed by the channels. These features makes the channels completely different with regard to computation. Hence, not all the matrix elements are equal. The matrix elements of the Hamiltonian corresponding to these eight arms excluding the rhombus are called channel matrix elements. For detailed calculations of the channel matrix elements refer to the Appendix II (A). Also, to improve the efficiency of computation, most channel matrix elements were evaluated using mathematical handbook [18]. The channel matrix elements J_{C_n} corresponding to the channels C_n (see figure 35) are given by

$$J_{C1} = J_{C2} = J_{C5} = J_{C6} = \frac{-\hbar^2 A^2 e^{-2\alpha} \sec\theta}{4m} \left[\frac{\alpha}{3} - \sin\theta\right] \tag{61}$$

and

$$J_{C3} = J_{C4} = J_{C7} = J_{C8} = \frac{-\hbar^2 A^2 e^{-2\alpha} \sec\theta}{4m} \left[\frac{\alpha}{3} + \sin\theta\right] \tag{62}$$

The total channel matrix elements for the channels C_n is given by

$$\begin{aligned}
\langle H\rangle_C &= J_{C1} + J_{C2} + J_{C3} + J_{C4} + J_{C5} + J_{C6} + J_{C7} + J_{C8} \\
&= 2J_{C1} + 2J_{C3} + 2J_{C5} + 2J_{C7} \\
&= 4\left(J_{C1} + J_{C3}\right) \\
&= 4\left(\frac{-\hbar^2 A^2 e^{-2\alpha} \sec\theta}{4m}\left[\frac{\alpha}{3} - \sin\theta\right] + \frac{-\hbar^2 A^2 e^{-2\alpha} \sec\theta}{4m}\left[\frac{\alpha}{3} + \sin\theta\right]\right) \\
&= \frac{-2\hbar^2 A^2 \alpha e^{-2\alpha} \sec\theta}{3m}
\end{aligned} \tag{63}$$

This is the part of the ground state energy of an electron associated with the channels only. In the next section, we calculate the part of the ground state energy contributed by the rhombus (intersection region).

B. Rhombus matrix elements

The skewed geometry of the nanowires intersection is a rhombus. This rhombus consist of four identical segments in $x' - y'$ plane. These four oblique quadrants are labeled as R_1, R_2, R_3 and R_4 (see figure 35). The geometrical area occupied by these quadrants are the same but are different with respect to the orientation relative to the origin. Hence, not all the matrix elements of the Hamiltonian are equal. The matrix element of the Hamiltonian operator evaluated over these oblique quadrants excluding four semi-infinite channels are called rhombus matrix elements. For detailed calculations of the rhombus matrix elements refer to the Appendix II (B). Also, to improve the efficiency of computation, most rhombus matrix elements were evaluated using mathematical handbook [17]. The rhombus matrix elements I_{R_n} corresponding to the oblique quadrants R_n (see figure 35) are given by

$$I_{R_1} = -\frac{3\hbar^2 A^2}{4\,m} \sin\theta \sec\theta\, e^{-2\alpha} = I_{R_3} \tag{64}$$

and

$$I_{R_2} = \frac{3\hbar^2 A^2}{4\,m} \sin\theta \sec\theta\, e^{-2\alpha} = I_{R_4} \tag{65}$$

The total rhombus matrix elements is given by

$$\begin{aligned} \langle H \rangle_R &= I_{R_1} + I_{R_2} + I_{R_3} + I_{R_4} \\ &= 0 \end{aligned} \tag{66}$$

Hence, the rhombus matrix elements add to zero. This means that there is no contribution to the ground state energy for an electron from the intersection region. It will be seen shortly in the next section, that the major contribution to the energy comes from the rooflines.

C. Rooflines matrix elements

The most important feature of this problem is the evaluation of the rooflines matrix elements. The rooflines are the regions of discontinuity of the trial functions. Referring to

the figure 35, the rooflines are categorized into three basic types. The first type are the outer four arms which are defined by the following relations:

$$\left.\begin{array}{l} x' = b \quad \text{to} \quad x' = \infty \ \text{and} \quad x' = -\infty \quad \text{to} \quad x' = -b \end{array}\right\} \quad \text{at} \quad y' = 0 \tag{67}$$

$$\left.\begin{array}{l} y' = b \quad \text{to} \quad y' = \infty \ \text{and} \quad y' = -\infty \quad \text{to} \quad y' = -b \end{array}\right\} \quad \text{at} \quad x' = 0 \tag{68}$$

The first relation represents the outer right and outer left arms respectively. The second relation represents the outer top and the outer bottom arms respectively (see figure 35). The Hamiltonian operator consist of the kinetic energy operator in one direction (either x' or y' direction) and the second order cross derivative term associated with the skewed geometry only. For detailed calculations of the rooflines matrix elements refer to the Appendix III (A). Also, mathematical handbook [17] was extensively used to improve the efficiency of computation. The matrix elements of the Hamiltonian $(K_n, n = \overline{1,4})$ corresponding to the outer right arm is given by

$$K_1 = \frac{\hbar^2 \, A^2 \, e^{-2\alpha} \sec\theta}{2m\alpha} \tag{69}$$

Following the same steps of calculations for the other three arms with proper Hamiltonian and the trial functions, we get

$$K_2 = K_3 = K_4 = K_1 \tag{70}$$

The total contribution to the matrix elements of the Hamiltonian from the four outer arms is given by

$$\begin{aligned} K_I &= \sum_{i=1}^{4} K_i = 4\, K_1 \\ &= \frac{2\,\hbar^2 \, A^2 \, e^{-2\alpha} \sec\theta}{m\,\alpha} \end{aligned} \tag{71}$$

The second type of rooflines are the inner four arms, which are defined by the following relations:

$$\left.\begin{array}{l} x' = 0 \quad \text{to} \quad x' = b \ \text{and} \quad x' = -b \quad \text{to} \quad x' = 0 \end{array}\right\} \quad \text{at} \quad y' = 0 \tag{72}$$

$$\left.\begin{array}{l} y' = 0 \quad \text{to} \quad y' = b \ \text{and} \quad y' = -b \quad \text{to} \quad y' = 0 \end{array}\right\} \quad \text{at} \quad x' = 0 \tag{73}$$

The first relation represents the inner right and inner left arms respectively. The second relation represents the inner top and the inner bottom arms respectively (see figure 35).

Here too, the Hamiltonian operator consist of the kinetic energy operator in one direction (either x' or y' direction) and the second order cross derivative term associated with the skewed geometry only. For detailed calculations of the rooflines matrix elements refer to the Appendix III (B). Most of the integrals were evaluated using mathematical handbook [17]. The matrix elements of the Hamiltonian $(L_n, n = \overline{1,4})$ corresponding to the inner right arm is given by

$$L_1 = \frac{\hbar^2 A^2 e^{-2\alpha} \sec\theta}{2m} \tag{74}$$

With simple analogy with L_1 (matrix elements of the Hamiltonian for the inner right arm), the matrix elements for the inner left, inner top and the inner bottom arms are respectively given by

$$L_2 = L_1, \quad L_3 = L_1 \quad \text{and} \quad L_4 = L_1 \tag{75}$$

$$\begin{aligned} K_{II} &= \sum_{i=1}^{4} L_i = 4\, L_1 \\ &= \frac{2\,\hbar^2\, A^2\, e^{-2\alpha} \sec\theta}{m} \end{aligned} \tag{76}$$

The third type of rooflines are the outer eight sides, which are defined by the following relations:

$$\left.\begin{array}{l} y' = 0 \quad \text{to} \quad y' = b \ \text{ and } \quad y' = -b \quad \text{to} \quad y' = 0 \end{array}\right\} \quad \text{at} \quad x' = \pm b \tag{77}$$

$$\left.\begin{array}{l} x' = 0 \quad \text{to} \quad x' = b \ \text{ and } \quad x' = -b \quad \text{to} \quad x' = 0 \end{array}\right\} \quad \text{at} \quad y' = \pm b \tag{78}$$

Also, the Hamiltonian operator consist of the kinetic energy operator in one direction (either x' or y' direction) and the second order cross derivative term associated with the skewed geometry only. For detailed calculations of the rooflines matrix elements refer to the Appendix III (C). Most of the integrals were evaluated using mathematical handbook [17]. Also, Mathematica package was used for the evaluation of the integrals. The integrals involving θ and δ functions were manually calculated. The matrix elements of the Hamiltonian $(S_n, n = \overline{1,8})$ corresponding to the outer first side is given by

$$S_1 = \frac{\hbar^2 A^2 e^{-2\alpha} \sec\theta}{2m} \left(\frac{2\alpha - 1}{6}\right) \tag{79}$$

Use of appropriate trial functions for the remaining seven sides, it can be shown that the matrix elements S_n are equal. Hence, the total contribution to the matrix elements of the

Hamiltonian from the eight sides is given by

$$\begin{aligned} K_{III} = 8S_1 &= 8\left[\frac{\hbar^2 A^2 e^{-2\alpha}\sec\theta}{2m}\left(\frac{2\alpha-1}{6}\right)\right] \\ &= \frac{2\hbar^2 A^2 e^{-2\alpha}\sec\theta}{3m}(2\alpha-1) \end{aligned} \tag{80}$$

D. Matrix element of the Hamiltonian

The contribution to the matrix element of the Hamiltonian for all the rooflines is given by

$$\begin{aligned} \langle H(\alpha)\rangle_{Rooflines} &= K_I + K_{II} + K_{III} \\ &= \frac{2\hbar^2 A^2 e^{-2\alpha}\sec\theta}{m\alpha} + \frac{2\hbar^2 A^2 e^{-2\alpha}\sec\theta}{m} + \frac{2\hbar^2 A^2 e^{-2\alpha}\sec\theta}{3m}(2\alpha-1) \\ &= \frac{2\hbar^2 A^2 e^{-2\alpha}\sec\theta}{m}\left(\frac{1}{\alpha}+1+\frac{2\alpha-1}{3}\right) \\ &= \frac{2\hbar^2 A^2 e^{-2\alpha}\sec\theta}{m}\left(\frac{2\alpha^2+2\alpha+3}{3\alpha}\right) \end{aligned} \tag{81}$$

Hence, the matrix element of the Hamiltonian for the entire cross-wire system consists of the contribution coming from the channels, oblique quadrants and the rooflines.

$$\begin{aligned} \langle H(\alpha)\rangle &= \langle H\rangle_C + \langle H\rangle_R + \langle H(\alpha)\rangle_{Rooflines} \\ &= \frac{-2\hbar^2 A^2 \alpha e^{-2\alpha}\sec\theta}{3m} + 0 + \frac{2\hbar^2 A^2 e^{-2\alpha}\sec\theta}{m}\left(\frac{2\alpha^2+2\alpha+3}{3\alpha}\right) \\ &= \frac{2\hbar^2 A^2 e^{-2\alpha}\sec\theta}{m}\left(-\frac{\alpha}{3}+\frac{2\alpha^2+2\alpha+3}{3\alpha}\right) \\ &= \frac{2\hbar^2 A^2 e^{-2\alpha}\sec\theta}{m}\left(\frac{\alpha^2+2\alpha+3}{3\alpha}\right) \\ &= \frac{2\hbar^2 e^{-2\alpha}\sec\theta}{m}\left(\frac{\alpha^2+2\alpha+3}{3\alpha}\right)\frac{9\alpha e^{2\alpha}}{2b^2(11\alpha+6)\sec\theta} \\ &= \frac{3\hbar^2}{mb^2}\left(\frac{\alpha^2+2\alpha+3}{11\alpha+6}\right) \\ &= \frac{3\hbar^2}{mb^2}\frac{(\alpha^2+2\alpha+3)}{(11\alpha+6)} \end{aligned} \tag{82}$$

where, the value of the normalization constant A have been used to obtain the final expression. This is the expectation value of the Hamiltonian for an electron in the entire cross-wire system. In the following chapter, this expression is used to evaluate the ground state energy of an electron in the oblique cross-wire geometry.

V. BOUND STATE ENERGY

A. Threshold energy vs bound state energy

The threshold energy or the propagation threshold for the channels intersecting at an arbitrary angle can be obtained by solving $2D$ Schrödinger equation given by

$$\left(\nabla'^2 - 2\,\sin(\theta_1-\theta_2)\frac{\partial^2}{\partial x'\partial y'} + \frac{2\,m\,E}{\hbar^2}\right)\Phi(x',y') = 0$$

$$\text{or,}\quad \left(\frac{\partial^2}{\partial x'^2} + \frac{\partial^2}{\partial y'^2} - 2\,\sin(\theta_1-\theta_2)\frac{\partial^2}{\partial x'\partial y'} + \frac{2\,m\,E}{\hbar^2}\right)\Phi(x',y') = 0 \tag{83}$$

with the boundary conditions that

$$\begin{aligned}\Phi(\pm b, y') &= 0 \quad \text{for} \quad |y'| > b \\ \Phi(x', \pm b) &= 0 \quad \text{for} \quad |x'| > b\end{aligned} \tag{84}$$

Using the inverse transformation

$$\begin{pmatrix} x \\ y \end{pmatrix} = \frac{1}{\Delta}\begin{bmatrix} \cos\theta_2 & \sin\theta_1 \\ -\sin\theta_2 & \cos\theta_1 \end{bmatrix}\begin{pmatrix} x' \\ y' \end{pmatrix}, \tag{85}$$

the $2D$ Schrödinger equation becomes

$$\left(\frac{\partial^2}{\partial x^2} + \frac{\partial^2}{\partial y^2} + \frac{2\,m\,E}{\hbar^2}\right)\Phi(x,y) = 0 \tag{86}$$

with the following new boundary conditions

$$\begin{aligned}\Phi(\pm a, y) &= 0 \quad \text{for} \quad |y| > a \\ \Phi(x, \pm a) &= 0 \quad \text{for} \quad |x| > a.\end{aligned} \tag{87}$$

Using the technique of separation of variables, we can write

$$\Phi(x,y) = X(x)Y(y) \tag{88}$$

From Eqn.86, we get

$$\frac{1}{X(x)}\frac{d^2X(x)}{dx^2} + \frac{1}{Y(y)}\frac{d^2Y(y)}{dy^2} + \frac{2mE}{\hbar^2} = 0 \tag{89}$$

Let

$$\frac{1}{X(x)}\frac{d^2X(x)}{dx^2} = -\kappa_x^2 \tag{90}$$

$$\frac{1}{Y(y)}\frac{d^2Y(y)}{dy^2} = -\kappa_y^2 \tag{91}$$

Hence, energy E is related to the separation constants κ_x and κ_y by

$$E = \frac{\hbar^2}{2m}\left(\kappa_x^2 + \kappa_y^2\right) \tag{92}$$

Since all channels are equivalent, we consider the channel in the first quadrant such that the wave is guided along x-axis [16]. The solution for the region $x > a$ along x- direction is given by

$$X(x) = Ae^{i\kappa_x x} + Be^{-i\kappa_x x} \tag{93}$$

In the channel, the wave moving from the right towards negative x-direction is represented by $e^{-i\kappa_x x}$. Since, we consider the case of the wave propagating towards positive x-direction only ($B = 0$), we have

$$X(x) = Ae^{i\kappa_x x} \tag{94}$$

The above equation represents a traveling wave along positive for $x >> a$. This means that the propagation wave vector has to be positive, that is

$$\kappa_x^2 > 0 \tag{95}$$

For the region $x >> a$, the wave function in the transverse direction is given by

$$Y(y) = C\cos(\kappa_y y) + D\sin(\kappa_y y) \tag{96}$$

Using the boundary conditions at $y = \pm a$ for $|x| >> a$, we get

$$Y(a) = 0 = C\cos(\kappa_y a) + D\sin(\kappa_y a) \tag{97}$$

$$Y(-a) = 0 = C\cos(\kappa_y a) - D\sin(\kappa_y a) \tag{98}$$

Adding and subtracting above equations, we get

$$2C\cos(\kappa_y a) = 0 \tag{99}$$

$$2D\sin(\kappa_y a) = 0 \tag{100}$$

Also

$$\begin{aligned} C \neq 0 \Rightarrow \cos(\kappa_y a) &= 0 \\ \kappa_y a &= \frac{n\pi}{2}, \quad n = 1, 3, 5, ... \\ \kappa_y &= \frac{n\pi}{2a} \end{aligned} \tag{101}$$

Again from the above equation, $D \neq 0$ gives

$$\begin{aligned} \sin(\kappa_y a) &= 0 \\ \kappa_y a &= \frac{n\pi}{2}, \quad n = 0, 2, 4, ... \\ \kappa_y &= \frac{n\pi}{2a} \end{aligned} \tag{102}$$

For $n = 0$, $Y(x) = Const.$, which is a trivial solution. Hence for both odd and even cases, we have

$$\begin{aligned} \kappa_y &= \frac{n\pi}{2a}, \quad n = 1, 2, 3, 4..... \\ \kappa_y &= \frac{n\pi}{w} \end{aligned} \tag{103}$$

where $w = 2a$ is the width of the channel. The free propagation along the channel with transverse quantization is a typical feature of quantum wire. The value of the transverse propagation constant is minimum when $n = 1$ and is given by

$$(\kappa_y)_{min} = \frac{\pi}{w} \tag{104}$$

The energy corresponding to the lowest quantization state along y-direction and free propagation along x-direction is given by

$$\begin{aligned} E &\geq \frac{\hbar^2}{2m}\left(\kappa_x^2 + (\kappa_y)_{min}^2\right) \\ E &\geq \frac{\hbar^2}{2m}\left(\kappa_x^2 + (\frac{\pi}{w})^2\right) \end{aligned} \tag{105}$$

There is no boundary condition that restrict the values of κ_x. It can have continuum of real values greater than or equal to zero. Since $\kappa_x^2 > 0$, the lowest energy that can propagate off to infinity along the channel is given by putting $\kappa_x = 0$ in the above expression.

$$E_t = \frac{\hbar^2\pi^2}{2mw^2} \tag{106}$$

This is the threshold energy for the propagation along the channel [1]. The threshold energy does not depend on the angle between the crossed wires. This is obvious because inside an infinite channel, which is far from the crossed intersection, there is no tunneling from the other channel. Any state with energy less than E_t will give the bound state. Hence, the condition of existence of localized states for energy E within the channel is

$$E < E_t \tag{107}$$

In our approach, the energy E is obtained by variational method, so it correspond to the minimum energy E_{min}. Many literatures, discussed earlier, show that for a single straight wire in two and three dimensions, localization is possible only in the presence of corners or the bents [9]. The bents and corners subsequently lower the energy of the system due to quantum effects and hence trapped states are formed. The energy corresponding to the bound states in the crossed channels is the bound state energy. Also, we have used variational principle to estimate the energy, hence the energy is the ground state bound energy. It is given by

$$E_b = E_t - E_{min} \tag{108}$$

The choice of the energy scale is completely arbitrary. In our calculations, for convenience, the origin of the energy scale was chosen as the threshold energy E_t. In such a case, the bound state will simply be given by

$$E_b = -E_{min} \tag{109}$$

The propagation threshold E_t is a constant for the given width of the channels.

B. Calculation of the bound state energy

According to the variational principle, the expectation value of the Hamiltonian is minimized with respect to the variational α. This means that the first differential of the expectation value of the Hamiltonian ($\langle H(\alpha)\rangle$) with respect to the variational parameter (α) must vanish at some value α_0 (say). Hence, from Eqn.82, we get

$$\begin{aligned}
\frac{\partial\langle H(\alpha)\rangle}{\partial\alpha}\,|_{\alpha_0} &= 0 \\
\Rightarrow \frac{3\hbar^2}{mb^2}\frac{\partial}{\partial\alpha}\left(\frac{\alpha^2+2\alpha+3}{11\alpha+6}\right)|_{\alpha_0} &= 0 \\
\Rightarrow \frac{(11\alpha_0+6)(2\alpha_0+2)-(\alpha_0^2+2\alpha_0+3)11}{(11\alpha_0+6)^2} &= 0 \\
\Rightarrow 11\alpha_0^2+12\alpha_0-21 &= 0 \\
\alpha_0 &= 0.94001
\end{aligned} \tag{110}$$

Also, we find that

$$\frac{\partial^2\langle H(\alpha)\rangle}{\partial\,\alpha^2}\,|_{\alpha_0} > 0.$$

This α_0 is the value of variational parameter which minimizes the expectation value of Hamiltonian. And the minimum energy is obtained by substituting α_0 in $\langle H \rangle$, which is given by

$$\begin{aligned} E_{min} &= \langle H(\alpha_0) \rangle \\ &= \frac{3\hbar^2}{mb^2}\left(\frac{2\alpha_0 + 2}{11}\right) \\ &= \frac{6\hbar^2}{mb^2}\left(\frac{\alpha_0 + 1}{11}\right) \\ &= 1.058\frac{\hbar^2}{ma^2}\Delta^2 \end{aligned} \tag{111}$$

The threshold energy is found to be

$$E_t = \frac{\pi^2\hbar^2}{2mw^2} \tag{112}$$

Since the maximum value of Δ is one, E_{min} is less than the threshold energy E_t. The bound states exist in the classically unbound system of cross wires which is purely due to quantum mechanical effect. This minimum energy corresponds to the binding energy of an electron in the cross wires. Hence, the bound state energy (E_b) of the electron taking the threshold energy as zero level is given by

$$\begin{aligned} E_b = -E_{min} &= -1.058\frac{\hbar^2}{ma^2}\Delta^2 \\ &= -4.232\frac{\hbar^2}{mw^2}\cos^2(\theta_1 - \theta_2) \\ &= -4.232\frac{\hbar^2}{mw^2}\cos^2\theta \end{aligned} \tag{113}$$

For the symmetrically crossed wire system, $\theta = 0$ and energy $E_{min} = 0.8575E_t$. Here, E_t is the unit of energy representing a factor equal to $(\pi^2\hbar^2)/(2mw^2)$ (see Eqn.112). This unit is chosen because we have not specified the nanowire material and there is no particular values for effective mass (m) and the width (w). The angular dependence of the bound state energy can be expressed in terms of the threshold energy as

$$E_b = -0.8575E_t\cos^2\theta \tag{114}$$

The typical values of bound state energies for the typical rotation angles $30°, 45°$ and $60°$ are $-0.6431E_t$, $-0.4287E_t$ and $-0.2143E_t$ respectively.

C. Angular dependence of the bound state energy

In our calculations, trial wave functions were so chosen that they vanish outside the rhombus region even in the channels. The variation parameter "α" was found to be independent of the relative orientation of the channels. This means that "α" has no any dependence on the angle of rotation (θ). The upper bound to the ground state energy was found to depend on the squared cosine of the angle by which one channel is rotated with respect to the other. The angle of rotation θ represent the relative rotation ($\theta_1 - \theta_2$) between the two arms of the cross-wire system (see figure 24). When $\theta = 0$, that is, if each arms of the cross-wire system is rotated by equal angle with respect to the fixed axis, the wires intersect at right angle. This case of classically unbound system is known to posses a quantum bound state [1]. This very fact is supplemented by the model (skewed geometry) formulated in this thesis project. It is clear from our results that when two channels intersect exactly at right angle

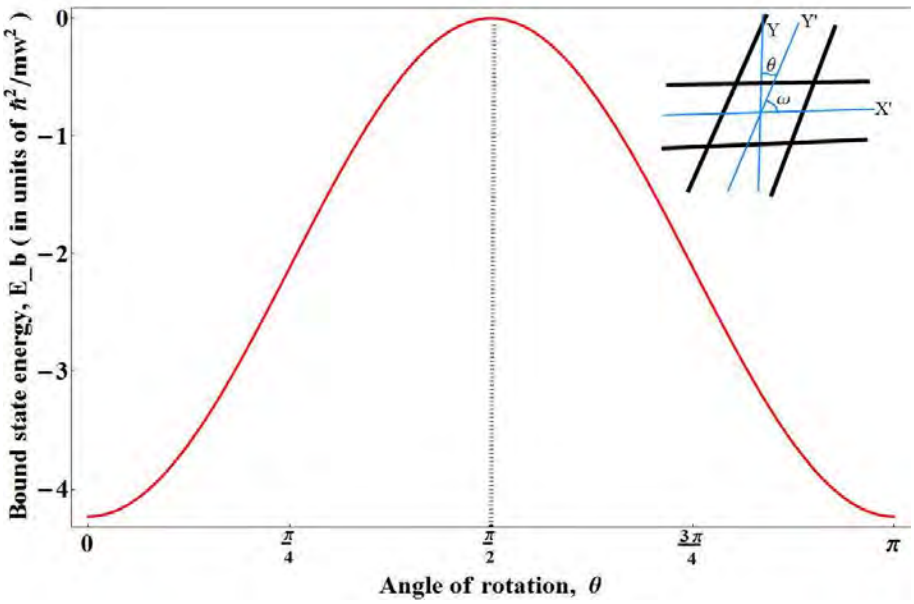

FIG. 36. Variation of bound state energy of an electron with the angle of rotation $\theta = \theta_1 - \theta_2$. The angle of rotation (θ) is shown in the adjoining figure.

($\theta = 0$), the system is in strongly bound state and for all other angles the system is less strongly bound (see figure 36). This is because, in the absence of rotation ($\theta = 0$), the trial wave function for an electron is localized well inside the intersection region (see figure 25). The probability of finding an electron is maximum inside the square region shown by sharp

kinks in the density plot (see figure 26). In the case of finite rotation angle, the trial wave functions get spread out of the intersection region due to change in the shape of the corners. This feature is depicted in the figures [Fig.27-Fig.32]. When two channels overlap ($\theta = \pi/2$), the wave function is confined to a single channel (see figure 33). The probability densities becomes uniform in the channels. The probability of finding an electron in such a case will be anywhere from $-\infty$ to $+\infty$ along the channel (see figure 34). The bound state energy is zero and that the electron can never be trapped in a single straight channel. This means that an electron becomes a free particle. Thus, bound state energy of an electron trapped in a cross nanowires varies with the angular deviation ($\theta_1 - \theta_2 = \theta$) as an integral multiple of π. The bound state energy corresponding to an angle θ of rotation is identical to that of rotation by an angle $(\pi - \theta)$. This energy is symmetric about the vertical line through the angle of rotation of $\pi/2$. This must be true because the geometry of cross-wire system for the two angles differing by π is exactly the same.

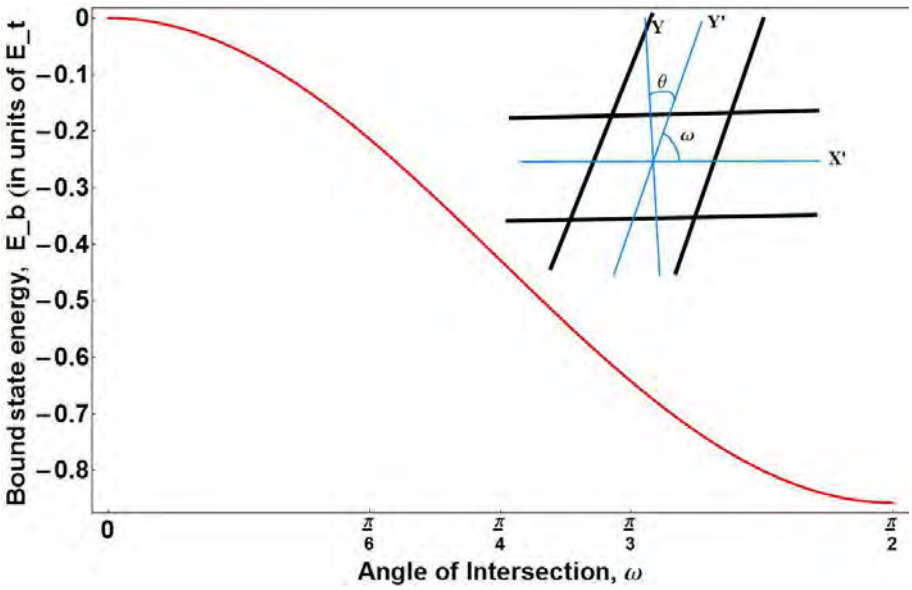

FIG. 37. Variation of bound state energy with the angle of intersection of the cross-wire system ω. The angle ω is shown in the adjoining figure.

The dependence of the bound state energy with the angle of intersection is shown in the figure 37. The bound state energy is expressed in the units of the threshold energy (E_t) for free propagation. It is clear from this plot that the bound state energy varies as squared sine of the intersection angle of the cross-wire system. This energy variation is symmetric about $\omega = \pi/2$ and odd multiple of it. The variation of bound state energy with the intersection

angle is complementary to that of energy variation with the angle of rotation (see figure 36). The energy corresponding to two angles of intersection differing by 180° is identical. This fact is obvious from the geometrical consideration. The geometry for the intersection angle ω is exactly the same as its supplementary angle. The bound state energy approaches maximum value as the angle of intersection goes to 90°. Also, as the origin of the energy scale is taken as the threshold energy itself, bound state energy is zero when $\omega = 0°$. This means that an electron can freely propagate along the channels of the cross-wire system.

Thus, the bound state energy of an electron trapped at the skew-symmetric cross-wire intersection varies as squared sine of the angle of intersection which is equivalent to the squared cosine of the relative rotation of the channels. Analytically, the ground state bound energy of an electron for our model system can be written as

$$E_b = -4.232\frac{\hbar^2}{mw^2}\cos^2\theta = -4.232\frac{\hbar^2}{mw^2}\sin^2\omega \tag{115}$$

where, the rotation angle (θ) and the intersection angle (ω) are related by

$$\theta + \omega = \frac{\pi}{2} \tag{116}$$

The squared sine dependence of the ground state bound energy on the cross-wire intersection angle implies that there exist unique solution for the angular domain $[\pi/2 \geq \omega \geq 0]$. The system considered here represent both bound and unbound states. The existence of bound states is mainly determined by the angle of the intersection of the cross-wire system. This also means that electron is trapped by the presence of corners and bents. If corners and bents do not exist as in the case of a single wires ($\theta = \pi/2$), then the system is unbounded. In case of finite rotation angle ($\theta \neq \pi/2$) there exist bound state due to quantum effects which has no any classical counterpart.

VI. RESULTS AND DISCUSSIONS

A. Summary of the results

The present work can be summarized as follows:

1. We have found that the bound state energy of an electron trapped at the intersection of the quantum nanowires in the skewed geometry depend on the angle of intersection of the channels. The ground state bound energy varies as squared cosine of the relative rotation of the channels. The bound state energy corresponding to an angle θ of rotation is identical to that of rotation by an angle $(\pi - \theta)$. In fact, it must be true because the geometry of cross-wire system for the two angles differing by π is exactly the same. Also parity conservation laws require that the energy be a true scalar, hence it must be invariant under reflection symmetry.

2. The results of our calculations show that the role of tilted nanowire geometry is to decrease the bound state energy. This is due to the fact that in the tilted configuration, one pair of the opposite corners become sharper than 90° while the other opposite corners become shallower, making the system elongated in one direction, thus delocalizing the electron. In the absence of any rotation of cross-wires the angle of intersection is 90°. This is a classically unbound system and is known to have quantum bound states due to the presence of corners, which was previously reported by Schult et al. [1]. Our calculations show that for any finite rotation of the nanowire, no matter however small it may be, there is always a decrease of the bound state energy. This is because in case of no rotation, all four corners are identical (included angle is 90°) and the spatial extend of an electron wave function is well within the square region (see figure 25). But in case of finite rotation, the electron wave functions get spread out into the channels of the cross-wire system due to change in the geometrical constraints (the shape of the corners), making the system expanded and therefore less bound. These features can be visualized directly from the figures [Fig.27-Fig.34] in Chapter III. Another remarkable property is that, when the angle of rotation is $\pi/2$ or an odd integral multiple of it, the wave function is further spread out along the channel, the system is no longer a cross-wire but a single wire (see figures 33 and 34). This is a case of free propagation and the quantum bound states no longer exist (see figure 36). The transition from

quantum bound state to unbound state due to rotation of the nanowire is the intrinsic feature which can be useful for device applications.

3. Different geometries of the cross-wire systems explored earlier (all crossed at right angles) show the effects of the bound states on the electron transport properties such as tunneling, transmission and reflection [1, 7]. Various ways of observing the bound states were also suggested through measurement of the conductance using two dimensional electron gas model [2]. The results of our model system (cross-wire intersecting at an *arbitrary* angle) not only supplement the theory of quantum bound state in a classically unbound system but give the quantitative explanation of the angular dependence of the bound state energy.

In order to arrive at these results, many steps were taken in sequential pattern. They are

- Firstly, after extensive study of the literatures on the cross-wire systems in two dimension, the problem that takes into account the angular dependence of the bound state energy for an electron was determined as a distinct one.

- Secondly, the model was set up using two orthogonal coordinate systems rigidly fixed on each nanowires and orthogonal transformation was applied to obtain new intersection geometry (rhombus).

- Thirdly, using the variational principle with suitable trial wave functions for the oblique geometry, calculations were carried out to estimate the upper bound to the ground state energy for an electron located inside the cross-wire system.

- Lastly, the results were visualized using Mathematica programming package.

B. Potential applications

As it has been stated above, our results supplement a theory of quantum bound states in classically unbound systems and may be useful to interpret electron transport peculiarities in realistic systems such as semiconductor nanowire films, intersecting nanorods and carbon nanotube bundles [7]. Some of the potential applications of this thesis work can be summarized as follows:

1. Transistors and switching devices. The model formulated here explains the effect of intersection angle of nanowires on the bound states at the crossed region. The bound state energy for an electron at the crossed intersection decreases as the angle between the nanowires decreases. This feature of the cross-wire system can be exploited to design ultra-sensitive transistors and switching devices with carbon nanotubes, in particular. In practice, carbon nanotube bundles can be regarded as a collection of asymmetrically crossed nanowires. The model developed here could be used to interpret electron transport peculiarities in such nanotube bundles. Since nanotubes are very rigid structures and can carry high densities of electric current without losing their properties, the crossed nanotubes structure could be a potential candidate for devices such as single-electron transistors [19]. Recently, resonances have been observed in the metallic and semiconducting carbon nanotubes intersection confirming the existence of localized states [7].

2. Amplifiers. Semiconductor quantum wires in crossed configuration provide superior performance of semiconductor optical amplifiers (SOAs) as opposed to the amplifiers built on quantum dots, and so they are potential candidates for future solid-state quantum information and communication devices [20]. With the development of lithographic and etching techniques, it is now possible to manipulate cross-wire semiconductors to design amplifiers. The model suggested here could be of immense value for controlling the quality factor of such amplifiers. This is because the crossed nanowires can be interchanged from bound states to unbound states simply by varying the angle of intersection. This property of the cross-nanowire system could be used to develop power efficient amplifiers.

3. Photo-detectors. The theory developed here can be used to study the performance of quantum wire photodetectors. In the crossed nanowire system, an electron is bound to the intersection region at some energy level. This electron can be excited by the light radiation (photon) of suitable wavelength that scales with electron bound state energy. The photocurrent will be produced as a result of these light illumination of the system. These essential properties can be exploited to design photo-detectors which can be manipulated and controlled by varying the bound state energy of an electron at the cross-wire intersection.

4. Lasers. Lasers may be designed from quantum wires which have desirable properties with regard to their performances [21]. Quantum wire lasers are predicted to have a high efficiency, low threshold current densities, and low temperature dependence of the threshold current [22]. It has been proved that quantum wire lasers have lower threshold current density as compared to the quantum dots lasers [23]. The energy spectrum of the crossed quantum wires can be varied over a wide range by simply changing the angle of intersection between them. The population inversion can be achieved by controlling the voltage across the crossed wires and also varying the intersection angle. Thus, the use of crossed quantum wires may offer possibilities for power-efficient nonlinear devices in semiconductor technology.

5. Solar cells. The theory developed here can be used to design the energy conversion devices such as solar cells. Quantum wire solar cells have the potential to increase the maximum attainable conversion efficiency of solar photon conversion by utilizing hot photogenerated carriers to produce higher photovoltages or higher photocurrents. The nanowire geometry provides potential advantages over planar wafer-based or thin-film solar cells in every step of the photoconversion process [24]. Knowledge of the quantum bound states in the cross-nanowire system is useful to explain the conversion of photon flux into an electron flux through the nanowire channels. In the crossed geometry, the nanowires will have greater resistance to the flow of electron than the corresponding parallel configuration. Therefore, understanding the properties of the crossed nanowire system would allow one to improve the efficiency of the quantum wire solar cells as compared to the conventional solar cells.

Finally, it can be concluded that the existence of bound states in the cross-wire system, which is classically unbound system demonstrates that the laws governing microscopic world are inherently quantum mechanical. Extension of this work to incorporate more realistic models of the confining potential, inhomogeneous external fields and temperature fluctuations appear fascinating but still remains to be done.

VII. BIBLIOGRAPHY

[1] R. L. Schult, D. G. Ravenhall, and H. W. Wyld, "Quantum bound states in a classically unbound system of crossed wires," *Phys. Rev. B*, vol. 39, pp. 5476–5479, Mar 1989.

[2] K.-F. Berggren and Z.-l. Ji, "Resonant tunneling via quantum bound states in a classically unbound system of crossed, narrow channels," *Phys. Rev. B*, vol. 43, pp. 4760–4764, Feb 1991.

[3] K.-F. Berggren and C.-K. Wang, "Different orbitals for different electrons in a system of intersecting quantum wires," vol. 63, pp. 667–673, June 1997.

[4] Z.-L. Ji and K.-F. Berggren, "Quantum bound states in narrow ballistic channels with intersections," *Phys. Rev. B*, vol. 45, pp. 6652–6658, Mar 1992.

[5] D. G. Ravenhall, H. W. Wyld, and R. L. Schult, "Quantum hall effect at a four-terminal junction," *Phys. Rev. Lett.*, vol. 62, pp. 1780–1783, Apr 1989.

[6] Y. Takagaki and K. Ploog, "Quantum transmission in an out-of-plane crossed-wire junction," *Phys. Rev. B*, vol. 48, pp. 11508–11511, Oct 1993.

[7] D. Makogon, N. de Jeu, and C. M. Smith, "Coupled quantum wires: Explaining the observed localized states at the crossing of metallic and semiconducting nanotubes," *Phys. Rev. B*, vol. 78, p. 115123, Sep 2008.

[8] Y. Avishai, D. Bessis, B. G. Giraud, and G. Mantica, "Quantum bound states in open geometries," *Phys. Rev. B*, vol. 44, pp. 8028–8034, Oct 1991.

[9] P. Exner, P. Seba, and P. St'ovicek, "On existence of a bound state in an l-shaped waveguide," *Czechoslovak Journal of Physics B*, vol. 39, no. 11, pp. 1181–1191, 1989.

[10] Y. Takagaki and K. H. Ploog, "Transport properties in anisotropic cross junctions by tight-binding calculations," *Phys. Rev. B*, vol. 74, p. 075325, Aug 2006.

[11] K.-K. Voo, S.-C. Chen, C.-S. Tang, and C.-S. Chu, "Connecting wave functions at a three-leg junction of one-dimensional channels," *Phys. Rev. B*, vol. 73, p. 035307, Jan 2006.

[12] S. C. Nepal, L. Zhemchuzhna, A. Meliksetyan, and I. Bondarev, "Bound electron states in skew-symmetric quantum wire intersections," *Bulletin of the American Physical Society (APS)*, vol. 59, p. 1, Mar 2014.

[13] V. V. Paranjape, "Bound quantum states in crossed-wire systems," *Journal of Physics: Condensed Matter*, vol. 3, no. 35, p. 6715, 1991.

[14] E. Abers, *Quantum Mechanics*. Pearson Prentice Hall, 2004.

[15] J. J. J. Sakurai and J. Napolitano, *Modern Quantum Mechanics*. International edition, Addison-Wesley, 2011.

[16] D. Griffiths, *Introduction to Quantum Mechanics*. Pearson Prentice Hall, 2005.

[17] F. W. Olver, D. W. Lozier, R. F. Boisvert, and C. W. Clark, *NIST Handbook of Mathematical Functions*. New York, NY, USA: Cambridge University Press, 1st ed., 2010.

[18] M. Abramowitz, *Handbook of Mathematical Functions, With Formulas, Graphs, and Mathematical Tables,*. Dover Publications, Incorporated, 1974.

[19] R. H. Baughman, A. A. Zakhidov, and W. A. de Heer, "Carbon nanotubes–the route toward applications," *Science*, vol. 297, no. 5582, pp. 787–792, 2002.

[20] M. A. M. Versteegh, P. J. S. van Capel, and J. I. Dijkhuis, "Ultrafast all-optical gated amplifier based on zno nanowire lasing," *Applied Physics Letters*, vol. 101, no. 2, pp. –, 2012.

[21] H. Takiguchi, H. Kudo, M. Taneya, and S. Sugahara, "Quantum wire laser," Jan. 18 1994. US Patent 5,280,493.

[22] H.-J. Choi, J. C. Johnson, R. He, S.-K. Lee, F. Kim, P. Pauzauskie, J. Goldberger, R. J. Saykally, and P. Yang, "Self-organized gan quantum wire uv lasers," *The Journal of Physical Chemistry B*, vol. 107, no. 34, pp. 8721–8725, 2003.

[23] S. Tiwari, G. D. Pettit, K. R. Milkove, F. Legoues, R. J. Davis, and J. M. Woodall, "High efficiency and low threshold current strained v groove quantum wire lasers," *Applied Physics Letters*, vol. 64, no. 26, 1994.

[24] L. Tsakalakos, J. Balch, J. Fronheiser, B. A. Korevaar, O. Sulima, and J. Rand, "Silicon nanowire solar cells," *Applied Physics Letters*, vol. 91, no. 23, pp. –, 2007.

VIII. APPENDIX I

A. Calculation of the normalization constant

For oblique quadrants R_n For the oblique quadrants defined by R_n where, $n = \overline{1,4}$, the trial functions are:

$$\Phi(x', y') = A\left(1 - \frac{|x'y'|}{b^2}\right) e^{-\alpha} \quad for \quad |x'| \leq b, \quad |y'| \leq b \tag{117}$$

For an oblique quadrant R_1: We take the trial function as

$$\Phi_1(x', y') = A\left(1 - \frac{x'y'}{b^2}\right) e^{-\alpha} \tag{118}$$

and the region of integration are from $x' = 0$ to $x' = b$ and $y' = 0$ to $y' = b$. Hence,

$$\begin{aligned}
R_1 &= \int_{x'=0}^{b}\int_{y'=0}^{b} \Phi_1^*(x', y')\,\Phi_1(x', y')\,\sec\theta\,dx'\,dy' \\
&= A^2\,\sec\theta\int_{x'=0}^{b}\int_{y'=0}^{b}\left(1 - \frac{x'\,y'}{b^2}\right)^2 e^{-2\alpha}\,dx'\,dy' \\
&= A^2\,\sec\theta\,e^{-2\alpha}\int_{x'=0}^{b}\int_{y'=0}^{b}\left(1 - \frac{x'\,y'}{b^2}\right)^2 dx'\,dy' \\
&= A^2\,\sec\theta\,e^{-2\alpha}\int_{x'=0}^{b}\int_{y'=0}^{b}\left(1 - \frac{2\,x'\,y'}{b^2} + \frac{x'^2\,y'^2}{b^4}\right) dx'\,dy' \\
&= A^2\,\sec\theta\,e^{-2\alpha}\left(b^2 - \frac{2\,b^2\,b^2}{4\,b^2} + \frac{b^3\,b^3}{9\,b^4}\right) \\
&= A^2\,\sec\theta\,e^{-2\alpha}\left(b^2 - \frac{b^2}{2} + \frac{b^2}{9}\right) \\
&= A^2\,b^2\,\sec\theta\,e^{-2\alpha}\left(\frac{1}{2} + \frac{1}{9}\right) \\
&= A^2\,b^2\,\sec\theta\,e^{-2\alpha}\left(\frac{11}{18}\right) \\
&= \frac{11}{18}\,A^2\,b^2\,\sec\theta\,e^{-2\alpha}
\end{aligned} \tag{119}$$

For an oblique quadrant R_2: We have trial function as

$$\Phi_2(x', y') = A\left(1 + \frac{x'\,y'}{b^2}\right) e^{-\alpha} \tag{120}$$

and the region of integration are from $x' = -b$ to $x' = 0$ and $y' = 0$ to $y' = b$. Hence,

$$R_2 = \int_{x'=-b}^{0}\int_{y'=0}^{b} \Phi_2^*(x', y')\,\Phi_2(x', y')\,\sec\theta\,dx'\,dy'$$

$$= A^2 \sec\theta \int_{x'=-b}^{0}\int_{y'=0}^{b} \left(1+\frac{x'\,y'}{b^2}\right)^2 e^{-2\alpha}\,dx'\,dy'$$
$$= -A^2 \sec\theta\, e^{-2\alpha} \int_{x'=0}^{-b}\int_{y'=0}^{b} \left(1+\frac{x'\,y'}{b^2}\right)^2 dx'\,dy'$$

Let $u=-x'$, so that $du=-dx'$, therefore, when $x'=0, u=0$ and when $x'=-b, u=b$. Therefore,

$$R_2 = A^2 \sec\theta\, e^{-2\alpha} \int_{u=0}^{b}\int_{y'=0}^{b} \left(1-\frac{u\,y'}{b^2}\right)^2 du\,dy' = R_1 \tag{121}$$

For an oblique quadrant R_3: We take the trial function as

$$\Phi_3(x',y') = A\left(1-\frac{x'\,y'}{b^2}\right)\exp(-\alpha) \tag{122}$$

and the region of integration are from $x'=-b$ to $x'=0$ and $y'=-b$ to $y'=0$. Hence,

$$R_3 = \int_{x'=-b}^{0}\int_{y'=-b}^{0} \Phi_3^*(x',y')\,\Phi_3(x',y')\,\sec\theta\,dx'\,dy'$$
$$= A^2 \sec\theta \int_{x'=-b}^{0}\int_{y'=-b}^{0} \left(1-\frac{x'\,y'}{b^2}\right)^2 e^{-2\alpha}\,dx'\,dy'$$
$$= A^2 \sec\theta\, e^{-2\alpha} \int_{x'=0}^{-b}\int_{y'=0}^{-b} \left(1-\frac{x'\,y'}{b^2}\right)^2 dx'\,dy'$$

Let $u=-x'$, so that $du=-dx'$, therefore, when $x'=0, u=0$ and when $x'=-b, u=b$. also let $v=-y'$, so that $dv=-dy'$, therefore, when $y'=0, v=0$ and when $y'=-b, v=b$. Therefore,

$$R_3 = A^2 \sec\theta\, e^{-2\alpha} \int_{u=0}^{b}\int_{v=0}^{b} \left(1-\frac{u\,v}{b^2}\right)^2 du\,dv = R_1 \tag{123}$$

and finally, **For an oblique quadrant** R_4: We have the trial function as

$$\Phi_4(x',y') = A\left(1+\frac{x'\,y'}{b^2}\right)e^{-\alpha} \quad for \quad x'>0,\, y'<0 \tag{124}$$

and the region of integration are from $x'=0$ to $x'=b$ and $y'=-b$ to $y'=0$. Hence,

$$R_4 = \int_{x'=0}^{b}\int_{y'=-b}^{0} \Phi_4^*(x',y')\,\Phi_4(x',y')\,\sec\theta\,dx'\,dy'$$
$$= A^2 \sec\theta \int_{x'=0}^{b}\int_{y'=-b}^{0} \left(1+\frac{x'\,y'}{b^2}\right)^2 e^{-2\alpha}\,dx'\,dy'$$
$$= -A^2 \sec\theta\, e^{-2\alpha} \int_{x'=0}^{b}\int_{y'=0}^{-b} \left(1+\frac{x'\,y'}{b^2}\right)^2 dx'\,dy'$$

Let $v = -y'$, so that $dv = -dy'$, therefore, when $y' = 0, v = 0$ and when $y' = -b, v = b$. Therefore,

$$R_4 = A^2 \sec\theta\, e^{-2\alpha} \int_{x'=0}^{b}\int_{v=0}^{b} \left(1 - \frac{x'\,v}{b^2}\right)^2 dx'\,dv = R_1 \tag{125}$$

The total contribution to the normalization integral from the regions R_n is given by

$$\begin{aligned} I_1 &= \sum_{i=1}^{4} R_i \\ &= 4\,R_1 \\ &= 4\left(\frac{11}{18}\right) A^2\,b^2 \sec\theta\, e^{-2\alpha} \\ &= \frac{22}{9}\,A^2\,b^2 \sec\theta\, e^{-2\alpha} \end{aligned} \tag{126}$$

For the open channels C_n For the open channels defined by C_n where, $n = \overrightarrow{(1,8)}$, the trial functions are:

$$\begin{aligned} \phi(x',y') &= A\left(1 - \frac{|y'|}{b}\right) e^{-\frac{\alpha\,|x'|}{b}} \quad for \quad |x'| > b,\ |y'| \le b \\ &= A\left(1 - \frac{|x'|}{b}\right) e^{-\frac{\alpha\,|y'|}{b}} \quad for \quad |y'| > b,\ |x'| \le b \end{aligned} \tag{127}$$

For the channel C_1: We get

$$\phi_1(x',y') = A\left(1 - \frac{y'}{b}\right) e^{-\frac{\alpha\,x'}{b}} \tag{128}$$

and the region of integration are from $x' = b$ to $x' = \infty$ and $y' = 0$ to $y' = b$. Hence,

$$\begin{aligned} C_1 &= \int_{x'=b}^{\infty}\int_{y'=0}^{b} \phi_1^*(x',y')\,\phi_1(x',y') \sec\theta\,dx'\,dy' \\ &= A^2 \sec\theta \int_{x'=b}^{\infty}\int_{y'=0}^{b} \left(1 - \frac{y'}{b}\right)^2 e^{-\frac{2\alpha\,x'}{b}}\,dx'\,dy' \\ &= A^2 \sec\theta \left[\int_{x'=b}^{\infty} e^{-\frac{2\alpha\,x'}{b}}\,dx'\right]\left[\int_{y'=0}^{b}\left(1 - \frac{y'}{b}\right)^2 dy'\right] \\ &= A^2 \sec\theta \left[\frac{-b}{2\alpha}\left(0 - e^{-2\alpha}\right)\right]\left[\frac{b}{3}\right] \\ &= A^2 \sec\theta \left[\frac{b}{2\alpha}\,e^{-2\alpha}\right]\left[\frac{b}{3}\right] \\ &= \frac{A^2}{6\alpha}\,b^2 \sec\theta\, e^{-2\alpha} \end{aligned} \tag{129}$$

For the channel C_2: We have

$$\phi_2(x',y') = A\left(1 - \frac{x'}{b}\right) e^{-\frac{\alpha\,y'}{b}} \tag{130}$$

and the region of integration are from $x' = 0$ to $x' = b$ and $y' = b$ to $y' = \infty$. Hence,

$$\begin{aligned} C_2 &= \int_{x'=0}^{b} \int_{y'=b}^{\infty} \phi_2^*(x', y')\, \phi_2(x', y')\, \sec\theta\, dx'\, dy' \\ &= A^2\, \sec\theta \int_{x'=0}^{b} \int_{y'=b}^{\infty} \left(1 - \frac{x'}{b}\right)^2 e^{-\frac{2\alpha\, y'}{b}}\, dx'\, dy' \\ &= A^2\, \sec\theta \left[\int_{x'=0}^{b} \left(1 - \frac{x'}{b}\right)^2 dx'\right] \left[\int_{y'=b}^{\infty} e^{-\frac{2\alpha\, y'}{b}}\, dy'\right] \\ &= A^2\, \sec\theta \left[\frac{b}{3}\right] \left[\frac{b}{2\alpha}\, e^{-2\alpha}\right] = C_1 \end{aligned} \tag{131}$$

For the channel C_3: We have

$$\phi_3(x', y') = A \left(1 + \frac{x'}{b}\right) e^{-\frac{\alpha\, y'}{b}} \tag{132}$$

and the region of integration are from $x' = -b$ to $x' = 0$ and $y' = b$ to $y' = \infty$.

Hence,

$$\begin{aligned} C_3 &= \int_{x'=-b}^{0} \int_{y'=b}^{\infty} \phi_3^*(x', y')\, \phi_3(x', y')\, \sec\theta\, dx'\, dy' \\ &= A^2\, \sec\theta \int_{x'=-b}^{0} \int_{y'=b}^{\infty} \left(1 + \frac{x'}{b}\right)^2 e^{-\frac{2\alpha\, y'}{b}}\, dx'\, dy' \\ &= -A^2\, \sec\theta \left[\int_{x'=0}^{-b} \left(1 + \frac{x'}{b}\right)^2 dx'\right] \left[\int_{y'=b}^{\infty} e^{-\frac{2\alpha\, y'}{b}}\, dy'\right] \end{aligned} \tag{133}$$

Let $u = -x'$, so that $du = -dx'$, therefore, when $x' = 0, u = 0$ and when $x' = -b, u = b$. Therefore,

$$\begin{aligned} C_3 &= A^2\, \sec\theta \left[\int_{u=0}^{b} \left(1 - \frac{u}{b}\right)^2 du\right] \left[\int_{y'=b}^{\infty} e^{-\frac{2\alpha\, y'}{b}}\, dy'\right] \\ &= A^2\, \sec\theta \left[\frac{b}{3}\right] \left[\frac{b}{2\alpha}\, e^{-2\alpha}\right] = C_1 \end{aligned} \tag{134}$$

For the channel C_4:The trial function is taken as

$$\phi_4(x', y') = A \left(1 - \frac{y'}{b}\right) e^{\frac{\alpha\, x'}{b}} \tag{135}$$

and the region of integration are from $x' = -\infty$ to $x' = -b$ and $y' = 0$ to $y' = b$. Hence,

$$C_4 = \int_{x'=-\infty}^{-b} \int_{y'=0}^{b} \phi_4^*(x', y')\, \phi_4(x', y')\, \sec\theta\, dx'\, dy'$$

$$= A^2 \sec\theta \int_{x'=-\infty}^{-b} \int_{y'=0}^{b} \left(1 - \frac{y'}{b}\right)^2 e^{\frac{2\alpha\, x'}{b}}\, dx'\, dy'$$
$$= -A^2 \sec\theta \left[\int_{x'=-b}^{-\infty} e^{\frac{2\alpha\, x'}{b}}\, dx'\right] \left[\int_{y'=0}^{b} \left(1 - \frac{y'}{b}\right)^2 dy'\right] \tag{136}$$

Let $u = -x'$, so that $du = -dx'$, therefore, when $x' = -b, u = a$ and when $x' = -\infty, u = \infty$. Therefore,

$$C_4 = A^2 \sec\theta \left[\int_{u=a}^{\infty} e^{\frac{-2\alpha\, u}{b}}\, du\right] \left[\int_{y'=0}^{b} \left(1 - \frac{y'}{b}\right)^2 dy'\right]$$
$$= A^2 \sec\theta \left[\frac{b}{2\alpha}\, e^{-2\alpha}\right] \left[\frac{b}{3}\right] = C_1 \tag{137}$$

For the channel C_5: The trial function is taken as

$$\phi_5(x', y') = A \left(1 + \frac{y'}{b}\right) e^{\frac{\alpha\, x'}{b}} \tag{138}$$

and the region of integration are from $x' = -\infty$ to $x' = -b$ and $y' = -b$ to $y' = 0$. Hence,

$$C_5 = \int_{x'=-\infty}^{-b} \int_{y'=-b}^{0} \phi_5^*(x', y')\, \phi_5(x', y') \sec\theta\, dx'\, dy'$$
$$= A^2 \sec\theta \int_{x'=-\infty}^{-b} \int_{y'=-b}^{0} \left(1 + \frac{y'}{b}\right)^2 e^{\frac{2\alpha\, x'}{b}}\, dx'\, dy'$$
$$= A^2 \sec\theta \left[\int_{x'=-\infty}^{-b} e^{\frac{2\alpha\, x'}{b}}\, dx'\right] \left[\int_{y'=-b}^{0} \left(1 + \frac{y'}{b}\right)^2 dy'\right] \tag{139}$$

Let $u = -x'$, so that $du = -dx'$, therefore, when $x' = -\infty, u = \infty$ and when $x' = -b, u = b$. also, let $v = -y'$, so that $dv = -dy'$, therefore, when $y' = 0, v = 0$ and when $y' = -b, v = b$. Therefore,

$$C_5 = A^2 \sec\theta \left[\int_{u=b}^{\infty} e^{\frac{-2\alpha\, u}{b}}\, du\right] \left[\int_{v=0}^{b} \left(1 - \frac{v}{b}\right)^2 dv\right]$$
$$= A^2 \sec\theta \left[\frac{b}{2\alpha}\, e^{-2\alpha}\right] \left[\frac{b}{3}\right] = C_1 \tag{140}$$

For the channel C_6: The trial function is taken as

$$\phi_6(x', y') = A \left(1 + \frac{x'}{b}\right) e^{\frac{\alpha\, y'}{b}} \tag{141}$$

and the region of integration are from $x' = -b$ to $x' = 0$ and $y' = -\infty$ to $y' = -b$. Hence,

$$\begin{aligned} C_6 &= \int_{x'=-b}^{0} \int_{y'=-\infty}^{-b} \phi_6^*(x', y')\, \phi_6(x', y')\, \sec\theta\, dx'\, dy' \\ &= A^2\, \sec\theta \int_{x'=-b}^{0} \int_{y'=-\infty}^{-b} \left(1 + \frac{x'}{b}\right)^2 e^{\frac{2\alpha\, y'}{b}}\, dx'\, dy' \\ &= A^2\, \sec\theta \left[\int_{x'=-b}^{0} \left(1 + \frac{x'}{b}\right)^2 dx'\right] \left[\int_{y'=-\infty}^{-b} e^{\frac{2\alpha\, y'}{b}}\, dy'\right] \end{aligned} \tag{142}$$

Let $u = -x'$, so that $du = -dx'$, therefore, when $x' = -b, u = b$ and when $x' = 0, u = 0$. also, let $v = -y'$, so that $dv = -dy'$, therefore, when $y' = -\infty, v = \infty$ and when $y' = -b, v = b$. Therefore,

$$\begin{aligned} C_6 &= A^2\, \sec\theta \left[\int_{u=0}^{b} \left(1 - \frac{u}{b}\right)^2 du\right] \left[\int_{v=b}^{\infty} e^{-\frac{2\alpha\, v}{b}}\, dv\right] \\ &= A^2\, \sec\theta \left[\frac{b}{3}\right] \left[\frac{b}{2\alpha}\, e^{-2\alpha}\right] = C_1 \end{aligned} \tag{143}$$

For the channel C_7: The trial function is taken as

$$\phi_7(x', y') = A \left(1 - \frac{x'}{b}\right) e^{\frac{\alpha\, y'}{b}} \tag{144}$$

and the region of integration are from $x' = 0$ to $x' = b$ and $y' = -\infty$ to $y' = -b$. Hence,

$$\begin{aligned} C_7 &= \int_{x'=0}^{b} \int_{y'=-\infty}^{-b} \phi_7^*(x', y')\, \phi_7(x', y')\, \sec\theta\, dx'\, dy' \\ &= A^2\, \sec\theta \int_{x'=0}^{b} \int_{y'=-\infty}^{-b} \left(1 - \frac{x'}{b}\right)^2 e^{\frac{2\alpha\, y'}{b}}\, dx'\, dy' \\ &= A^2\, \sec\theta \left[\int_{x'=0}^{b} \left(1 - \frac{x'}{b}\right)^2 dx'\right] \left[\int_{y'=-\infty}^{-b} e^{\frac{2\alpha\, y'}{b}}\, dy'\right] \end{aligned} \tag{145}$$

Let $v = -y'$, so that $dv = -dy'$, therefore, when $y' = -b, v = b$ and when $y' = -\infty, v = \infty$. Therefore,

$$\begin{aligned} C_7 &= A^2\, \sec\theta \left[\int_{x'=0}^{b} \left(1 - \frac{x'}{b}\right)^2 dx'\right] \left[\int_{v=b}^{\infty} e^{\frac{-2\alpha\, v}{b}}\, dv\right] \\ &= A^2\, \sec\theta \left[\frac{b}{3}\right] \left[\frac{b}{2\alpha}\, e^{-2\alpha}\right] = C_1 \end{aligned} \tag{146}$$

For the channel C_8: The trial function is taken as

$$\phi_8(x', y') = A \left(1 + \frac{y'}{b}\right) e^{\frac{-\alpha\, x'}{b}} \tag{147}$$

and the region of integration are from $x' = b$ to $x' = \infty$ and $y' = -b$ to $y' = 0$. Hence,

$$\begin{aligned} C_8 &= \int_{x'=b}^{\infty}\int_{y'=-b}^{0} \phi_8^*(x',y')\,\phi_8(x',y')\,\sec\theta\,dx'\,dy' \\ &= A^2\,\sec\theta\int_{x'=b}^{\infty}\int_{y'=-b}^{0}\left(1+\frac{y'}{b}\right)^2 e^{\frac{-2\alpha\,x'}{b}}\,dx'\,dy' \\ &= A^2\,\sec\theta\left[\int_{x'=b}^{\infty} e^{\frac{-2\alpha\,x'}{b}}\,dx'\right]\left[\int_{y'=-b}^{0}\left(1+\frac{y'}{b}\right)^2\,dy'\right] \end{aligned} \tag{148}$$

Let $v = -y'$, so that $dv = -dy'$, therefore, when $y' = 0, v = 0$ and when $y' = -b, v = b$. Therefore,

$$\begin{aligned} C_8 &= A^2\,\sec\theta\left[\int_{x'=b}^{\infty} e^{\frac{-2\alpha\,x'}{b}}\,dx'\right]\left[\int_{v=0}^{b}\left(1-\frac{v}{b}\right)^2\,dv\right] \\ &= A^2\,\sec\theta\left[\frac{b}{2\alpha}\,e^{-2\alpha}\right]\left[\frac{b}{3}\right] = C_1 \end{aligned} \tag{149}$$

The total contribution to the normalization integral from the channels C_n is given by

$$\begin{aligned} J_1 &= \sum_{i=1}^{8} C_i \\ &= 8\,C_1 \\ &= 8\left(\frac{A^2}{6\alpha}\,b^2\,\sec\theta\,e^{-2\alpha}\right) \\ &= \frac{4\,A^2}{3\,\alpha}\,b^2\,\sec\theta\,e^{-2\alpha} \end{aligned} \tag{150}$$

Hence, from the normalization condition we have,

$$\begin{aligned} I_1 + J_1 &= 1 \\ \frac{22}{9}\,A^2\,b^2\,\sec\theta\,e^{-2\alpha} + \frac{4\,A^2}{3\,\alpha}\,b^2\,\sec\theta\,e^{-2\alpha} &= 1 \\ \frac{2\,A^2\,b^2\,\sec\theta\,e^{-2\alpha}}{9\,\alpha}\,(11\alpha+6) &= 1 \\ A^2 &= \frac{9\,\alpha\,e^{2\alpha}}{2\,b^2\,(11\alpha+6)\,\sec\theta} \\ A &= \sqrt{\frac{9\,\alpha\,e^{2\alpha}}{2\,b^2\,(11\alpha+6)\,\sec\theta}} \end{aligned} \tag{151}$$

This is the required normalization constant for the given set of trial functions.

IX. APPENDIX II

A. Calculation of channel integrals

For the regions C_n (n=1 to 8)

For channel C_1: $x' = b$ to $x' = \infty$ and $y' = 0$ to $y' = b$, $x', y' > 0$

$$\varphi_1 = A\left(1 - \frac{y'}{b}\right) e^{\frac{-\alpha x'}{b}}$$

and

$$\hat{H} \equiv \frac{-\hbar^2}{2m}\left(\frac{\partial^2}{\partial x'^2} + \frac{\partial^2}{\partial y'^2} - 2\sin\theta \frac{\partial^2}{\partial x' \partial y'}\right) \tag{152}$$

$$\begin{aligned}
\frac{\partial \varphi_3}{\partial y'} &= A\left(\frac{-\alpha}{b}\right)\left(1 + \frac{x'}{b}\right) e^{\frac{-\alpha y'}{b}} \\
\frac{\partial^2 \varphi_3}{\partial y'^2} &= A\left(\frac{\alpha}{b}\right)^2 \left(1 + \frac{y'}{b}\right) e^{\frac{-\alpha y'}{b}} \\
\frac{\partial^2 \varphi_3}{\partial x'^2} &= 0 \\
\frac{\partial^2 \varphi_3}{\partial x' \partial y'} &= -\frac{A\alpha}{b^2} e^{\frac{-\alpha y'}{b}} \\
\hat{H}\varphi_3 &= \frac{-\hbar^2 A\alpha}{2m\, b^2}\left[\alpha\left(1 + \frac{x'}{b}\right) + 2\sin\theta\right] e^{\frac{-\alpha y'}{b}}
\end{aligned}$$

Hence, the matrix element of $\hat{H}$ is given by

$$\begin{aligned}
J_{C1} &= \langle \varphi_1(x', y') | \hat{H} | \varphi_1(x', y') \rangle \\
&= \frac{-\hbar^2 A^2 \alpha}{2mb^2} \int_{x'=b}^{\infty} \int_{y'=0}^{b} \left(1 - \frac{y'}{b}\right) e^{\frac{-\alpha x'}{b}} \left[\alpha\left(1 - \frac{y'}{b}\right) - 2\sin\theta\right] \sec\theta\, dx' dy' \\
&= \frac{-\hbar^2 A^2 \alpha}{2mb^2} \int_{x'=b}^{\infty} e^{\frac{-\alpha x'}{b}} dx' \int_{y'=0}^{b} \left(1 - \frac{y'}{b}\right) \left[\alpha\left(1 - \frac{y'}{b}\right) - 2\sin\theta\right] dy' \\
&= \frac{-\hbar^2 A^2 \alpha \sec\theta}{2mb^2} \left[\frac{b}{2\alpha} e^{-2\alpha}\right] \left[\alpha\left(\frac{b}{3}\right) - 2\sin\theta\left(\frac{b}{2}\right)\right] \\
&= \frac{-\hbar^2 A^2 e^{-2\alpha} \sec\theta}{4m} \left[\frac{\alpha}{3} - \sin\theta\right]
\end{aligned} \tag{153}$$

For channel C_2: $x' = 0$ to $x' = b$ and $y' = b$ to $y' = \infty$, $x', y' > 0$

$$\varphi_2 = A\left(1 - \frac{x'}{b}\right) e^{\frac{-\alpha y'}{b}} \tag{154}$$

From symmetry, it is clear that $J_{C2} = J_{C1}$.

For channel C_3: $x' = -b$ to $x' = 0$ and $y' = b$ to $y' = \infty$, $x' < 0, y' > b$

$$\varphi_3 = A\left(1 + \frac{x'}{b}\right) e^{\frac{-\alpha y'}{b}} \tag{155}$$

and

$$\begin{aligned}
\frac{\partial \varphi_3}{\partial y'} &= A\left(\frac{-\alpha}{b}\right)\left(1 + \frac{x'}{b}\right) e^{\frac{-\alpha y'}{b}} \\
\frac{\partial^2 \varphi_3}{\partial y'^2} &= A\left(\frac{\alpha}{b}\right)^2\left(1 + \frac{y'}{b}\right) e^{\frac{-\alpha y'}{b}} \\
\frac{\partial^2 \varphi_3}{\partial x'^2} &= 0 \\
\frac{\partial^2 \varphi_3}{\partial x' \partial y'} &= -\frac{A\alpha}{b^2} e^{\frac{-\alpha y'}{b}} \\
\hat{H}\varphi_3 &= \frac{-\hbar^2 A\alpha}{2mb^2}\left[\alpha\left(1 + \frac{x'}{b}\right) + 2\sin\theta\right] e^{\frac{-\alpha y'}{b}}
\end{aligned}$$

Hence, the matrix element of $\hat{H}$ is given by

$$\begin{aligned}
J_{C3} &= \langle \varphi_3(x', y') | \hat{H} | \varphi_3(x', y') \rangle \\
&= \frac{-\hbar^2 A^2 \alpha}{2mb^2} \int_{x'=-b}^{0} \int_{y'=b}^{\infty} \left(1 + \frac{x'}{b}\right) e^{\frac{-\alpha y'}{b}} \left[\alpha\left(1 + \frac{x'}{b}\right) + 2\sin\theta\right] \sec\theta \, dx' dy' \\
&= \frac{-\hbar^2 A^2 \alpha \sec\theta}{2mb^2} \int_{y'=b}^{\infty} e^{\frac{-2\alpha y'}{b}} dy' \int_{x'=-b}^{0} \left(1 + \frac{x'}{b}\right) \left[\alpha\left(1 + \frac{x'}{b}\right) + 2\sin\theta\right] dx'
\end{aligned}$$

Let $u = -x'$, so that $du = -dx'$, therefore, when $x' = 0, u = 0$ and when $x' = -b, u = b$. Therefore

$$\begin{aligned}
J_{C3} &= \frac{\hbar^2 A^2 \alpha \sec\theta}{2mb^2} \int_{y'=b}^{\infty} e^{\frac{-2\alpha y'}{b}} dy' \int_{u=b}^{0} \left(1 - \frac{u}{b}\right) \left[\alpha\left(1 - \frac{u}{b}\right) + 2\sin\theta\right] du \\
&= \frac{-\hbar^2 A^2 \alpha \sec\theta}{2mb^2} \int_{y'=b}^{\infty} e^{\frac{-2\alpha y'}{b}} dy' \int_{u=0}^{b} \left(1 - \frac{u}{b}\right) \left[\alpha\left(1 - \frac{u}{b}\right) + 2\sin\theta\right] du \\
&= \frac{-\hbar^2 A^2 \alpha \sec\theta}{2mb^2} \left[\frac{b}{2\alpha} e^{-2\alpha}\right] \left[\alpha\left(\frac{a}{3}\right) + 2\sin\theta\left(\frac{b}{2}\right)\right] \\
&= \frac{-\hbar^2 A^2 e^{-2\alpha} \sec\theta}{4m} \left[\frac{\alpha}{3} + \sin\theta\right]
\end{aligned} \tag{156}$$

For channel C_4: $x' = -\infty$ to $x' = -b$ and $y' = 0$ to $y' = b$, $x' < 0, y' > 0$

$$\varphi_4 = A\left(1 - \frac{y'}{b}\right) e^{\frac{\alpha x'}{b}} \tag{157}$$

From symmetry, it is clear that $J_{C4} = J_{C3}$.

For channel C_5: $x' = -\infty$ to $x' = -b$ and $y' = -b$ to $y' = 0$, $x', y' < 0$

$$\varphi_5 = A\left(1 + \frac{y'}{b}\right) e^{\frac{\alpha x'}{b}} \tag{158}$$

and

$$\begin{aligned}
\frac{\partial \varphi_5}{\partial x'} &= A\left(\frac{\alpha}{b}\right)\left(1 + \frac{y'}{b}\right) e^{\frac{\alpha x'}{b}} \\
\frac{\partial^2 \varphi_5}{\partial x'^2} &= A\left(\frac{\alpha}{b}\right)^2\left(1 + \frac{y'}{b}\right) e^{\frac{\alpha x'}{b}} \\
\frac{\partial^2 \varphi_5}{\partial y'^2} &= 0 \\
\frac{\partial^2 \varphi_5}{\partial x' \partial y'} &= \frac{A\alpha}{b^2} e^{\frac{\alpha x'}{b}} \\
\hat{H}\varphi_5 &= \frac{-\hbar^2 A\alpha}{2mb^2}\left[\alpha\left(1 + \frac{y'}{b}\right) - 2\sin\theta\right] e^{\frac{\alpha x'}{b}}
\end{aligned}$$

Hence, the matrix element of $\hat{H}$ is given by

$$\begin{aligned}
J_{C5} &= \langle \varphi_5(x', y') | \hat{H} | \varphi_5(x', y') \rangle \\
&= \frac{-\hbar^2 A^2 \alpha}{2mb^2} \int_{x'=-\infty}^{-b} \int_{y'=-b}^{0} \left(1 + \frac{y'}{b}\right) e^{\frac{\alpha x'}{b}} \left[\alpha\left(1 + \frac{y'}{b}\right) - 2\sin\theta\right] \sec\theta \, dx' dy' \\
&= \frac{-\hbar^2 A^2 \alpha \sec\theta}{2mb^2} \int_{x'=-\infty}^{-b} e^{\frac{2\alpha x'}{b}} dx' \int_{y'=-b}^{0} \left(1 + \frac{y'}{b}\right) \left[\alpha\left(1 + \frac{y'}{b}\right) - 2\sin\theta\right] dy'
\end{aligned}$$

Let $u = -x'$, so that $du = -dx'$, therefore, when $x' = -b, u = b$ and when $x' = -\infty, u = \infty$. also, let $v = -y'$, so that $dv = -dy'$, therefore, when $y' = -b, v = b$ and when $y' = 0, v = 0$. Therefore,

$$\begin{aligned}
J_{C5} &= \frac{-\hbar^2 A^2 \alpha \sec\theta}{2mb^2} \int_{u=\infty}^{b} e^{\frac{-2\alpha u}{b}} du \int_{v=b}^{0} \left(1 - \frac{v}{b}\right) \left[\alpha\left(1 - \frac{v}{b}\right) - 2\sin\theta\right] dv \\
&= \frac{-\hbar^2 A^2 \alpha \sec\theta}{2mb^2} \int_{u=b}^{\infty} e^{\frac{-2\alpha u}{b}} du \int_{v=0}^{b} \left(1 - \frac{v}{b}\right) \left[\alpha\left(1 - \frac{v}{b}\right) - 2\sin\theta\right] dv \\
&= \frac{-\hbar^2 A^2 \alpha \sec\theta}{2mb^2} \left[\frac{b}{2\alpha} e^{-2\alpha}\right] \left[\alpha\left(\frac{b}{3}\right) - 2\sin\theta\left(\frac{b}{2}\right)\right] \\
&= \frac{-\hbar^2 A^2 e^{-2\alpha} \sec\theta}{4m} \left[\frac{\alpha}{3} - \sin\theta\right]
\end{aligned} \tag{159}$$

For channel C_6: $x' = -b$ to $x' = 0$ and $y' = -\infty$ to $y' = -b$, $x' < 0, y' < 0$

$$\varphi_6 = A\left(1 + \frac{x'}{b}\right) e^{\frac{\alpha y'}{b}} \tag{160}$$

From symmetry, it is clear that $J_{C6} = J_{C5}$.

For channel C_7: $x' = 0$ to $x' = b$ and $y' = -\infty$ to $y' = -b$, $x' > 0, y' < 0$

$$\varphi_7 = A\left(1 - \frac{x'}{b}\right) e^{\frac{\alpha y'}{b}} \tag{161}$$

and

$$\begin{aligned}
\frac{\partial \varphi_7}{\partial y'} &= A\left(\frac{\alpha}{b}\right)\left(1 - \frac{x'}{b}\right) e^{\frac{\alpha y'}{b}} \\
\frac{\partial^2 \varphi_7}{\partial y'^2} &= A\left(\frac{\alpha}{b}\right)^2\left(1 - \frac{x'}{b}\right) e^{\frac{\alpha y'}{b}} \\
\frac{\partial^2 \varphi_7}{\partial x'^2} &= 0 \\
\frac{\partial^2 \varphi_7}{\partial x' \partial y'} &= -\frac{A\alpha}{b^2} e^{\frac{\alpha y'}{b}} \\
\hat{H}\varphi_7 &= \frac{-\hbar^2 A\alpha}{2mb^2}\left[\alpha\left(1 - \frac{x'}{b}\right) + 2\sin\theta\right] e^{\frac{\alpha y'}{b}}
\end{aligned}$$

Hence the matrix element of $\hat{H}$ is given by

$$\begin{aligned}
J_{C7} &= \langle \varphi_7(x', y') | \hat{H} | \varphi_7(x', y') \rangle \\
&= \frac{-\hbar^2 A^2 \alpha}{2mb^2} \int_{x'=0}^{b} \int_{y'=-\infty}^{-b} \left(1 - \frac{x'}{b}\right) e^{\frac{2\alpha y'}{b}} \left[\alpha\left(1 - \frac{x'}{b}\right) + 2\sin\theta\right] \sec\theta \, dx' dy' \\
&= \frac{-\hbar^2 A^2 \alpha \sec\theta}{2mb^2} \int_{y'=-\infty}^{-b} e^{\frac{2\alpha y'}{b}} dy' \int_{x'=0}^{b} \left(1 - \frac{x'}{b}\right) \left[\alpha\left(1 - \frac{x'}{b}\right) + 2\sin\theta\right] dx'
\end{aligned}$$

Let $v = -y'$, so that $dv = -dy'$, therefore, when $y' = -\infty, v = \infty$ and when $y' = -b, v = b$. Therefore,

$$\begin{aligned}
J_{C7} &= \frac{\hbar^2 A^2 \alpha \sec\theta}{2mb^2} \int_{v=\infty}^{b} e^{\frac{-2\alpha v}{b}} dv \int_{x'=0}^{b} \left(1 - \frac{x'}{b}\right) \left[\alpha\left(1 - \frac{x'}{b}\right) + 2\sin\theta\right] dx' \\
&= \frac{-\hbar^2 A^2 \alpha \sec\theta}{2mb^2} \int_{v=b}^{\infty} e^{\frac{-2\alpha v}{b}} dv \int_{x'=0}^{b} \left(1 - \frac{x'}{b}\right) \left[\alpha\left(1 - \frac{x'}{b}\right) + 2\sin\theta\right] dx' \\
&= \frac{-\hbar^2 A^2 \alpha \sec\theta}{2mb^2} \left[\frac{b}{2\alpha} e^{-2\alpha}\right] \left[\alpha\left(\frac{b}{3}\right) + 2\sin\theta\left(\frac{b}{2}\right)\right] \\
&= \frac{-\hbar^2 A^2 e^{-2\alpha} \sec\theta}{4m} \left[\frac{\alpha}{3} + \sin\theta\right]
\end{aligned} \tag{162}$$

For channel C_8: $x' = b$ to $x' = \infty$ and $y' = -b$ to $y' = 0$, $x' > 0, y' < 0$

$$\varphi_8 = A\left(1 + \frac{y'}{b}\right) e^{-\frac{\alpha x'}{b}} \tag{163}$$

From symmetry, it is clear that $J_{C8} = J_{C7}$ and therefore

$$J_{C1} = J_{C2} = J_{C5} = J_{C6}$$

and

$$J_{C3} = J_{C4} = J_{C7} = J_{C8}$$

The total the matrix element of $\hat{H}$ is given by for the channels C_n is given by

$$\begin{aligned}
\langle H \rangle_C &= J_{C1} + J_{C2} + J_{C3} + J_{C4} + J_{C5} + J_{C6} + J_{C7} + J_{C8} \\
&= 2J_{C1} + 2J_{C3} + 2J_{C5} + 2J_{C7} \\
&= 4\left(J_{C1} + J_{C3}\right) \\
&= 4\left(\frac{-\hbar^2 A^2 e^{-2\alpha}\sec\theta}{4m}\left[\frac{\alpha}{3} - \sin\theta\right] + \frac{-\hbar^2 A^2 e^{-2\alpha}\sec\theta}{4m}\left[\frac{\alpha}{3} + \sin\theta\right]\right) \\
&= \frac{-2\hbar^2 A^2 \alpha e^{-2\alpha}\sec\theta}{3m}
\end{aligned} \tag{164}$$

B. Calculation of rhombus integrals

For the regions R_n (n=1 to 4)

For oblique quadrant R_1: $x' = 0$ to $x' = b$ and $y' = 0$ to $y' = b$ $\quad x', y' > 0$

$$\varphi_1 = A\left(1 - \frac{x'\,y'}{b^2}\right) e^{-\alpha} \tag{165}$$

and the Hamiltonian operator is given by

$$\hat{H} \equiv \frac{-\hbar^2}{2m}\left(\frac{\partial^2}{\partial x'^2} + \frac{\partial^2}{\partial y'^2} - 2\,\sin\theta \frac{\partial^2}{\partial x'\partial y'}\right) \tag{166}$$

So we have

$$\begin{aligned}
\frac{\partial\varphi_1}{\partial x'} &= -\frac{A}{b^2}\,y'\,e^{-\alpha} \\
\frac{\partial^2\varphi_1}{\partial x'\,\partial y'} &= -\frac{A}{b^2}\,e^{-\alpha} \\
\frac{\partial^2\varphi_1}{\partial x'^2} &= 0 \\
\frac{\partial^2\varphi_1}{\partial y'^2} &= 0
\end{aligned}$$

$$\begin{aligned}
\hat{H}\varphi_1 &= \frac{-\hbar^2}{2m}\left(-2\,\sin\theta\,(-\frac{A}{b^2}\,e^{-\alpha})\right) \\
&= -\frac{A\,\hbar^2\,\sin\theta}{m\,b^2}\,e^{-\alpha}
\end{aligned}$$

Hence the matrix element of $\hat{H}$ is given by

$$\begin{aligned} I_{R_1} &= \langle \varphi_1(x', y') | \hat{H} | \varphi_1(x', y') \rangle \\ &= -\frac{A\,\hbar^2\,\sin\theta}{m\,b^2}\,e^{-\alpha}\int_{x'=0}^{b}\int_{y'=0}^{b} A\left(1-\frac{x'y'}{b^2}\right)\,e^{-\alpha}\,\sec\theta\,dx'\,dy' \\ &= -\frac{A^2\,\hbar^2\,\sin\theta\sec\theta}{m\,b^2}\,e^{-2\alpha}\int_{x'=0}^{b}\int_{y'=0}^{b}\left(1-\frac{x'y'}{b^2}\right)\,dx'\,dy' \\ &= -\frac{A^2\,\hbar^2\,\sin\theta\sec\theta}{m\,b^2}\,e^{-2\alpha}\left(b^2-\frac{b^2}{4}\right) \\ &= -\frac{3\hbar^2\,A^2}{4\,m}\,\sin\theta\sec\theta\,e^{-2\alpha} \end{aligned} \tag{167}$$

For oblique quadrant R_2: $x' = -b$ to $x' = 0$ and $y' = 0$ to $y' = b \quad x' < 0, y' > 0$

$$\varphi_2 = A\left(1+\frac{x'y'}{b^2}\right)\,e^{-\alpha} \tag{168}$$

Hence, we get

$$\begin{aligned} \frac{\partial\varphi_2}{\partial x'} &= \frac{A}{b^2}\,y'\,e^{-\alpha} \\ \frac{\partial^2\varphi_2}{\partial x'\,\partial y'} &= \frac{A}{b^2}\,e^{-\alpha} \\ \frac{\partial^2\varphi_2}{\partial x'^2} &= 0 \\ \frac{\partial^2\varphi_2}{\partial y'^2} &= 0 \end{aligned}$$

$$\begin{aligned} \hat{H}\varphi_2 &= \frac{-\hbar^2}{2m}\left(-2\,\sin\theta\,(\frac{A}{b^2}\,e^{-\alpha})\right) \\ &= \frac{A\,\hbar^2\,\sin\theta}{m\,b^2}\,e^{-\alpha} \end{aligned}$$

Hence, the matrix element of $\hat{H}$ is given by

$$\begin{aligned} I_{R_2} &= \langle \varphi_2(x', y') | \hat{H} | \varphi_2(x', y') \rangle \\ &= \frac{A\,\hbar^2\,\sin\theta}{m\,b^2}\,e^{-\alpha}\int_{x'=-b}^{0}\int_{y'=0}^{b} A\left(1+\frac{x'y'}{b^2}\right)\,e^{-\alpha}\,\sec\theta\,dx'\,dy' \\ &= \frac{A^2\,\hbar^2\,\sin\theta\sec\theta}{m\,b^2}\,e^{-2\alpha}\int_{x'=-b}^{0}\int_{y'=0}^{b}\left(1+\frac{x'y'}{b^2}\right)\,dx'\,dy' \end{aligned}$$

Let $u = -x'$, so that $du = -dx'$, therefore, when $x' = 0, u = 0$ and when $x' = -b, u = b$. Therefore

$$I_{R2} = -\frac{A^2\,\hbar^2\,\sin\theta\sec\theta}{m\,b^2}\,e^{-2\alpha}\int_{u=b}^{0}\int_{y'=0}^{b}\left(1-\frac{uy'}{b^2}\right)\,du\,dy'$$

$$= \frac{A^2\,\hbar^2\,\sin\theta\sec\theta}{m\,b^2}\,e^{-2\alpha}\int_{u=0}^{b}\int_{y'=0}^{b}\left(1-\frac{u\,y'}{b^2}\right)\,du\,dy'$$
$$= -I_{R_1} \tag{169}$$

For oblique quadrant R_3: $x' = -b$ to $x' = 0$ and $y' = -b$ to $y' = 0 \quad x' < 0, y' < 0$

$$\varphi_3 = A\left(1-\frac{x'y'}{b^2}\right)\,e^{-\alpha} \tag{170}$$

$$\frac{\partial\varphi_3}{\partial x'} = -\frac{A}{b^2}\,y'\,e^{-\alpha}$$
$$\frac{\partial^2\varphi_3}{\partial x'\,\partial y'} = -\frac{A}{b^2}\,e^{-\alpha}$$
$$\frac{\partial^2\varphi_3}{\partial x'^2} = 0$$
$$\frac{\partial^2\varphi_3}{\partial y'^2} = 0$$

$$\hat{H}\varphi_3 = \frac{-\hbar^2}{2m}\left(-2\,\sin\theta\,(-\frac{A}{b^2}\,e^{-\alpha})\right)$$
$$= -\frac{A\,\hbar^2\,\sin\theta}{m\,b^2}\,e^{-\alpha}$$

Hence the matrix element of $\hat{H}$ is given by

$$I_{R3} = \langle\varphi_3(x',y')|\hat{H}|\varphi_3(x',y')\rangle$$
$$= -\frac{A\,\hbar^2\,\sin\theta}{m\,b^2}\,e^{-\alpha}\int_{x'=-b}^{0}\int_{y'=-b}^{0}A\left(1-\frac{x'y'}{b^2}\right)\,e^{-\alpha}\,\sec\theta\,dx'\,dy'$$
$$= -\frac{A^2\,\hbar^2\,\sin\theta\sec\theta}{m\,b^2}\,e^{-2\alpha}\int_{x'=-b}^{0}\int_{y'=-b}^{0}\left(1-\frac{x'y'}{b^2}\right)\,dx'\,dy'$$

Let $u = -x'$, so that $du = -dx'$, therefore, when $x' = 0, u = 0$ and when $x' = -b, u = b$. also, let $v = -y'$, so that $dv = -dy'$, therefore, when $y' = 0, v = 0$ and when $y' = -b, v = b$. Therefore, we get

$$I_{R_3} = -\frac{A^2\,\hbar^2\,\sin\theta\sec\theta}{m\,b^2}\,e^{-2\alpha}\int_{u=b}^{0}\int_{v=b}^{0}\left(1-\frac{uv}{b^2}\right)\,du\,dv$$
$$= -\frac{A^2\,\hbar^2\,\sin\theta\sec\theta}{m\,b^2}\,e^{-2\alpha}\int_{u=0}^{b}\int_{v=0}^{b}\left(1-\frac{uv}{b^2}\right)\,du\,dv$$
$$= I_{R_1} \tag{171}$$

For oblique quadrant R_4: $x' = 0$ to $x' = b$ and $y' = -b$ to $y' = 0 \quad x' > 0, y' < 0$

$$\varphi_4 = A\left(1+\frac{x'y'}{b^2}\right)\,e^{-\alpha} \tag{172}$$

$$\frac{\partial \varphi_4}{\partial x'} = \frac{A}{b^2}\, y'\, e^{-\alpha}$$
$$\frac{\partial^2 \varphi_4}{\partial x'\, \partial y'} = \frac{A}{b^2}\, e^{-\alpha}$$
$$\frac{\partial^2 \varphi_4}{\partial x'^2} = 0$$
$$\frac{\partial^2 \varphi_2}{\partial y'^2} = 0$$

$$\begin{aligned}\hat{H}\varphi_4 &= \frac{-\hbar^2}{2m}\left(-2\,\sin\theta\,(\frac{A}{b^2}\,e^{-\alpha})\right)\\ &= \frac{A\,\hbar^2\,\sin\theta}{m\,b^2}\,e^{-\alpha}\end{aligned}$$

Hence, the matrix element of $\hat{H}$ is given by

$$\begin{aligned}I_{R_4} &= \langle\varphi_4(x',y')|\hat{H}|\varphi_4(x',y')\rangle\\ &= \frac{A\,\hbar^2\,\sin\theta}{m\,b^2}\,e^{-\alpha}\int_{x'=0}^{b}\int_{y'=-b}^{0} A\left(1+\frac{x'y'}{b^2}\right)\,e^{-\alpha}\,\sec\theta\,dx'\,dy'\\ &= \frac{A^2\,\hbar^2\,\sin\theta\sec\theta}{m\,b^2}\,e^{-2\alpha}\int_{x'=0}^{b}\int_{y'=-b}^{0}\left(1+\frac{x'y'}{b^2}\right)\,dx'\,dy'\end{aligned}$$

Let $v = -y'$, so that $dv = -dy'$, therefore, when $y' = 0, v = 0$ and when $y' = -b, v = b$. Therefore, we have

$$\begin{aligned}I_{R4} &= -\frac{A^2\,\hbar^2\,\sin\theta\sec\theta}{m\,b^2}\,e^{-2\alpha}\int_{x'=0}^{b}\int_{v=b}^{0}\left(1-\frac{x'v}{b^2}\right)\,dx'\,dv\\ &= \frac{A^2\,\hbar^2\,\sin\theta\sec\theta}{m\,b^2}\,e^{-2\alpha}\int_{x'=0}^{b}\int_{v=0}^{b}\left(1-\frac{x'v}{b^2}\right)\,dx'\,dv\\ &= -I_{R_1}\end{aligned} \tag{173}$$

The total the matrix element of $\hat{H}$ is given by for the region R_n is given by

$$\begin{aligned}\langle H\rangle_R &= I_{R_1} + I_{R_2} + I_{R_3} + I_{R_4}\\ &= I_{R1} - I_{R_1} + I_{R_1} - I_{R_1}\\ &= 0\end{aligned} \tag{174}$$

X. APPENDIX III

A. Calculation of matrix elements for outer four arms

The outer four arms are defined by the following conditions:

$$\begin{aligned} x' = b \quad &\text{to} \quad x' = \infty, y' = 0 \\ x' = -\infty \quad &\text{to} \quad x' = -b, y' = 0 \\ y' = b \quad &\text{to} \quad y' = \infty, x' = 0 \\ y' = -\infty \quad &\text{to} \quad y' = -b, x' = 0 \end{aligned}$$

For the right arm, $x' = b$ to $x' = \infty, y' = 0$ and the trial function near its proximity is given by

$$\psi_1 = A \left(1 - \frac{|y'|}{b}\right) e^{\frac{-\alpha\, x'}{b}} \tag{175}$$

The Hamiltonian operator is given by

$$\hat{H} \equiv \frac{-\hbar^2}{2m} \left(\frac{\partial^2}{\partial x'^2} + \frac{\partial^2}{\partial y'^2} - 2\, \sin\theta \frac{\partial^2}{\partial x' \partial y'}\right) \tag{176}$$

As there is no discontinuity in the derivative of ψ_1 with respect to x', $\frac{\partial^2}{\partial x'^2}$ contribution is not taken in the calculation of matrix element of $\hat{H}$ in this roof line as it is already taken into account in the bulk integration. Hence, we have to consider $\hat{H}$ as

$$\hat{H} \equiv \frac{-\hbar^2}{2m} \left(\frac{\partial^2}{\partial y'^2} - 2\, \sin\theta \frac{\partial^2}{\partial x' \partial y'}\right) \tag{177}$$

Using,$|y'|$=$y'\,[\theta(y') - \theta(-y')]$, and $\delta(y') = \delta(-y')$ we get,

$$\begin{aligned} \frac{\partial}{\partial y'} \left(1 - \frac{|y'|}{b}\right) &= \frac{-1}{b}\, [\theta(y') - \theta(-y')] \\ \frac{\partial^2}{\partial y'^2} \left(1 - \frac{|y'|}{b}\right) &= \frac{-1}{b}\, [\delta(y') + \delta(-y')] \\ &= \frac{-2}{b}\, \delta(y') \\ \frac{\partial}{\partial x'} \left(1 - \frac{|y'|}{b}\right) e^{\frac{-\alpha\, x'}{b}} &= \frac{-\alpha}{b} \left(1 - \frac{|y'|}{b}\right) e^{\frac{-\alpha\, x'}{b}} \\ \frac{\partial^2}{\partial x' \partial y'} \left(1 - \frac{|y'|}{b}\right) e^{\frac{-\alpha\, x'}{b}} &= \frac{\alpha}{b^2}\, [\theta(y') - \theta(-y')]\, e^{\frac{-\alpha\, x'}{b}} \\ \hat{H}\psi_1 &= A\, \frac{-\hbar^2}{2m} \left[\frac{-2}{b}\, \delta(y') - 2\, \sin\theta \frac{\alpha}{b^2}\, (\theta(y') - \theta(-y'))\right] e^{\frac{-\alpha\, x'}{b}} \end{aligned}$$

Hence, the first roof line integral can be evaluated as

$$
\begin{aligned}
K_1 &= \langle\psi_1(x',y')|\hat{H}|\psi_1(x',y')\rangle \\
&= \frac{-\hbar^2\,A^2}{2m}\int_{x'=b}^{\infty}\int_{y'=0-\epsilon}^{0+\epsilon}\left(1-\frac{|y'|}{b}\right)\,e^{\frac{-2\alpha\,x'}{b}}\left[\frac{-2}{b}\delta(y')-2\,\sin\theta\frac{\alpha}{b^2}\,(\theta(y')-\theta(-y'))\right]\sec\theta\,dx'dy' \\
&= \frac{-\hbar^2\,A^2}{2m}\int_{x'=b}^{\infty}\,e^{\frac{-2\alpha\,x'}{b}}\,dx'\int_{y'=-\epsilon}^{+\epsilon}\left(1-\frac{|y'|}{b}\right)\left[\frac{-2}{b}\,\delta(y')-\frac{2\,\alpha\,\sin\theta}{b^2}\,(\theta(y')-\theta(-y'))\right]\,dy' \\
&= \frac{-\hbar^2A^2}{2m}\left[\frac{b}{2\,\alpha}e^{-2\alpha}\right] \\
&\times\left[\int_{y'=-\epsilon}^{+\epsilon}\left(1-\frac{|y'|}{b}\right)\frac{-2}{b}\delta(y')dy'-\frac{2\alpha\sin\theta}{b^2}\int_{y'=-\epsilon}^{+\epsilon}\left(1-\frac{|y'|}{b}\right)(\theta(y')-\theta(-y'))\right]dy' \\
&= \frac{-\hbar^2\,A^2\sec\theta}{2m}\,\left[\frac{b}{2\,\alpha}\,e^{-2\alpha}\right]\left[-\frac{2}{b}-\frac{2\,\alpha}{b^2}\,(0)\right] \\
&= \frac{\hbar^2\,A^2\,e^{-2\alpha}\sec\theta}{2m\alpha}
\end{aligned}
\tag{178}
$$

For the left arm, $x'=-\infty$ to $x'=-b, y'=0$ and the trial function near its proximity is given by

$$\psi_2 = A\left(1-\frac{|y'|}{b}\right)\,e^{\frac{\alpha\,x'}{b}} \tag{179}$$

Using, $|y'|{=}y'\,[\theta(y')-\theta(-y')]$, and $\delta(y')=\delta(-y')$, we get

$$
\begin{aligned}
\frac{\partial}{\partial y'}\left(1-\frac{|y'|}{b}\right) &= \frac{-1}{b}\,[\theta(y')-\theta(-y')] \\
\frac{\partial^2}{\partial y'^2}\left(1-\frac{|y'|}{b}\right) &= \frac{-1}{b}\,[\delta(y')+\delta(-y')] \\
&= \frac{-2}{b}\,\delta(y') \\
\frac{\partial}{\partial x'}\left(1-\frac{|y'|}{b}\right)\,e^{\frac{\alpha\,x'}{b}} &= \frac{\alpha}{b}\,\left(1-\frac{|y'|}{b}\right)\,e^{\frac{\alpha\,x'}{b}} \\
\frac{\partial^2}{\partial x'\partial y'}\left(1-\frac{|y'|}{b}\right)\,e^{\frac{\alpha\,x'}{b}} &= -\frac{\alpha}{b^2}\,[\theta(y')-\theta(-y')]\,e^{\frac{\alpha\,x'}{b}} \\
\hat{H}\psi_2 &= A\,\frac{-\hbar^2}{2m}\left[\frac{-2}{b}\,\delta(y')+\frac{2\,\alpha\,\sin\theta}{b^2}\,(\theta(y')-\theta(-y'))\right]\,e^{\frac{-\alpha\,x'}{b}}
\end{aligned}
$$

Hence, the second roof line integral can be evaluated as

$$
\begin{aligned}
K_2 &= \langle\psi_2(x',y')|\hat{H}|\psi_2(x',y')\rangle \\
&= \frac{-\hbar^2\,A^2}{2m}\int_{x'=-\infty}^{-b}\int_{y'=0-\epsilon}^{0+\epsilon}\left(1-\frac{|y'|}{b}\right)\,e^{\frac{2\alpha\,x'}{b}} \\
&\times\left[\frac{-2}{b}\,\delta(y')+\frac{2\,\alpha\,\sin\theta}{b^2}\,(\theta(y')-\theta(-y'))\right]\sec\theta\,dx'\,dy'
\end{aligned}
$$

$$= \frac{-\hbar^2 A^2}{2m} \int_{x'=-\infty}^{-b} e^{\frac{2\alpha x'}{b}} dx' \int_{y'=-\epsilon}^{+\epsilon} \left(1 - \frac{|y'|}{b}\right) \times \left[\frac{-2}{b}\delta(y') + \frac{2\,\alpha\,\sin\theta}{b^2}\,(\theta(y') - \theta(-y'))\right] dy' \tag{180}$$

Using transformation $u = -x'$, so that $du = -dx'$, therefore, when $x' = -b, u = b$ and when $x' = -\infty, u = \infty$.

$$\begin{aligned}
K_2 &= -\frac{-\hbar^2 A^2 \sec\theta}{2m} \int_{u=\infty}^{b} e^{\frac{-2\alpha u}{b}} du \int_{y'=-\epsilon}^{+\epsilon} \left(1 - \frac{|y'|}{b}\right) \\
&\times \left[\frac{-2}{b}\delta(y') + \frac{2\alpha\sin\theta}{b^2}\,(\theta(y') - \theta(-y'))\right] dy' \\
&= \frac{-\hbar^2 A^2 \sec\theta}{2m} \int_{u=b}^{\infty} e^{\frac{-2\alpha u}{b}} du \int_{y'=-\epsilon}^{+\epsilon} \left(1 - \frac{|y'|}{b}\right) \\
&\times \left[\frac{-2}{b}\delta(y') + \frac{2\alpha\sin\theta}{b^2}\,(\theta(y') - \theta(-y'))\right] dy' \\
&= \frac{-\hbar^2 A^2 \sec\theta}{2m} \left[\frac{b}{2\alpha} e^{-2\alpha}\right] \\
&\times \left[\int_{y'=-\epsilon}^{+\epsilon} \left(1 - \frac{|y'|}{b}\right) \frac{-2}{b}\delta(y')\,dy' + \frac{2\alpha\sin\theta}{b^2} \int_{y'=-\epsilon}^{+\epsilon} \left(1 - \frac{|y'|}{b}\right) (\theta(y') - \theta(-y'))\right] dy' \\
&= \frac{-\hbar^2\,A^2 \sec\theta}{2m} \left[\frac{b}{2\alpha} e^{-2\alpha}\right] \left[-\frac{2}{b} + \frac{2\alpha}{b^2}\,(0)\right] \\
&= \frac{\hbar^2 A^2 e^{-2\alpha} \sec\theta}{2m\alpha} \\
&= K_1
\end{aligned} \tag{181}$$

For the top arm, $y' = b$ to $y' = \infty, x' = 0$ and the trial function is given by

$$\psi_3 = A\left(1 - \frac{|x'|}{b}\right) e^{\frac{-\alpha\,y'}{b}} \tag{182}$$

As there is no discontinuity in the derivative of ψ_3 with respect to y', $\frac{\partial^2}{\partial y'^2}$ contribution is not taken in the calculation of matrix element of $\hat{H}$ in this roof line as it is already taken into account in the bulk integration. Hence, we have to consider $\hat{H}$ as

$$\hat{H} \equiv \frac{-\hbar^2}{2m}\left(\frac{\partial^2}{\partial x'^2} - 2\,\sin\theta \frac{\partial^2}{\partial x' \partial y'}\right) \tag{183}$$

For the bottom arm, $y' = -\infty$ to $y' = -b, x' = 0$ and the trial function is given by

$$\psi_3 = A\left(1 - \frac{|x'|}{b}\right) e^{\frac{\alpha\,y'}{b}} \tag{184}$$

With simple analogy with K_1 and K_2 integrals, it is clear that $K_3 = K_1$ and $K_4 = K_1$. Hence,

$$\begin{aligned} K_I &= \sum_{i=1}^{4} K_i \\ &= 4\,K_1 \\ &= \frac{2\,\hbar^2\,A^2\,e^{-2\alpha}\sec\theta}{m\,\alpha} \end{aligned} \tag{185}$$

B. Calculation of matrix elements for inner four arms

The inner four arms are defined by the following equations:

$$\begin{aligned} x' = 0 \quad &\text{to} \quad x' = b, y' = 0 \\ x' = -b \quad &\text{to} \quad x' = 0, y' = 0 \\ y' = 0 \quad &\text{to} \quad y' = b, x' = 0 \\ y' = -b \quad &\text{to} \quad y' = 0, x' = 0 \end{aligned}$$

For the inner right arm, $x' = 0$ to $x' = b, y' = 0$ and the trial function is given by

$$\Psi_1 = A\left(1 - \frac{x'\,|y'|}{b^2}\right) e^{-\alpha} \tag{186}$$

As there is no discontinuity in the derivative of Ψ_1 with respect to x', $\frac{\partial^2}{\partial x'^2}$ contribution is not taken in the calculation of matrix element of $\hat{H}$ in this roof line as it is already taken into account in the bulk integration. Hence, we have to consider $\hat{H}$ as

$$\hat{H} \equiv \frac{-\hbar^2}{2m}\left(\frac{\partial^2}{\partial y'^2} - 2\,\sin\theta\,\frac{\partial^2}{\partial x'\partial y'}\right) \tag{187}$$

Note: Theta functions are the special class of functions which is defined by

$$\begin{aligned} \theta(x - x') &= 1 \quad \text{when} \quad (x - x') > 0 \\ &= 0 \quad \text{when} \quad (x - x') < 0 \end{aligned}$$

Also, another important property of theta function is it's derivative is Dirac-delta function, that is

$$\frac{d}{dx}\left(\theta(x - x')\right) = \delta(x - x')$$

and Dirac-delta function is defined by

$$\begin{aligned}\delta(x-x') &= 1 \quad \text{when} \quad x-x'=0\\ &= 0 \quad \text{when} \quad x-x'\neq 0\end{aligned}$$

In the following calculations, we make use of these properties of both functions to arrive at the result.

Using, $|y'|{=}y'\left[\theta(y')-\theta(-y')\right]$, and $\delta(y')=\delta(-y')$, we get

$$\begin{aligned}\frac{\partial^2\Psi_1}{\partial x'^2} &= 0\\ \frac{\partial^2\Psi_1}{\partial y'^2} &= -\frac{2Ax'}{b^2}\delta(y')e^{-\alpha}\\ \frac{\partial\Psi_1}{\partial x'} &= -\frac{Ae^{-\alpha}}{b^2}|y'|\\ \text{and} \qquad \frac{\partial^2\Psi_1}{\partial x'\partial y'} &= -\frac{Ae^{-\alpha}}{b^2}\left[\theta(y')-\theta(-y')\right]\\ \hat{H}\Psi_1 &= A\frac{-\hbar^2}{2m}\left[\frac{-2x'}{b}\delta(y')+\frac{2\cos\theta}{b^2}\left(\theta(y')-\theta(-y')\right)\right]e^{-\alpha}\end{aligned}$$

Hence, for this case the roof line integral can be evaluated as

$$\begin{aligned}L_1 &= \langle\Psi_1(x',y')|\hat{H}|\Psi_1(x',y')\rangle\\ &= \frac{-\hbar^2A^2\,e^{-2\alpha}}{2m}\int_{x'=0}^{b}\int_{y'=0-\epsilon}^{0+\epsilon}\left(1-\frac{x'|y'|}{b^2}\right)\\ &\times\left[\frac{-2x'}{b^2}\delta(y')+\frac{2\sin\theta}{b^2}\underbrace{\left(\theta(y')-\theta(-y')\right)}\right]\sec\theta dx'dy'\\ &= \frac{-\hbar^2A^2e^{-2\alpha}\sec\theta}{2m}\int_{x'=0}^{b}\left[\frac{-2\,x'}{b^2}+\frac{2\sin\theta}{b^2}\underbrace{(0)}\right]dx'\\ &= \frac{-\hbar^2A^2e^{-2\alpha}\sec\theta}{2m}\left[\left(\frac{-2}{b^2}\right)\int_{x'=0}^{b}x'dx'+0\right]\\ &= \frac{-\hbar^2A^2e^{-2\alpha}\sec\theta}{2m}\left[\left(\frac{-2}{b^2}\right)\frac{b^2}{2}\right]\\ &= \frac{\hbar^2A^2e^{-2\alpha}\sec\theta}{2m}\end{aligned} \tag{188}$$

For the inner left arm, $x'=-b$ to $x'=0, y'=0$ and the trial function is given by

$$\Psi_2 = A\left(1+\frac{x'\,|y'|}{b^2}\right)e^{-\alpha} \tag{189}$$

Using, $|y'|{=}y'\left[\theta(y')-\theta(-y')\right]$, and $\delta(y')=\delta(-y')$, we get

$$\frac{\partial^2\Psi_2}{\partial x'^2} = 0$$

$$\frac{\partial^2\Psi_2}{\partial y'^2} = \frac{2Ax'}{b^2}\delta(y')e^{-\alpha}$$
$$\frac{\partial\Psi_2}{\partial x'} = \frac{A\,e^{-\alpha}}{b^2}|y'|$$
$$\frac{\partial^2\Psi_2}{\partial x'\partial y'} = \frac{Ae^{-\alpha}}{b^2}\left[\theta(y') - \theta(-y')\right]$$
$$\hat{H}\Psi_2 = A\,\frac{-\hbar^2}{2m}\left[\frac{2\,x'}{b}\,\delta(y') - \frac{2\sin\theta}{b^2}\left(\theta(y') - \theta(-y')\right)\right]e^{-\alpha}$$

The roof line integral can be obtained as

$$\begin{aligned}
L_2 &= \langle\Psi_2(x',y')|\hat{H}|\Psi_2(x',y')\rangle \\
&= \frac{-\hbar^2A^2e^{-2\alpha}}{2m}\int_{x'=-b}^{0}\int_{y'=0-\epsilon}^{0+\epsilon}\left(1+\frac{x'|y'|}{b^2}\right) \\
&\times\left[\frac{2x'}{b^2}\delta(y') - \frac{2\sin\theta}{b^2}\underbrace{\left(\theta(y')-\theta(-y')\right)}\right]\sec\theta dx'dy' \\
&= \frac{-\hbar^2A^2e^{-2\alpha}\sec\theta}{2m}\int_{x'=b}^{0}\left[\frac{2x'}{b^2} - \frac{2\sin\theta}{b^2}\underbrace{(0)}\right]dx'
\end{aligned}$$

Using substitution $u=-x'$, so that $du=-dx'$, therefore, when $x'=-b, u=b$ and when $x'=0, u=0$.

$$\begin{aligned}
&= \frac{\hbar^2A^2e^{-2\alpha}\sec\theta}{2m}\left[\left(-\frac{2}{b^2}\right)\int_{u=b}^{0}u\,du+0\right] \\
&= \frac{\hbar^2A^2e^{-2\alpha}\sec\theta}{2m}\left[\left(\frac{2}{b^2}\right)\int_{u=0}^{b}u\,du\right] \\
&= \frac{\hbar^2A^2e^{-2\alpha}\sec\theta}{2m}\left[\left(\frac{2}{b^2}\right)\frac{b^2}{2}\right] \\
&= \frac{\hbar^2A^2e^{-2\alpha}\sec\theta}{2m} \\
&= L_1
\end{aligned} \tag{190}$$

For the inner top arm, $y'=0$ to $y'=b, x'=0$ and the trial function is given by

$$\Psi_3 = A\left(1-\frac{|x'|\,y'}{b^2}\right)e^{-\alpha} \tag{191}$$

In the same analogy as integral L_1, it can be shown that integral for the inner top arm $L_3=L_1$. For the inner bottom arm, $y'=-b$ to $y'=0, x'=0$ and the trial function is given by

$$\Psi_4 = A\left(1+\frac{|x'|\,y'}{b^2}\right)e^{-\alpha} \tag{192}$$

With the same calculations as integral L_2, it can be shown that integral for the inner bottom arm $L_4 = L_2$. Hence,

$$\begin{aligned} K_{II} &= \sum_{i=1}^{4} L_i \\ &= 4\, L_1 \\ &= \frac{2\,\hbar^2\, A^2\, e^{-2\alpha} \sec\theta}{m} \end{aligned} \tag{193}$$

C. Calculation of matrix elements for outer eight sides

The outer eight arms are mathematically defined by the following sets of equations:

$$\begin{aligned} y' = 0 \quad \text{to} \quad y' = b, \text{at} \quad x' = b \\ y' = -b \quad \text{to} \quad y' = 0, \text{at} \quad x' = b \\ y' = 0 \quad \text{to} \quad y' = b, \text{at} \quad x' = -b \\ y' = -b \quad \text{to} \quad y' = 0, \text{at} \quad x' = -b \\ x' = 0 \quad \text{to} \quad x' = b, \text{at} \quad y' = b \\ x' = -b \quad \text{to} \quad x' = 0, \text{at} \quad y' = b \\ x' = 0 \quad \text{to} \quad x' = b, \text{at} \quad y' = -b \\ x' = -b \quad \text{to} \quad x' = 0, \text{at} \quad y' = -b \end{aligned}$$

For the side, $y' = 0$ to $y' = b$ at $x' = b$, the trial function is given by

$$\begin{aligned} \varphi_a &= A\left(1 - \frac{x'y'}{b^2}\right) e^{-\alpha} \quad for \quad x' < b \\ &= A\left(1 - \frac{y'}{b}\right) e^{\frac{-\alpha\, x'}{b}} \quad for \quad x' > b \end{aligned}$$

The Hamiltonian operator is given by

$$\hat{H} \equiv \frac{-\hbar^2}{2m}\left(\frac{\partial^2}{\partial x'^2} + \frac{\partial^2}{\partial y'^2} - 2\,\sin\theta \frac{\partial^2}{\partial x' \partial y'}\right) \tag{194}$$

As there is no discontinuity in the derivative of φ_a with respect to y', contribution from $\frac{\partial^2}{\partial y'^2}$ is not taken in the calculation of matrix element of $\hat{H}$ for this side as it is already taken into account in the bulk integration. If this term in Hamiltonian operator is not dropped then we get the extra contribution which is incorrect. Hence, we have to consider $\hat{H}$ without the

second term as

$$\hat{H} \equiv \frac{-\hbar^2}{2m}\left(\frac{\partial^2}{\partial x'^2} - 2\,\sin\theta\frac{\partial^2}{\partial x'\partial y'}\right) \tag{195}$$

Using θ-function, the trial function can be written as

$$\varphi_a = A\left(1 - \frac{y'}{b}\left[\theta(x'-b) + \frac{x'}{b}\,\theta(b-x')\right]\right)\, e^{-\alpha\left[\theta(b-x')+\frac{x'}{b}\,\theta(x'-b)\right]} \tag{196}$$

$$\begin{aligned}
\frac{\partial\varphi_a}{\partial\, x'} &= A\left(-\frac{y'}{b}\left[\underbrace{\delta(x'-b) - \frac{x'}{b}\delta(b-x')}_{=0} + \frac{1}{b}\theta(b-x')\right]\right) e^{-\alpha\left[\theta(b-x')+\frac{x'}{b}\theta(x'-b)\right]} \\
&\quad + A\left(1 - \frac{y'}{b}\left[\theta(x'-b) + \frac{x'}{b}\theta(b-x')\right]\right) e^{-\alpha\left[\theta(b-x')+\frac{x'}{b}\theta(x'-b)\right]} \\
&\quad \times \left[\underbrace{\alpha\,\delta(b-x') - \frac{\alpha\,x'}{b}\delta(x'-b)}_{=0} - \frac{\alpha}{b}\theta(x'-b)\right] \\
&= -\frac{A}{b}\left[\frac{y'}{b}\theta(b-x') + \alpha\theta(x'-b)\left(1-\frac{y'}{b}\right)\right] e^{-\alpha\left[\theta(b-x')+\frac{x'}{b}\theta(x'-b)\right]}
\end{aligned} \tag{197}$$

Let

$$\begin{aligned}
g(x',y') &= \frac{y'}{b}\,\theta(b-x') + \alpha\,\theta(x'-b)\,\left(1-\frac{y'}{b}\right) \\
\text{and} \qquad f(x') &= -\alpha\left[\theta(b-x') + \frac{x'}{b}\,\theta(x'-b)\right] \\
\frac{\partial g}{\partial\, x'} &= -\frac{y'}{b}\,\delta(b-x') + \alpha\,\delta(x'-b)\,\left(1-\frac{y'}{b}\right) \\
\frac{\partial f}{\partial\, x'} &= -\alpha\left[\underbrace{-\delta(b-x') + \frac{x'}{b}\,\delta(x'-b)}_{=0} + \frac{1}{b}\,\theta(x'-b)\right] \\
&= \frac{-\alpha}{b}\,\theta(x'-b) \\
\text{Therefore} \qquad \frac{\partial\varphi_a}{\partial\, x'} &= -\frac{A}{b}\,g(x',y')\,e^{f(x')} \\
\frac{\partial^2\varphi_a}{\partial\, x'^2} &= -\frac{A}{b}\left[\frac{\partial g}{\partial\, x'} + g\,\frac{\partial f}{\partial\, x'}\right]\, e^{f(x')} \\
&= -\frac{A}{b}\,e^{f(x')}\left(\delta(b-x')\left[-\frac{y'}{b} + \alpha\,(1-\frac{y'}{b})\right] - \underbrace{\frac{\alpha^2}{b}\,(1-\frac{y'}{b})\,\theta(x'-b)}_{\text{Integral}=0}\right) \\
&= -\frac{A}{b}\,e^{-\alpha)}\,\delta(x'-b)\left[\alpha - (\alpha+1)\,\frac{y'}{b}\right]
\end{aligned} \tag{198}$$

Also,

$$\begin{aligned}
\frac{\partial^2 \varphi_a}{\partial\, x' \partial\, y'} &= -\frac{A}{b}\frac{\partial}{\partial\, y'}\left[g(x', y')e^{f(x')}\right] \\
&= -\frac{A}{b}e^{f(x')}\frac{\partial\, g}{\partial\, y'} \\
&= -\frac{A}{b}e^{f(x')}\left[\frac{1}{b}\theta(b - x') - \frac{\alpha}{b}\theta(x' - b)\right] \\
&= -\frac{A}{b^2}e^{f(x')}\left[\underbrace{\theta(b - x') - \alpha\theta(x' - b)}_{\text{Integral}=0}\right] \\
&= 0
\end{aligned}$$

$$\text{Therefore} \qquad \hat{H}\varphi_a = \frac{-\hbar^2}{2m}\left[-\frac{A}{b}e^{-\alpha}\delta(x' - b)\left(\alpha - (\alpha + 1)\frac{y'}{b}\right)\right] \tag{199}$$

Hence, for the side at $x' = b$ extending from $y' = 0$ to $y' = b$, the integral is given by

$$\begin{aligned}
S_1 &= \langle\varphi_a(x', y')|\hat{H}|\varphi_a(x', y')\rangle \\
&= -\frac{\hbar^2}{2\,m}\int_{y'=0}^{b}\int_{x'=b-\epsilon}^{b+\epsilon}\varphi_a(x', y')\left[-\frac{A}{b}\,e^{-\alpha}\,\delta(x' - b)\left(\alpha - (\alpha + 1)\,\frac{y'}{b}\right)\right]\sec\theta\,dx'\,dy' \\
&= \frac{\hbar^2\sec\theta}{2\,m}\left(\frac{A}{b}\right)\,e^{-\alpha}\int_{y'=0}^{b}\varphi_a(b, y')\left[\alpha - (\alpha + 1)\,\frac{y'}{b}\right]\,dy' \\
&= \frac{\hbar^2\sec\theta}{2\,m}\left(\frac{A}{b}\right)\,e^{-\alpha}\int_{y'=0}^{b}A\left(1 - \frac{y'}{b}\right)\,e^{-\alpha}\left[\alpha - (\alpha + 1)\,\frac{y'}{b}\right]\,dy' \\
&= \frac{\hbar^2\,A^2\,e^{-2\alpha}\sec\theta}{2\,m\,b}\int_{y'=0}^{b}\left(1 - \frac{y'}{b}\right)\left[\alpha - (\alpha + 1)\,\frac{y'}{b}\right]\,dy' \\
&= \frac{\hbar^2\,A^2\,e^{-2\alpha}\sec\theta}{2\,m\,b}\int_{y'=0}^{b}\left[\alpha - (2\alpha + 1)\,\frac{y'}{b} + (\alpha + 1)\,\frac{y'^2}{b^2}\right]\,dy' \\
&= \frac{\hbar^2\,A^2\,e^{-2\alpha}\sec\theta}{2\,m\,b}\left[\alpha\,b - (2\alpha + 1)\,\frac{b^2}{2\,b} + (\alpha + 1)\,\frac{b^3}{3\,b^2}\right] \\
&= \frac{\hbar^2\,A^2\,e^{-2\alpha}\sec\theta}{2\,m\,b}\left[\alpha\,b - (2\alpha + 1)\,\frac{b}{2} + (\alpha + 1)\,\frac{b}{3}\right] \\
&= \frac{\hbar^2\,A^2\,e^{-2\alpha}\sec\theta}{2\,m}\left[\alpha - \frac{2\alpha + 1}{2} + \frac{\alpha + 1}{3}\right] \\
&= \frac{\hbar^2\,A^2\,e^{-2\alpha}\sec\theta}{2\,m}\left(\frac{\alpha}{3} - \frac{1}{6}\right) \\
&= \frac{\hbar^2\,A^2\,e^{-2\alpha}\sec\theta}{2\,m}\left(\frac{2\,\alpha - 1}{6}\right)
\end{aligned} \tag{200}$$

Use of appropriate trial functions for the other sides, it can be shown that the integrals S_n, where $n = \overrightarrow{(1, 8)}$ are equal. Hence, the total contribution to the integrals from the eight

sides is obtained as

$$\begin{aligned} K_{III} &= 8\, S_1 \\ &= 8\, \left[\frac{\hbar^2\, A^2\, e^{-2\alpha} \sec\theta}{2\, m}\, \left(\frac{2\,\alpha - 1}{6} \right) \right] \\ &= \frac{2\,\hbar^2\, A^2\, e^{-2\alpha} \sec\theta}{3\, m}\, (2\,\alpha - 1) \end{aligned} \tag{201}$$

The matrix element of $\hat{H}$ for all the roof lines is given by

$$\begin{aligned} \langle H(\alpha) \rangle_{Rooflines} &= K_I + K_{II} + K_{III} \\ &= \frac{2\,\hbar^2\, A^2\, e^{-2\alpha} \sec\theta}{m\alpha} + \frac{2\,\hbar^2\, A^2\, e^{-2\alpha} \sec\theta}{m} + \frac{2\,\hbar^2\, A^2\, e^{-2\alpha} \sec\theta}{3\, m}\, (2\,\alpha - 1) \\ &= \frac{2\,\hbar^2\, A^2\, e^{-2\alpha} \sec\theta}{m} \left(\frac{1}{\alpha} + 1 + \frac{2\,\alpha - 1}{3} \right) \\ &= \frac{2\,\hbar^2\, A^2\, e^{-2\alpha} \sec\theta}{m} \left(\frac{2\,\alpha^2 + 2\,\alpha + 3}{3\,\alpha} \right) \end{aligned} \tag{202}$$